Engineering New Methods to Investigate Cyclic Dinucleotides

Alex J. Pollock

A dissertation submitted in partial fulfillment of the
requirements for the degree of

Doctor of Philosophy

University of Washington

2021

Reading Committee:

Joshua Woodward, Chair

Samuel Miller

Christoph Grundner

Program Authorized to Offer Degree:

Microbiology

University of Washington

ABSTRACT

Engineering New Methods to Investigate Cyclic Dinucleotides

Alex J. Pollock

Chair of the Supervisory Committee:
Joshua J. Woodward
Department of Microbiology

Nucleotide second messengers are nucleotide-based small molecules which orchestrate cellular responses to internal cues and adaptation to environmental conditions. These messengers are ubiquitous throughout life and their flux coordinates diverse processes via binding response regulator proteins or riboswitches to induce post-translational, translational, or transcriptional responses. Some of the best studied nucleotide second messengers include cAMP which regulates carbon source utilization, (p)ppGpp which regulates biosynthetic metabolism in response to nutrient limitation, and 3′3′-c-di-GMP which regulates motility and biofilm production. Nucleotide second messengers are hypothesized to be ubiquitous because they are rapidly diffusible and can be quickly synthesized from and hydrolyzed into common substrates making them amenable to effective cellular coordination. This work focuses on the recently discovered nucleotide second messengers 3′3′-c-di-AMP and 2′3′-cGAMP which are respectively an essential bacterial molecule regulating virulence, cell wall homeostasis, and osmotic regulation and a mammalian innate immune signaling molecule signaling mis-localized double stranded DNA. These second messengers are synthesized by the condensation of two ATPs or an ATP and a GTP molecule, respectively, and have been the subject of increasing academic and clinical interest in the last decade. Despite significant advances in these fields, quantitative, single cell, and kinetic tools to detect these important nucleotide second messengers are lacking. This dearth has resulted in many important investigations being intractable. In response, we have generated FRET biosensors for both 2′3′-cGAMP and 3′3′-c-di-AMP. These adaptable biosensors allow for entirely new perspectives of bacterial and metazoan cyclic-di-nucleotide signaling. Additionally, we have also developed a luminescence-based coupled enzyme assay to facilitate higher-throughput population level quantification of 3′3′-c-di-AMP. We note that the recently discovered bacteriophage-defense signaling molecule, 3′3′-cGAMP can also be detected using this coupled enzyme assay but utility will be limited until a high affinity binding protein is found and adapted to extract 3′3′-cGAMP from complex samples. The tools developed in this work will facilitate diverse investigations of immune signaling and bacterial regulation with implications for immunotherapy, autoimmune disease, viral and bacterial restriction, and vaccine development.

This is for my family.

Table of Contents

List of Figures and Tables

Chapter 1

Chapter 2

Chapter 3

Acknowledgements

I first want to thank my mentor, Joshua Woodward, for his unwavering support both personally and professionally. You have simultaneously provided the structure and freedom to develop as a scientist and follow my interests. More than anything else, you created an environment where I felt supported, could speak freely, and not fear failure. Of course, your insights were also invaluable, but your mentorship allowed me to grow into an independent scientist and I can think of no greater praise. It was a rewarding experience to have been with the lab through so many transitions: from cash strapped and scrappy to flush with funding, from trudging through failure to stumbling upon success, and from startup to established – I'm excited to see what comes next! Josh, thank you for everything. I know this is only the beginning of our relationship.

Mentorship is necessary but not sufficient, the support of incredible labmates is also required. I want to thank Shivam Zaver and Hannah Tabakh in particular who have become some of my closest friends in addition to being valuable co-authors and collaborators. It feels fitting that we went on this journey together and are all graduating within a few months of each other (sorry Josh). I also want to thank all members past and present of the Woodward lab for their company, advice, and support including: Adelle McFarland, Kamakshi Sureka, Tu Anh Huynh, Fariah Ahmed-Qadri, Qing Tang, Melissa Locke, Chelsea Stamm, Aruna Menon, Kimberly Gutierrez, Samantha Hopp, and Maureen Thomason. I am thankful to have been surrounded by great compatriots from beginning to end. Please reach out if I can ever help and I'm sure our paths will cross again soon!

My experience was also enriched in innumerable ways by my cohort: Brittany Ruhland, Danny Vogt, Sofiya Shevchenko, Justin Ulrich-Lewis, and Renee Cruz as well as honorary members Monica Cesinger and Rochelle Glover. I am thankful to have a peer community with whom I can talk freely and see eye-to-eye with. Without you, I don't know how I would have made sense of the wild ride of graduate school. I appreciate your friendship and look forward to our next gathering.

As the saying goes, it takes a village. I would like to thank the entire Microbiology Department and associated individuals for their advice and support. I would like to specifically thank Michelle Reniere and her entire lab for invaluable joint lab meetings, the Microbiology administrators, particularly Amy Gundlach and Andrea Pardo for helping make this a smooth journey, members of the Mougous Lab, particularly See-Yeun Ting, for constantly sharing equipment and ideas, and my committee members: Samuel Miller, Joseph Mougous, Michelle Reniere, and Christoph Grundner for providing valuable advice and support when I insisted on pursuing an aggressive research program.

I also want to thank the Foster School of Business for making their classes freely available for PhD students. Pursuing the Technology Entrepreneurship Certificate provided me with an invaluable perspective on the business of science and connected me with the Washington Research Foundation (WRF). I am very thankful for all the members of WRF, in particular Will Canestaro and Kim Emmons, for giving me the opportunity to grow my business acumen and help support bioscience in Washington.

I also want to thank all my friends outside of the department, in particular, Adrien Ledin, Jonathan Winkle, David Bacsik, Hasib Yousefzai, Esther Adelstein, Jessica Wong, and Teddy Forscher for our excellent adventures and helping me keep perspective. There really isn't anything like hanging above the abyss to set your priorities straight. I appreciate your friendship and support.

I can't thank my family enough for nurturing me. Most of all, my parents: Bob and Lynn Pollock, for instilling a deep curiosity about life, drive to explore, and perspective to step back and enjoy all of life's grandeur. I love you more than I can say. My brothers, Zack and Mason, have also been amazing compatriots in this journey – I am proud of you, love you, and am thankful for your friendship. Finally, Phoenica, you have been with me through the entire process: from choosing a lab to graduation. You are an absolutely amazing partner and I love you so much. I learn from you every day and I look forward to exploring the rest of life together.

Chapter 1

A STING-based biosensor affords broad cyclic dinucleotide detection within single living eukaryotic cells

The majority of this chapter was published in:

Pollock, A.J., Zaver, S.A. & Woodward, J.J. A STING-based biosensor affords broad cyclic dinucleotide detection within single living eukaryotic cells. *Nature Communications* **11**, 3533 (2020).

Summary

Cyclic dinucleotides (CDNs) are second messengers conserved across all three domains of life. Within eukaryotes they mediate protective roles in innate immunity against malignant, viral, and bacterial disease and exert pathological effects in autoimmune disorders. Despite their ubiquitous role in diverse biological contexts, CDN detection methods are limited. In this chapter, using structure guided design of the murine STING CDN binding domain, we engineer a Förster resonance energy transfer (FRET)-based biosensor deemed BioSTING. Recombinant BioSTING affords real-time detection of CDN synthase activity and inhibition. Expression of BioSTING in live human cells allows quantification of localized bacterial and eukaryotic CDN levels in single cells with low nanomolar sensitivity. These findings establish BioSTING as a powerful kinetic in vitro platform amenable to high throughput screens and as a broadly applicable cellular tool to interrogate the temporal and spatial dynamics of CDN signaling in a variety of infectious, malignant, and autoimmune contexts.

Introduction

The mammalian innate immune system provides a critical first line of defense against invading microorganisms through a suite of germline encoded, invariant sentinel proteins called Pattern Recognition Receptors (PRRs). PRRs survey the extracellular and intracellular milieu for molecular signatures of microbial origin, termed pathogen associated molecular patterns (PAMPs)[1,2]. Upon engaging PAMPs, PRRs participate in signal transduction cascades to activate antimicrobial gene regulatory programs that ultimately facilitate pathogen clearance[1,2]. Microbial nucleic acids, including DNA and RNA species, constitute a major class of PAMPs. Although a number of nucleic acid sensing PRRs have been identified to-date, the enzyme cyclic GMP-AMP Synthase (cGAS) has emerged as one of the most important sensors of foreign and self double-stranded (ds) DNA[2-5].

Upon allosteric activation by dsDNA, cGAS catalyzes the production of the cyclic dinucleotide (CDN) second messenger 2'3'-cyclic GMP-AMP (c[G(2',5')pA(3',5')p], 2'3'-cGAMP, or cGAMP), which then directly binds to and activates the ER-resident scaffold protein STING[6-10]. In addition to 2'3'-cGAMP, STING also recognizes 3'3'-linked cyclic dipurines, including c-di-AMP, c-di-GMP, and 3'3'-cGAMP, produced in the context of infection with certain bacterial species, although with markedly reduced affinities[11-14.] CDN-mediated activation of STING facilitates the recruitment and activation of several kinases, culminating in transcription factor-mediated cytokine expression and induction of autophagy to sterilize the cytosol of the infected cell[15-19].

Despite significant advances in our understanding of cGAS and STING regulation, the development of methods for monitoring the kinetics and dynamics of CDN signaling, especially in living cells, is limited. Most studies have relied on type I interferon (IFN-I) induction downstream of STING activation as an indirect reporter of cGAS activity in cells[11,13,20]. While these assays are robust and sensitive, they are not specific as many PAMPs can elicit IFN-I responses. To that end, fluorescent-tagged STING constructs have been used as a more direct reporter for STING activation. These assays rely on the translocation of STING to a perinuclear punctate compartment upon CDN binding as a qualitative proxy for its activation and have recently

been employed to monitor 2'3'-cGAMP transfer via gap junctions[21]. These tools, however, are limited to a qualitative, binary localization readout. In lieu of these reporter assays, methods to directly measure cyclic dinucleotides, including mass spectrometry, enzyme immunoassays (EIA), ENPP1-based luciferase assays (cGAMP-luc), and RNA-based biosensors have been developed[3,4,6,13,22-25]. While these assays are specific, they range in their sensitivity and only provide bulk endpoint measurements following destruction of the biological sample.

FRET biosensors have been developed for the detection of small molecules, including the nucleotide second messengers cAMP[26,27] , cGMP[28], and cyclic-di-GMP[29,34]. Ligand binding to an intramolecular FRET biosensor results in a conformational shift that alters the relative distance and orientation of fused compatible donor and acceptor fluorophores. This, in turn, alters the excitation energy transfer between fluorophores, which can be quantitated by exciting the donor fluorophore and determining the ratio of acceptor fluorophore emission to donor fluorophore emission. This change in fluorescence is directly linked to ligand occupancy and thus reports on ligand concentration either in solution or within cells[35-37]. Because these biosensors are based on native ligand binding proteins, they are powerful, genetically encodable tools with biologically relevant binding affinities and responses. Use of these biosensors has provided fundamental insight into the spatial and temporal dynamics of nucleotide signaling, as well as the identification of activators and inhibitors following in vitro and cellular screens.

To address the limitations of current CDN detection techniques, we report the development of an intramolecular FRET biosensor deemed BioSTING, which is based on the eukaryotic CDN binding protein STING[38.] We demonstrate that recombinant BioSTING is a sensitive tool capable of detecting real-time CDN synthesis, drug inhibition, and extracted CDNs from cellular sources. Further, we show that BioSTING expressed in eukaryotic cells can be used to detect CDN synthesis, import, localization, and degradation by a viral protein. Thus, BioSTING affords a powerful in vitro and cellular platform for monitoring CDN levels and is likely to facilitate fundamental discoveries relating to CDN biology as well as translational drug discovery campaigns.

Results

Design and Development of BioSTING

CDN signal transduction is mediated by nucleotide binding to effector proteins. Ligand induced structural changes in the protein alter effector function to execute changes in response to altered cellular concentrations of the second messenger[39]. The mammalian protein STING is unique in its ability to bind a variety of CDNs of both mammalian and bacterial origin[6-14]. Structurally, STING is a multipass membrane protein with a C-terminal domain consisting of a dimerization region, a CDN binding domain, and a C-terminal tail (CTT) that is required for downstream signaling (Figure 1.1a)[15-19]. The CDN binding domain has been extensively characterized at atomic resolution. When the structures of human STING in the apo and c-di-GMP bound states are aligned, one monomer in each dimer was observed to overlap with nearly no change. However, the second monomer exhibited translocation of over 4 and 12 angstroms in the N and C-termini, respectively (Figures 1.1b and 1.2a, b). Because FRET is highly sensitive to the intermolecular distance between compatible fluorophores, we hypothesized that a fluorescent fusion protein with

the STING CTD would afford a platform for the development of a FRET-based CDN biosensor (Figure 1.1c)[39-41].

Unlike some human STING alleles, murine STING (mSTING) binds both bacterial and eukaryotic dipurine containing CDNs[6-14]. Therefore, to construct a reporter of broad utility, a prototype sensor was generated by fusing mSTING to the bright and photostable FRET pair mTFP and mKO2 at L152 and E335, respectively (Figure 1.1a)[35-37,42,43]. The residues contained within this region of mSTING include the dimerization domain and the CDN binding domain but exclude the amino-terminal transmembrane domains and CTT. Based on analysis of the crystal structure, we hypothesized that, upon cyclic dinucleotide binding, the C-terminus fused to mKO2 would shift in closer proximity to mTFP and increase the amount of FRET signal (Figure 1.1c). Indeed, we observed a modest ~7% FRET increase in the presence of cGAMP with purified recombinant protein (Figure 1.2c). While this observation demonstrated the utility of this approach, the FRET signal was deemed insufficient, and we sought to optimize this prototype to enhance the FRET signal. Notably, we did not observe a FRET change using the eCFP and eYFP FRET pair highlighting the importance of fluorophore orientation as a factor in generating a FRET response.

FRET is exquisitely sensitive to changes in distance and orientation. As such, a five amino acid GGSGG linker was added between mSTING-CTD and each fluorophore individually and in combination[44,45]. While addition of the linker between STING-CTD and mKO2 slightly diminished the FRET response, addition of GGSGG between mTFP and STING-CTD alone successfully increased the FRET change to over 20% (Figures 1.1d and 1.2c and Table 1.1). This modified FRET biosensor responded to 2'3'-cGAMP with a dynamic range of 12–125 nM and a limit of detection (signal-to-noise ratio 3:1) of approximately 12 nM (Table 1.1). Because a 20% FRET increase is more than sufficient for cellular applications, we named this protein BioSTING (Biosensor STING) and used this version in all further experiments.

Characterization of BioSTING-CDN Binding

Having generated BioSTING, we next sought to compare the biochemical parameters of nucleotide interactions between purified BioSTING and STING-CTD by DRaCALA analysis[46]. Radioactive cGAMP (Figure 1.2d) bound BioSTING and STING-CTD at a Kd of 56 and 61 nM, respectively (Figures 1.1e and 1.2e). Radioactive c-di-AMP (Figure 1.2d) bound BioSTING and STING-CTD at a Kd of 2.26 μM and 2.58 μM, respectively (Figures 1.1e and 1.2e). These results confirmed that the region of STING contained within BioSTING maintained CDN binding and that the addition of flanking FRET-fluorophores did not alter binding affinity or disrupt the dimer to which CDNs bind. To confirm that BioSTING retained binding specificity, we performed radioactive cGAMP binding analysis with both BioSTING and STING-CTD in the presence of a variety of unlabeled nucleotides. As expected, only 3'3'-cyclic and 2'3'-cyclic dinucleotides but not ATP, GTP, cAMP, or cGMP could compete off bound [^{32}P] 2'3'-cGAMP (Figures 1.1f and 1.2f). These findings reveal that fusion of the two FRET fluorophores to BioSTING has no discernable impact on nucleotide specificity or binding affinity relative to STING-CTD.

Finally, we monitored the dissociation kinetics by determining the rate that cold nucleotide could compete off bound radioactive nucleotide. Radioactive 2'3'-cGAMP was competed off BioSTING and STING-CTD by cold 2'3'-cGAMP with a half-life of 121 and 83 min, respectively (Figure

1.1g). Radioactive 3'3'-c-di-AMP was competed off of both proteins with a half-life of <10 s by cold 3'3'-c-di-AMP (Figure 1.1h). Together, these results show similar dissociation rates of CDNs from BioSTING relative to STING-CTD, consistent with the similarity in the observed Kd's for these nucleotides. In addition, due to the rapid dissociation rate of 3'3'-c-di-AMP, BioSTING is anticipated to afford rapid monitoring of both increases and decreases in nucleotide levels of 3'3'-CDNs. However, as a consequence of the relatively slow dissociation rate of 2'3'-cGAMP, BioSTING may afford real time monitoring of increases in 2'3'-cGAMP but may be limited in the temporal resolution associated with its decline. Notably, these results suggest that STING activation by 2'3'-cGAMP may be possible through a single binding event while activation by 3'3'-CDNs may require constant exposure to an activating concentration of ligand.

BioSTING provides a real-time readout of cyclic dinucleotide production in vitro

Current in vitro methods for monitoring CDN production employ sensitive EIA, mass spectrometry, and cGAMP-luc endpoint measures, as well as less sensitive continuous tools, including a cGAMP RNA biosensor and an indirect pyrophosphate release assay[3,4,6,22-25]. Given the limitations of current CDN detection methods, the ease of recombinant BioSTING production, and its capacity to directly report on a variety of CDNs at biologically relevant concentrations, we employed BioSTING to monitor in vitro CDN synthase activity and inhibition to demonstrate its utility for kinetic characterization and feasibility for high throughput screening related to these enzymes.

To demonstrate the ability of recombinant BioSTING to detect real time production of cyclic dinucleotides, we monitored DNA integrity scanning protein A (DisA) mediated synthesis of 3'3'-c-di-AMP, which occurs constitutively in the presence of ATP. In reactions consisting of BioSTING, ATP, and increasing concentrations of purified DisA, we observed increasing rates of FRET signal concomitant with increasing DisA concentrations (Figure 1.3a). Next, cGAS synthesis of 2'3'-cGAMP from ATP and GTP was monitored. As expected, the rate of BioSTING FRET signal correlated with increased cGAS protein and there was no 2'3'-cGAMP production without the addition of DNA, which is required for allosteric activation of the enzyme (Figures 1.3b and 1.4a).

BioSTING FRET assays are carried out in a 96-well format using a fluorescent plate reader making it amenable to in vitro high throughput screening efforts (Figure 1.4b). Recently, Pfizer reported the development of the cGAS inhibitor PF-06928215[52]. To test the use of BioSTING as a platform to characterize small molecule inhibitors, we performed dose response measurements with fixed cGAS and variable concentrations of PF-06928215 (Figure 1.3c). In parallel, we also titrated cGAS levels while keeping the concentration of PF-06928215 fixed (Figure 1.4c). The slope of the linear region was determined for each reaction, plotted versus PF-06928215 concentration, and fit to identify an IC50 of ~12 μM (Figure 1.3d), in close agreement with the reported IC50 of 5 μM[47]. Together these studies demonstrate that BioSTING affords robust, continuous detection of CDN levels in vitro and offers flexibility in assay design, making it amenable to high throughput screens and kinetic characterization studies of a variety of CDN synthases. In addition to screening for modulators of CDN synthase activity, BioSTING could also potentially be used to screen directly for STING agonists and antagonists.

BioSTING can detect 2'3'-cGAMP extracted from mammalian cells

Given the ease of producing recombinant BioSTING and its nanomolar affinity for 2'3'-cGAMP, we anticipated that it may provide an attractive method for measuring 2'3'-cGAMP from cellular extracts. To demonstrate this utility, we monitored FRET responses of BioSTING exposed to methanol extracts from HEK293T cells transfected with increasing concentrations of pCDNA3.1-cGAS. As expected, FRET responses were negligible with low concentrations of transfected pCDNA3.1-cGAS plasmid but saturated at elevated plasmid concentrations (Figure 1.3e). Notably, at lower levels of transfected plasmid we observed marginal FRET responses. This is likely a consequence of the simultaneous increase in both cGAS expression and activating DNA, as well as the dilution factor chosen for the experiment. To overcome this limitation, samples containing low levels of cGAMP can be diluted less or subjected to a cGAMP enrichment step using recombinant STING.

In addition, we observed signal saturation with higher levels of transfected plasmid. To overcome signal saturation, samples transfected with the highest amount of pCDNA3.1-cGAS were diluted to obtain readings within the sensor's linear range (Figure 1.3f). Multiplying the dilution factor by the diluted sample's cGAMP concentration calculated by interpolation into a standard curve of known cGAMP concentrations (Figure 1.1d), thus allows for determination of cGAMP in the undiluted sample. If cell volume assumptions are applied, an average intracellular cGAMP concentration can be calculated, in our case ~30 μM, which was in line with the concentration determined by EIA and within the range of concentrations previously reported by other methods (Figure 1.4d)[48.] Together, these findings suggest that recombinant BioSTING can be used as a bulk cell extract 2'3'-cGAMP detection method; although, other sensitive methods for end-point 2'3'-cGAMP detection exist[22,48].

BioSTING can detect 2'3'-cGAMP within live mammalian cells

The inability to directly monitor cyclic dinucleotides in individual living eukaryotic cells is currently one of the biggest limitations in the field. Encouraged by the in vitro characterization of BioSTING, we next sought to extend its application within this context. BioSTING was introduced into a pSLIK doxycycline inducible lentiviral system to generate stable HEK293T cell lines (Figure 1.5a)[49]. Fixed levels of either pCDNA3.1-cGAS or empty vector were transfected into cells expressing BioSTING and FRET signal was monitored using flow cytometry. In cells expressing cGAS relative to an empty vector control, we observed a greater than 20% BioSTING FRET increase, consistent with our in vitro assays (Figure 1.5b, c, and 1.6a-c). We also confirmed production of 2'3'-cGAMP in this experimental system by EIA analysis (Figure 1.6b). To ensure that BioSTING FRET responses were directly due to cGAMP recognition, we delivered purified cGAMP using both lipofection and nucleofection. Lipofectamine transfection produced a strong response, which plateaued below the BioSTING saturation level, likely as a consequence of the limited carrying capacity of the transfection reagent (Figure 1.5d). Nucleofection, on the other hand, was not limited in this manner, and we observed complete BioSTING activation (Figure 1.6d).

As intracellular cGAMP concentrations can range from low nanomolar to high micromolar[48], to quantitatively contextualize the observed BioSTING FRET response in cells, we titrated the levels

of cGAS expression vector and determined the intracellular concentration of cGAMP by EIA in parallel with BioSTING FRET measurements by flow cytometry. Using assumptions about cell volume, we then plotted FRET changes versus average intracellular cGAMP concentration from which we were able to estimate that 50% of the maximum BioSTING FRET signal corresponds to a concentration of approximately 5–50 nM cGAMP in cells, consistent with the in vitro measured affinity of BioSTING for cGAMP and supporting our expectation that BioSTING is responding to biologically relevant concentrations of cGAMP (Figure 1.6e, f).

Reanalysis of our flow cytometry data to detect FRET levels of single cells rather than the entire population confirmed our expectation that, under the conditions tested, there was a unimodal rather than bimodal shift in signal (Figure 1.5e). Because the entire population is responding with a normal distribution, we interrogated the possibility of using BioSTING as a platform for screening via flow cytometry. To estimate sorting potential, a FRET high gate was drawn above cells transfected with an empty vector and a FRET low gate drawn below cells transfected with a high amount of pCDNA3.1-cGAS (Figure 1.5f). We obtained ~10-fold enrichment for cells in the FRET low gate (Figure 1.6g) and ~100 fold enrichment of cells in the FRET high gate (Figure 1.6h). We hypothesize that the decreased selection in the FRET low gate is a consequence of a small percentage of cells evading efficient transfection. Thus, efficiency of selection could likely be improved using an integrated inducible or constitutive cGAS system. Overall, these encouraging results provide support for utilizing BioSTING as a platform for forward genetic screens to identify genes involved in regulating cGAS and cGAMP in living cells.

In order to assess the impacts of BioSTING expression levels on intracellular FRET responses, we again reanalyzed our flow cytometry results to compare cells expressing high and low levels of BioSTING (Figure 1.7a). These two populations had similar FRET response dynamics but with slightly different response magnitudes (Figure 1.7b-d). Thus, although there is flexibility in the expression level of cells, BioSTING expression levels should be tightly controlled when comparing FRET responses between samples.

Development and use of a cGAMP-blind BioSTING

A powerful control for an intramolecular FRET biosensor is a ligand blind version which differentiates changes due to bona fide binding from other effects (i.e., protein–protein interactions, fluorophore quenching, etc). A literature search highlighted the mutations Y240S and T263A in human STING (Y239S and T262A in murine STING) as ideal candidates which would diminish CDN binding without disrupting protein stability (Figure 1.8a)[50]. As expected, Y239S T262A BioSTING stably expressed and neither appreciably bound radioactive cGAMP nor produced a FRET change in response to cGAMP (Figure 1.8b, c). To determine if Y239S T262A BioSTING could act as a cGAMP control in cells, we titrated pCDNA3.1-cGAS in cells expressing WT or mutant biosensor. While WT BioSTING produced a robust FRET response, Y239S T262A BioSTING only generated a minor FRET change at exceptionally high levels of cGAS, thus supporting the use of Y239S T262A BioSTING as a control biosensor for 2’3’-cGAMP (Figure 1.8d).

Bacterial 3’3’-CDNs have been shown to be released during infection and to activate STING in the cytosol. To determine if WT BioSTING and Y239S T262A BioSTING can detect bacterial

CDNs in cells, we titrated increasing concentrations of expression vectors for *B. subtilis* DisA which synthesizes c-di-AMP and a constitutively active isoform of *P. aeruginosa* WspR (D70E), denoted WspR*, which synthesizes c-di-GMP (Figure 1.8e)[40]. All nucleotides resulted in a BioSTING FRET increase. However, while Y239S T262A BioSTING produced a minor response to the highest concentrations of cGAS, moderate responses were observed for DisA, and unexpectedly large responses were observed for WspR*. Levels of c-di-AMP are not expected to reach high levels in physiologically relevant contexts, therefore Y239S T262A BioSTING is likely to serve as an adequate control for c-di-AMP. In contrast, the lowest levels of WspR* tested induced a large response in Y239S T262A BioSTING demonstrating that it will not be an adequate control for c-di-GMP. Thus, despite its applicability as a control for other CDNs, the Y239S T262A BioSTING variant may be selectively used as a c-di-GMP biosensor within cells.

We hypothesized that further design may be used to generate other versions of BioSTING which exhibit selectivity for CDNs based upon their unique chemical properties, including phosphodiester linkage and/or base content. Previous studies identified naturally occurring mutations in human STING that abolish responsiveness to 3'3'-CDNs while retaining 2'3'-cGAMP sensing[8]. In an effort to engineer a universally blind control biosensor we subsequently made the R231A/H mutations previously reported to diminish IFN-β activation in Y239S T262A BioSTING. We also introduced these mutations to WT BioSTING in an effort to make a sensor capable of uncoupling bacterial versus eukaryotic CDNs. When cyclic dinucleotide cyclases are expressed in this mutant array, we unexpectedly found that these mutants alone only diminished the response to cGAMP but the triple mutant Y239S, T262A, and R231A diminished but did not completely abrogate the FRET response to c-di-GMP (Figure 1.9). More work will be required to determine whether this is related to 3'3'-c-di-GMP binding before this sensor could be employed as a control for c-di-GMP secretion. Therefore, we were unsuccessful in our attempt to uncouple sensing of 3'3'-CDNs from 2'3'-cGAMP. In future iterations of BioSTING, we hope to use unbiased approaches to make BioSTING variants with altered nucleotide specificities.

BioSTING exhibits broad utility for monitoring 2'3'-cGAMP dynamics in live cells

Based on our encouraging results highlighting BioSTING's ability to detect cGAMP in cells, we next sought to demonstrate BioSTING's utility to monitor modulation of cGAS activity. Previous experiments titrated pCDNA3.1-cGAS alone, resulting in simultaneous increases in both the CDN cyclase and stimulatory ligand, leading to titration curves with positive Hill coefficients. To directly measure cGAS activation we co-transfected cells with a fixed, low concentration of pCDNA3.1-cGAS and increasing amounts of calf thymus DNA (CT-DNA) ligand. As expected, at low CT-DNA levels we observed no detectable FRET increase, but as CT-DNA content was increased, we observed an elevated FRET signal that began to saturate at the highest concentration of stimulatory ligand tested (Figure 1.10a). These results suggest that BioSTING is a useful tool to investigate the kinetics of cGAS activation in live cells.

The cGAS-STING pathway is immensely important for controlling viral infection and many viruses have developed methods to inhibit this pathway. Recently, vaccinia virus was reported to antagonize cGAS-STING signaling through expression of Poxin, a 2'3'-cGAMP-selective phosphodiesterase[51]. To monitor cGAMP hydrolysis by Poxin in cells, we expressed a constant level of wild-type (WT) or catalytically dead (H17A) Poxin over a titration of cGAS plasmid.

Expression of Poxin in 293T cells was confirmed by [^{32}P] CDN hydrolysis assays (Figure 1.11a, b). In cells transfected with low levels of cGAS plasmid we observed high FRET from the H17A mutant and a greatly decreased FRET response in cells expressing the WT Poxin. As expected, expression of high cGAS levels overcame the capacity of Poxin to antagonize cGAMP levels (Figure 1.10b). Co-expression of Poxin with DisA or WspR* had no effect on 3'3'-CDN-mediated FRET responses as compared to empty vector controls, consistent with the role of Poxin as a 2'3'-cGAMP specific hydrolase (Figure 1.11c). These results demonstrate the utility of BioSTING to characterize modulators of cGAMP concentrations within living cells.

While cGAS production of cGAMP and subsequent STING activation both occur in the cytosol, recent findings have established that CDNs can be transmitted between cells through export and import mechanisms, as well as through gap junctions[22,21,48,52,53]. Such nucleotide transfer is reported to facilitate antitumor properties and cGAMP is being explored therapeutically both alone and in combination with PD-1 blockade[48,52-56]. The therapeutic utility of cGAMP in this context requires nucleotide import to the cytosol to promote STING inflammatory responses[20,48,52-54]. To investigate the utility of BioSTING for monitoring cellular import of cGAMP, we added increasing concentrations of cGAMP to the extracellular medium. After 6 h, cellular FRET signals in response to altered concentrations of cGAMP exhibited saturation like responses below the maximum signal associated with the sensor (Figure 1.10c). The observed saturation of the response may be due to saturation of the importer operative in these cells or a consequence of the establishment of import-export equilibrium. While a thorough account of the transport mechanisms is yet to be documented, these results demonstrate that BioSTING can detect cGAMP uptake from the extracellular space and may provide a valuable tool to identify and characterize the mechanism by which cGAMP is transferred among cells.

Despite being a well-studied system, conflicting reports regarding cGAS and cGAMP localization remain[57-61]. As a genetically encodable protein, we hypothesized that BioSTING could be localized to distinct cellular compartments through the introduction of specific signal sequences. As such, we introduced a nuclear localization signal (NLS) to BioSTING, which resulted in successful localization to the nucleus (Figures 1.10d, e and 1.11d, e). Using a cGAS titration, we were able to detect cGAMP in both the nucleus and the cytoplasm (Figure 1.10f). Consistently, the Y239S T262A BioSTING control sensor had very little change in FRET response providing additional evidence that we are detecting bona fide cGAMP in the nuclear compartment. Although these experiments only indicate that cGAMP can penetrate the nucleus, we anticipate that utilization of BioSTING in time-course and microscopy experiments will further elucidate the localization of cGAMP production under various activating conditions and may be used to reveal mediators of nucleotide transit between cellular compartments.

Finally, BioSTING, containing the dimerization domain of full-length STING, has the potential to heterodimerize with endogenous STING. To determine the consequences of heterodimerization, full-length, human STING was expressed alone or in combination with cGAS in HEK293T cells stably expressing BioSTING. Expression of human STING in this context decreased the response of BioSTING in the presence and absence of cGAS (Figure 1.10g). Observation of a FRET decrease upon expression of STING suggests that heterodimerization leads to an altered conformation and that cells must be deficient for STING in order to attain interpretable FRET responses. Taken together, these data demonstrate that our first-generation FRET biosensor,

BioSTING, is highly versatile for both in vitro and cellular studies, but its application is currently limited to a STING-deficient setting.

Concluding Remarks

Here, we report the development of BioSTING, a FRET-based intramolecular biosensor engineered to monitor CDNs in vitro and in cells. BioSTING maintains the native CDN binding properties of the parent protein upon which it was designed and as such exhibits CDN reporting capacity in physiological concentration ranges. Through a variety of in vitro and cellular studies we establish BioSTING as a robust sensor of a variety of CDNs, providing real-time detection of nucleotide levels with temporal and spatial resolution.

BioSTING's ease of recombinant production, native binding properties, and simple kinetic readout make it a promising tool for investigating cyclic dinucleotides in vitro. We show that BioSTING can detect extracted nucleotides from cellular samples, as well as enzymatic production of cyclic dinucleotides with recombinant protein. Although not investigated in this work, BioSTING can also likely be used to monitor phosphodiesterase activity for bacterial 3'3'-cyclic dinucleotides in real time. However, given the unexpectedly low dissociation rate, such application for 2'3-cGAMP hydrolysis may be limited. In addition to general enzymatic characterization of CDN synthesis, we also utilized BioSTING to characterize PF-06928215 inhibition of cGAS, demonstrating its robust utility for characterization of small molecule modulators of CDN synthases. A key limitation to be considered relates to the spectral properties of compounds under investigation. For instance, while several antimalarial compounds have been reported to inhibit cGAS activity, the intrinsic fluorescence of these compounds spectrally overlap with BioSTING and interfere with its application in this context. Although this limitation is important to consider, few compounds are expected to have conflicting autofluorescence. Additionally, the only clinically investigated cGAS inhibitor, PF-06928215, does not have conflicting autofluorescence demonstrating the potential of non-fluorescent molecules to selectively inhibit cGAS.

Despite impressive in vitro utility, the primary motivation for developing BioSTING was to create a tool capable of detecting 2'3'-cGAMP in live single cells. While the dynamic range of BioSTING is indeed narrower, our findings support that BioSTING binds and responds to cGAMP at physiologically relevant concentrations and with sensitivity comparable to commercially available EIA based approaches. In addition, we successfully measured FRET changes by flow cytometry, providing the first single cell measurements of CDN levels. In addition to single cell measurements, a key aspect of FRET based biosensors is the capacity to provide subcellular information about signaling dynamics. As a genetically encodable protein, localization tags can be added to target a sensor to specific cellular compartments. There is currently a debate about the localization of cGAS and therefore production of cGAMP in cells. By introducing an NLS to BioSTING we demonstrated the ability to restrict the sensor to the nucleus and monitor cGAMP within this compartment. Application of BioSTING in combination with rapid imaging microscopy is likely to provide important insight into when and where cGAMP is produced and if this differs depending upon the infectious insult, within distinct cell types, or in response to cellular damage versus pathogen encounter.

One particularly exciting application of BioSTING is for high throughput small molecule and forward genetic screening. In high throughput small molecule screening applications, BioSTING provides the ability to measure cGAMP production in live cells, which can simultaneously account for compound toxicity and cell permeability together with target engagement. In fact, Pfizer identified PF-06928215 as an inhibitor of cGAS through in vitro enzyme screening methods but the compound failed in development as a pharmaceutical due to its inability to access the cytosol. In addition, we anticipate that BioSTING will have utility in genetic screens to study modulation of cGAMP levels in cells. Because FRET measurements can be conducted using flow cytometry, BioSTING affords the ability to conduct these studies in batch culture. Combining BioSTING flow-based sorting with disruption or overexpression libraries from mammalian and microbial pathogens will afford genome wide interrogation of CDN signaling pathways, including molecular insight into pathogen associated antagonists, as well as cell intrinsic regulators of the pathway, namely cGAS activators and inhibitors and mediators of cGAMP hydrolysis, transport, and localization.

Though developed to investigate 2'3'-cGAMP cellular biology, BioSTING is also capable of investigating similar aspects of bacterial 3'3'-cyclic dinucleotides. We demonstrated through expression of DisA and WspR* that BioSTING can detect bacterial 3'3'-CDNs in the mammalian cytosol. Thus, the potential for BioSTING to be used as a tool to investigate the timing and magnitude of bacterial CDN release in biologically relevant contexts such as during *Listeria monocytogenes, Mycobacterium tuberculosis,* and *Chlamydia trachomatis* infection, among others, is evident. In our attempts to identify CDN blind variants of BioSTING, we inadvertently identified Y239S T262A BioSTING as a c-di-GMP specific reporter. These findings suggest that with further engineering of BioSTING it may be possible to identify mutants sensitive to specific CDNs. Such sensors would be useful to dissect mixed CDN interactions such as during *M. tuberculosis* infection, in which both cGAS produced 2'3'-cGAMP and bacterial derived c-di-AMP have been implicated in STING activation[62-64]. In addition, a wide array of bacterial cyclic dinucleotides of dipurine, dipyrimidine, and mixed purine pyrimidine content were recently reported; however, only cyclic dipurine containing nucleotides were shown to robustly bind to and activate STING[14,65]. It is feasible that BioSTING can be engineered through a mix of semi-randomized and rationally designed mutations to detect these more recently discovered signaling nucleotides. Finally, mutation of Tyrosine 167, which stabilizes CDN binding though a pi-stacking interaction, to an alanine or valine will likely generate an additional BioSTING control variant that is universally blind to all CDNs. Although outside the scope of this work, the intracellular concentration of bacterial CDNs have been reported to be similar to the Kd of BioSTING[13,32,64], thus it is likely that expression of BioSTING in bacterial cells will afford interrogation of CDN dynamics within these organisms as well.

BioSTING is a blue, orange-based rather than far-red or luminescence-based biosensor, which limits its use to cell culture due to the limited ability for blue-orange light to penetrate tissues. Although there are many important findings to be made in cell culture, as a clinically relevant molecule, there is also an immense interest in studying 2'3'-cGAMP in vivo. We believe that it will be possible to develop a far-red FRET or luminescent version of BioSTING by replacing mKO2-mTFP fluorophores with a small circularly rotated library of a red-shifted FRET pair, BRET pair, or split luciferase and screening for increased signal upon cGAMP binding[66-70]. Production of either a far-red (such as the 'Booster' FRET set) or luminescent derivative integrated

into the murine genome under either constitutive or cell specific promoters will allow for the detection of cGAMP in vivo and create a powerful model to study cGAMP activity in viral infection and autoimmune disease models.

As a STING-based biosensor, BioSTING is sensitive to heterodimerization with native STING. Thus, the sensitivity afforded by STING also leads to the limitation that BioSTING must be used in cells which either do not express or are genetically modified to lack STING. Although many important studies are tractable in this system, some investigations such as those coupling cGAMP measurements with STING-Interferon pathway activation or regulation in the same sample currently are not. To allow investigation of these exciting research areas we anticipate creating a version of BioSTING incapable of heterodimerization with WT STING through engineering of the dimerization interface. This updated version will increase BioSTING's versatility while retaining the impressive sensitivity and specificity of STING.

Overall BioSTING is a powerful tool that makes many fundamental and clinically important investigations of cyclic dinucleotide biology more tractable and in some instances feasible in the first place. In addition to the immediate application of current BioSTING versions, we believe there is immense promise in using BioSTING as a foundation to develop a wide array of biosensors with unique CDN binding or in vivo imaging capacities. In total, BioSTING represents a versatile tool to significantly advance the current limits of knowledge related to the ever expanding and clinically relevant field of cyclic dinucleotide signaling.

Materials and Methods

BioSTING cloning

Primers for BioSTING cloning are listed in Supplementary Table 2 and plasmids and strains are listed in Supplementary Table 3. Prototype and GGSGG linker versions of BioSTING were generated by amplifying STING CTD with Kapa HiFi polymerase (Kapa Biosystems) using a combination of primers 1, 2, 3, and 4 from pET28b-mSTING CTD. The resulting products were ligated into pET15b-mKO2-12AA-mTFP using Spe1/Kpn1 fast digest restriction endonuclease cloning (Thermo Fisher) and transformed into XL1-Blue chemically competent *E. coli*. Site directed mutagenesis was carried out by amplifying the generated pET15b-BioSTING sensor using primers 5, 6 or 7, 8 or 9, 10, or 11,12 using Kapa HiFi polymerase. PCR purified product was DpnI digested (NEB) and transformed into XL1-Blue chemically competent *E. coli*. To generate pSLIK-BioSTING, pET15b-BioSTING was amplified using primers 13 and 14 for cytoplasmic expression and primers 13 and 15 to add a nuclear localization signal (NLS) from c-MYC at the C-terminus. These products were then ligated into the BsiW1 (Thermo Fisher) site of pSLIK using InFusion (Takara) then transformed into Stbl3-OneShot competent cells (Thermo Fisher).

Protein expression and purification

Recombinant 6×-His tagged SUMO-mcGAS, *B. subtilis* (*B.s.*) DisA, mSTING-CTD, and mRECON were expressed and purified as summarized below[45]. Briefly, plasmids for mcGAS, DisA, mSTING-CTD, and mRECON expression were transformed into Rosetta (DE3)pLysS chemically competent cells. Overnight cultures of the resulting transformed bacteria were inoculated into 1.5 L of LB broth at a 1:100 dilution. Bacterial cultures were grown to OD_{600} 0.4–0.6 at 37 °C after which protein expression was induced by the addition of 0.5 mM isopropyl β-D-1-thiogalactopyranoside (IPTG) for 20 h at 16 °C. Bacteria were harvested by centrifugation, and the cell pellets were resuspended in Buffer A [50 mM Tris-Cl pH = 8.0, 300 mM NaCl, 20 mM Imidazole, 5 mM β-Mercaptoethanol (BME), and 1 mM phenylmethylsulfonyl fluoride (PMSF)]. Cells were lysed by sonication and clarified lysate was bound to HisPur NiNTA Resin (Thermo Scientific). The resin was washed with 100–200 column volumes of buffer A and bound proteins were eluted in Buffer B [50 mM Tris-Cl pH = 7.4, 300 mM NaCl, 300 mM Imidazole, 5 mM β-Mercaptoethanol (BME), and 1 mM phenylmethylsulfonyl fluoride (PMSF)]. Following NiNTA chromatography, His6-SUMO-mcGAS was exchanged into Buffer C [20 mM Tris-Cl pH 7.4, 250 mM NaCl, 1 mM dithiothreitol (DTT)] and further purified by Heparin Sepharose chromatography. Bound cGAS was eluted over 250 mM to 1000 mM NaCl gradient. The resulting purified proteins were analyzed by SDS-PAGE, exchanged into storage buffer [40 mM Tris pH 7.5, 100 mM NaCl, 20 mM $MgCl_2$] using PD-10 desalting columns (GE Healthcare), snap frozen, and stored at −80 °C until use.

For BioSTING expression, plasmids encoding BioSTING variants were transformed into Rosetta (DE3)pLysS chemically competent cells.Overnight cultures of the resulting transformed bacteria were inoculated into 1 L of LB broth and grown as above. At an OD_{600} of 0.5–0.7, protein expression was induced by the addition of 0.2 mM isopropyl β-D-1-thiogalactopyranoside (IPTG)

for 6 h at 18 °C. Bacteria were harvested by centrifugation, and the cell pellets were resuspended in Buffer D [50 mM Tris-Cl pH = 7.5, 100 mM NaCl, 20 mM Imidazole, 5 mM β-Mercaptoethanol (BME), and 1 mM phenylmethylsulfonyl fluoride (PMSF)]. Cells were lysed by sonication and clarified lysate was bound to HisPur NiNTA Resin (Thermo Scientific, Waltham, MA). The resin was washed with 100–200 column volumes of Buffer D and bound proteins were eluted in Buffer E [50 mM Tris-Cl pH = 7.5, 100 mM NaCl, 300 mM Imidazole, 5 mM β-Mercaptoethanol (BME), and 1 mM phenylmethylsulfonyl fluoride (PMSF)]. The resulting proteins were concentrated and further purified by gel filtration on a Superdex 200 column (GE Healthcare) using storage buffer [40 mM Tris pH 7.5, 100 mM NaCl, 30 mM $MgCl_2$, supplemented with 0.5 mM TCEP]. Protein samples were tested for purity by SDS-PAGE followed by Coomassie Brilliant Blue staining. Fractions with high purity were pooled, concentrated, flash frozen, and stored at −80 °C until use in biochemical assays.

Synthesis of [^{32}P] 2'3'-cyclic GMP-AMP and [^{32}P] 3'3'-cyclic di-AMP

[^{32}P] Radiolabeled cyclic dinucleotides (CDNs) were synthesized enzymatically using α-[^{32}P] ATP (Perkin-Elmer) and recombinant SUMO-mcGAS (2'3'-cGAMP) or *B.s*. DisA (3'3'-c-di-AMP) and affinity purified using mSTING-CTD and mRECON, as follows: [^{32}P] cGAMP was synthesized enzymatically by incubating 0.33 μM α-[^{32}P] ATP (Perkin-Elmer) with 250 μM unlabeled GTP, 1 μg of Interferon Stimulatory DNA 100mer, and 1 μM of recombinant His-tagged cGAS in binding buffer [40 mM Tris pH 7.5, 100 mM NaCl, 20 mM $MgCl_2$] at 37 °C overnight. Subsequently, recombinant cGAS was removed from the reaction mixture by incubation with HisPur Ni-NTA resin (Thermo Scientific) for 30 min. The sample was transferred to a minispin column (Thermo Scientific) to elute the crude [^{32}P] cGAMP sample. The resulting [^{32}P] cGAMP was purified further using recombinant mSTING-CTD. 100 μM mSTING-CTD was bound to HisPur Ni-NTA resin for 30 min on ice. The resin was washed two times to remove unbound mSTING-CTD. The resulting resin was incubated with the remaining crude cGAMP synthesis reaction mixture for 30 min on ice. Following removal of the supernatant, the Ni-NTA resin was washed five times with ice cold binding buffer. The resin was then incubated with 100 μL of binding buffer for 10 min at 95 °C and transferred to a minispin column to elute [^{32}P] cGAMP.

[^{32}P] c-di-AMP was synthesized as follows: briefly, 1 μM α-[^{32}P] ATP (Perkin-Elmer) was incubated with 1 μM of recombinant DisA in binding buffer at 37 °C overnight. The reaction mixture was boiled for 5 min at 95 °C and DisA was removed by incubation with HisPur Ni-NTA resin. The sample was transferred to a minispin column (Thermo Scientific) to elute the crude [^{32}P] c-di-AMP sample. The resulting [^{32}P] c-di-AMP was further purified using recombinant His-tagged mRECON. 100 μM His-tagged mRECON was bound to HisPur Ni-NTA resin for 30 min on ice. The resin was washed two times to remove unbound RECON. The resulting resin was incubated with the remaining crude [^{32}P] c-di-AMP sample for 30 min on ice. Following removal of the supernatant, the Ni-NTA resin was washed five times with ice cold binding buffer and then incubated with 100 μL of binding buffer for 5 min at 95 °C. The slurry was then transferred to a minispin column to elute [^{32}P] c-di-AMP.

Affinity purified CDNs were analyzed by Thin Layer Chromatography (TLC) on Polygram CEL300 PEI TLC plates (Machery-Nagel) in buffer containing 1:1.5 (vol/vol) saturated $(NH_4)_2SO_4$ and 1.5 M NaH_2PO_4 pH 3.6. [^{32}P] radiolabeled CDNs were visualized by exposure

onto PhosphorImager screens, which were developed using a Typhoon FLA 9000 biomolecular imager (GE Healthcare) and determined to be ~99% pure.

Nucleotide binding assays

[^{32}P] Radiolabeled cyclic dinucleotide binding assays were performed using DRaCALA[105]. Binding assays were performed in binding buffer [40 mM Tris pH 7.5, 100 mM NaCl, 20 mM $MgCl_2$] at room temperature. To determine binding affinities, two-fold serial dilutions of proteins were incubated with ~1 nM of [^{32}P] radiolabeled CDNs for at least 10 min. To determine binding specificities, proteins were pre-incubated with 500 μM excess, unlabeled nucleotides for 10 min, followed by incubation with ~1 nM of [^{32}P] radiolabeled CDNs for at least 10 min. Samples were then blotted onto nitrocellulose membranes and allowed to air dry. [^{32}P] radioactivity was visualized by exposure onto PhosphorImager screens, which were developed using a Typhoon FLA 9000 biomolecular imager (GE Healthcare). Non-radioactive 2'3'-cGAMP (Invivogen), 3'3'-cGAMP (Invivogen), 3'3'-c-di-AMP (Invivogen, San Diego, CA), and 3'3'-c-di-GMP (BIOLOG Life Science Institute, Bremen, Germany) were purchased and diluted in endotoxin free water.

In vitro FRET assays

5–10 μM purified BioSTING proteins were incubated with increasing concentrations of cyclic dinucleotides within a black flat bottom opaque 96-well plate (Greiner Bio-One) in activity buffer [40 mM Tris pH 7.5, 100 mM NaCl, 20 mM $MgCl_2$]. mTFP and FRET fluorescence was monitored using a fluorimeter (BioTek Synergy H1 Hybrid Reader, BioTek Instruments) with the following parameters (unless otherwise stated): 458 nm excitation, 490 nm emission for mTFP, and 600 nm emission for mKO2. Assay parameters were calculated using Prism Software. Kd and EC50 were determined using nonlinear fit and all other parameters were calculated using linear fit, according to literature precedent [26].
Enzyme activity assays

For DisA enzyme activity assays, 5–10 μM purified BioSTING was incubated with increasing concentrations of recombinant *B.s*. DisA within a black 96-well plate in activity buffer [40 mM Tris pH 7.5, 100 mM NaCl, 20 mM $MgCl_2$]. Enzyme assays were initiated by the addition of 1 mM ATP, and the enzyme reactions were allowed to proceed for 2 h at 37 °C.

For cGAS enzyme activity assays, 5–10 μM purified BioSTING was incubated with increasing concentrations of recombinant SUMO-mcGAS within a black 96-well plate in activity buffer [40 mM Tris pH 7.5, 100 mM NaCl, 20 mM $MgCl_2$]. Enzyme assays were initiated by the addition of 1 mM ATP, 1 mM GTP and 1 μg ISD (Figures 3.3b and 3.4a, b) or by the addition of 250 μM ATP, 250 μM GTP, and 50 ng ISD (Figures 3.3c, d and 3.4c). Enzyme assays were allowed to proceed for 2 h at 37 °C. cGAS inhibitor (PF-06928215) was purchased from Sigma-Aldrich and diluted in sterile DMSO.

For all assays, FRET activity was monitored as above.

2'3'-cGAMP extraction

HEK293T cells were plated at a density of 750,000 cells per well of a 6-well cell culture plate. The next day cells were transfected with the indicated amounts of pcDNA3.1-hcGAS vector using PEI transfection reagent (Polysciences). Twenty-four hours later the cells were harvested by centrifugation and washed once with ice-cold PBS. Cell pellets were resuspended in ice-cold 80% Optima, HPLC grade methanol (Fisher Scientific) and incubated on ice for 20 min. Cells were further lysed by sonication. Following centrifugation, cellular extracts were completely dried under vacuum and stored at −20 °C until use. For FRET assays, extracts were resuspended in activity buffer [40 mM Tris pH 7.5, 100 mM NaCl, 20 mM $MgCl_2$] containing 5–10 μM purified BioSTING and transferred to a black 96-well plate. FRET activity was monitored using a fluorimeter as described above. Quantification requires a standard curve of known cGAMP concentrations in the sample buffer done at the time of analysis.

Cell lines

Human Embryonic Kidney (HEK) 293 T cells were grown in Dulbecco's Modified Eagle Medium (DMEM) (Gibco) supplemented with 10% (v/v) heat-inactivated FBS (HyClone), 1 mM sodium pyruvate, 2 mM L-Glutamine (Thermo Fisher), 100 U mL^{-1} penicillin, 100 μg mL^{-1} streptomycin and maintained at 37 °C in 5% CO2 in a humidified incubator.

Lentivirus production and transduction

VSV-G pseudotyped, self-inactivating lentivirus was prepared by transfecting a semi-confluent 10 cm dish of HEK293T cells with 4 μg of psPAX2, 2 μg of pCMV-VSV-G, together with 4 μg of pSLIK lentiviral vector using Poly(ethyleneimine) (PEI). Growth medium was replaced 24 h after transfection and cell culture supernatants were collected at 48 and 72 h after transfection and filtered through a 0.45 μm filter.

For lentiviral transduction, HEK293T cells were seeded at a density of 2 to 4 million cells per 10 cm dish. The following day, cells were transduced with 5 mL of filtered lentiviral supernatant. 24 h later the cell culture medium was removed and replaced with standard cell culture medium supplemented with 2 μg per mL puromycin (Gibco). For all subsequent experiments, lentivirus-transduced cells were passaged and maintained in selection medium containing puromycin.

Intracellular FRET assays

For experiments using CDN cyclases, HEK293T cells stably expressing the indicated BioSTING constructs under a doxycycline-inducible promoter were plated at a density of 750,000 cells per well of a 6-well cell culture plate. The next day, the cells were transfected with the indicated amounts of cyclase-encoding plasmids using PEI transfection reagent. One hour later, biosensor expression was induced by the addition of Doxycycline Hydrochloride (1 μg mL^{-1}) (Sigma-Aldrich). Twenty four hours later the cells were harvested by centrifugation and resuspended in ice-cold PBS. Biosensor activity was determined by FACS analysis. To contextualize results, a negative control in which no cGAMP is present and a positive control where cGAMP is abundant should be run in each assay to quantify the lower and upper bounds of FRET activation.

For electroporation experiments, HEK293T cells stably expressing wild-type BioSTING were plated at a density of five million cells per 10 cm dish in cell culture medium supplemented with Doxycycline (1 μg mL^{-1}) to induce biosensor expression. The next day cells were harvested by trypsinization and electroporated with the indicated concentrations of 2'3'-cGAMP using SF Cell Line 4D-Nucleofector X Kit according to the manufacturer's protocols (Lonza). Following electroporation, the cells were resuspended in ice-cold PBS and analyzed by FACS analysis.
For extracellular 2'3'-cGAMP stimulations, HEK293T cells stably expressing wild-type BioSTING were plated at a density 750,000 cells per well of a 6-well cell culture plate in cell culture medium supplemented with Doxycycline (1 μg mL^{-1}) to induce biosensor expression. The next day, the indicated concentrations of 2'3'-cGAMP were added to the culture medium. 6 h later the cells were harvested by centrifugation and resuspended in ice-cold PBS. Biosensor activation was determined by FACS analysis.

Flow cytometry

To prepare cells for flow cytometry, cell culture media was aspirated, and the cells were harvested in ice-cold PBS. The resuspended cells were then analyzed using a LSR II flow cytometer (BD) with the following voltages: FSC-A/H/W-350, SSC-A/H/W-240, BV510(mTFP)-360, PE(mKO2)-380, and BV570(FRET)-375 volts. Data was then analyzed using FlowJo software (Tree Star).

2'3'-cGAMP enzyme immunoassay (EIA)

HEK293T cells were plated at a density of 750,000 cells per well of a 6-well cell culture plate. The next day cells were transfected with the indicated amounts of pcDNA3.1-hcGAS vector using PEI transfection reagent. Twenty-four hours later the cells were harvested by centrifugation and washed once with ice-cold PBS. Cell lysates were prepared using the 2'3'-cGAMP EIA protocol and 2'3'-cGAMP was quantified according to the manufacturer's instructions (Arbor Assays).

Western blotting

HEK293T cells were plated at a density of 750,000 cells per well of a 6-well cell culture plate. The next day cells were transfected with 1 μg pcDNA3.1-hcGAS or empty vector using PEI transfection reagent. Twenty-four hours later cells were harvested by centrifugation, and the cell pellets were lysed in Pierce RIPA buffer (Thermo Scientific) supplemented with Halt Protease and Phosphatase Inhibitor Cocktail (Thermo Scientific). Lysates were clarified by centrifugation, and protein content was normalized using Pierce BCA Protein Assay Kit (Thermo Scientific). In total, 30 μg of protein per condition were loaded onto Any kD Mini-PROTEAN TGX Precast Protein Gels (Bio-Rad) and separated by SDS-PAGE. Proteins were then transferred onto nitrocellulose membranes (Bio-Rad) at 100 V for 90 min at 4 °C. The membranes were then air dried for one hour and blocked in 5% Blotto, non-fat milk (Santa Cruz Biotechnology) dissolved in 1× TBS for one hour. Membranes were probed overnight in 5% Bovine Serum Albumin (Fisher Scientific) dissolved in 1 X TBS-T with anti-cGAS Rabbit mAb (1:1000) and anti-β-Actin Mouse mAb (1:1000) (Cell Signaling Technology). Proteins were visualized using IRDye 800CW Goat anti-Rabbit IgG Secondary Antibody (1:10000) and IRDye 680RD Goat anti-Mouse IgG Secondary Antibody (1:10000) (LI-COR Biosciences). All wash steps were carried out using 1× TBS-T. Blots

were imaged using an Odyssey Fc System (LI-COR Biosciences). Rabbit anti-cGAS (D1D3G; cat. no. 15102) and mouse anti-β-Actin (8H10D10; cat. no. 3700) monoclonal antibodies were obtained from Cell Signaling Technology.

Figures

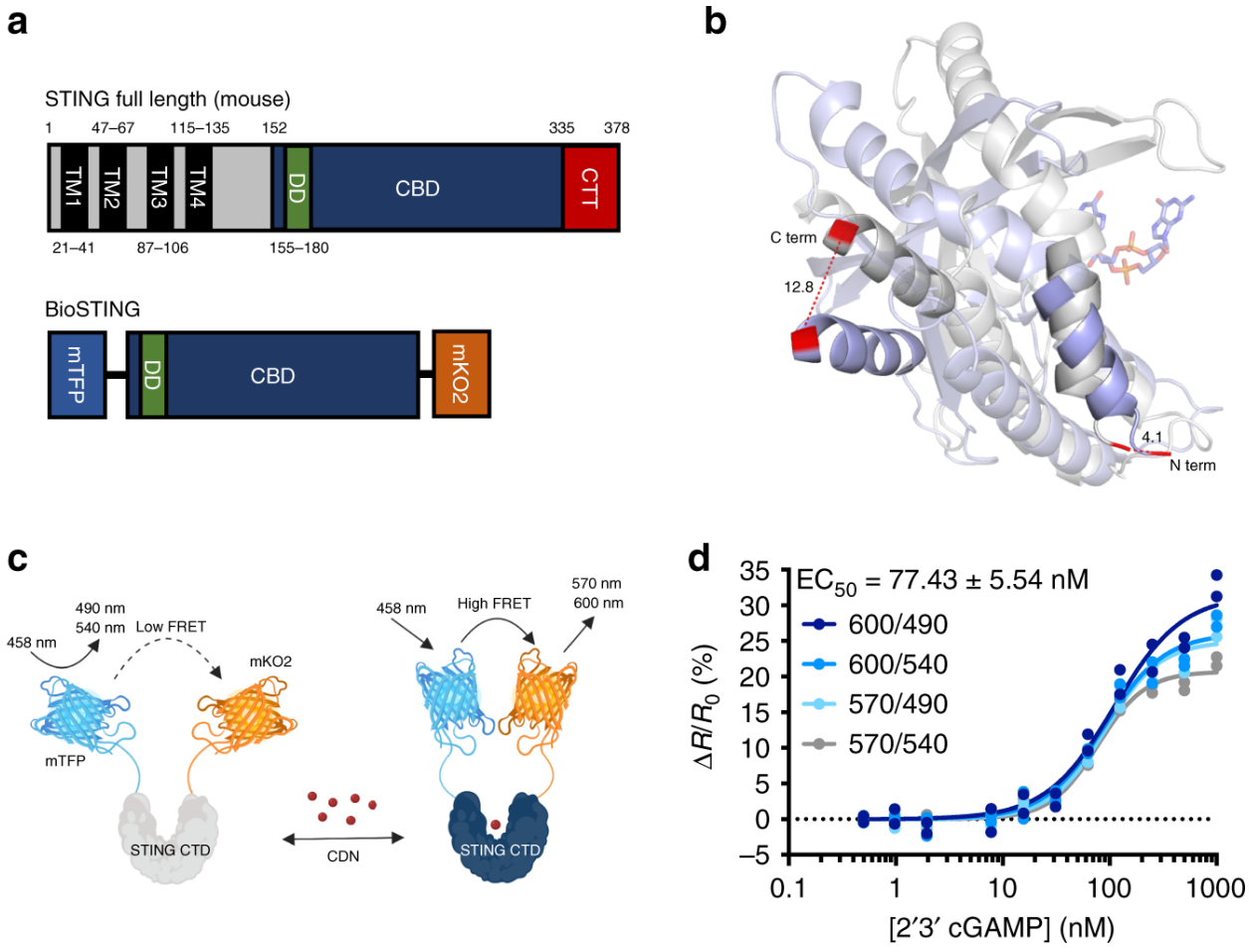

Figure 1.1: BioSTING Design and Optimization
(a) Schematic representation of full-length STING (top) and BioSTING with additional GGSGG linker between mTFP and STING-CTD (bottom). Abbreviations are defined as follows: TM (transmembrane region), DD (dimerization domain), CBD (CDN binding domain), and CTT (C-terminal tail). **(b)** Overlay and structural alignment of human STING CTD in apo (blue) and c-di-GMP bound (gray) states (PDB 4F5E and 4F5D, respectively). Only a single monomer, which exhibits the largest structural rearrangement upon ligand binding, is shown. The N and C-terminal helices of the CTD are highlighted with the terminal residues in red and their associated displacement following ligand binding labeled in angstroms. **(c)** Model of the FRET increase which occurs upon CDN binding. Generated with Biorender.com. **(d)** Recombinant BioSTING FRET response to increasing concentrations of 2′3′-cGAMP using 458 nm excitation and listed emission wavelengths.

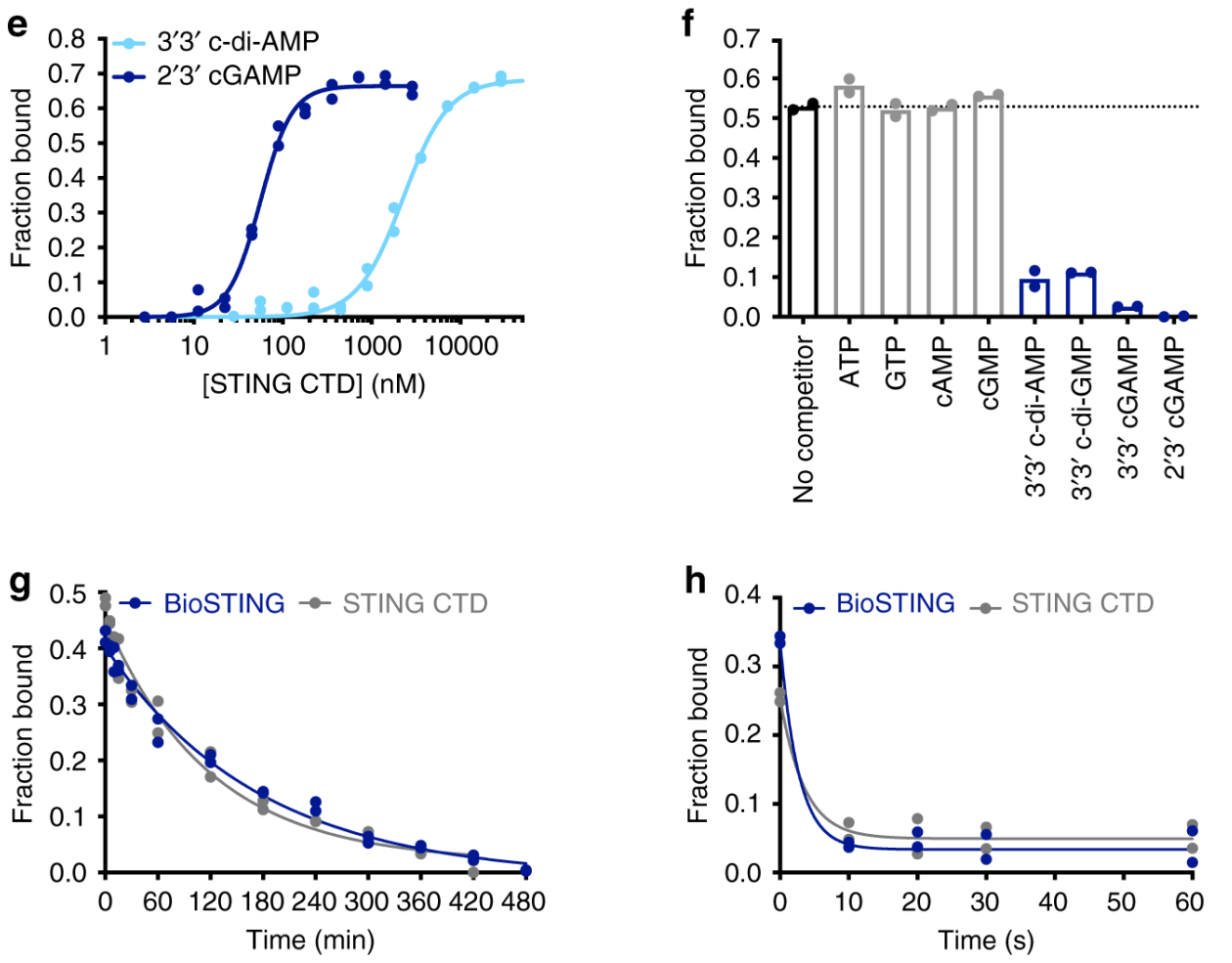

Figure 1.1 (continued): BioSTING Design and Optimization
(e) DRaCALA radioactive nucleotide binding assay of BioSTING using ~1 nM [^{32}P] labeled 2′3′-cGAMP and 3′3′-c-di-AMP. Corresponding STING-CTD binding curve is Figure 3.2e. **(f)** DRaCALA binding analysis of BioSTING using ~1 nM [^{32}P] labeled 2′3′-cGAMP in the presence of excess (500 µM) unlabeled nucleotides. Corresponding STING-CTD competition is Figure 3.2f. **(g)** Time course of excess unlabeled 2′3′-cGAMP competing off bound [^{32}P] labeled 2′3′-cGAMP from BioSTING (blue) and STING-CTD (gray). **(h)** Time course of excess unlabeled 3′3′-c-di-AMP competing off bound [^{32}P] labeled c-di-AMP from BioSTING (blue) and STING-CTD (gray). In panels g and h, BioSTING was pre-incubated with ~1 nM of [^{32}P] labeled CDNs for 10 min followed by the addition of 1 mM unlabeled 2′3′-cGAMP (g) or 3′3′-c-di-AMP (h). In all panels, individual data points of $n = 2$ biological replicates are shown.

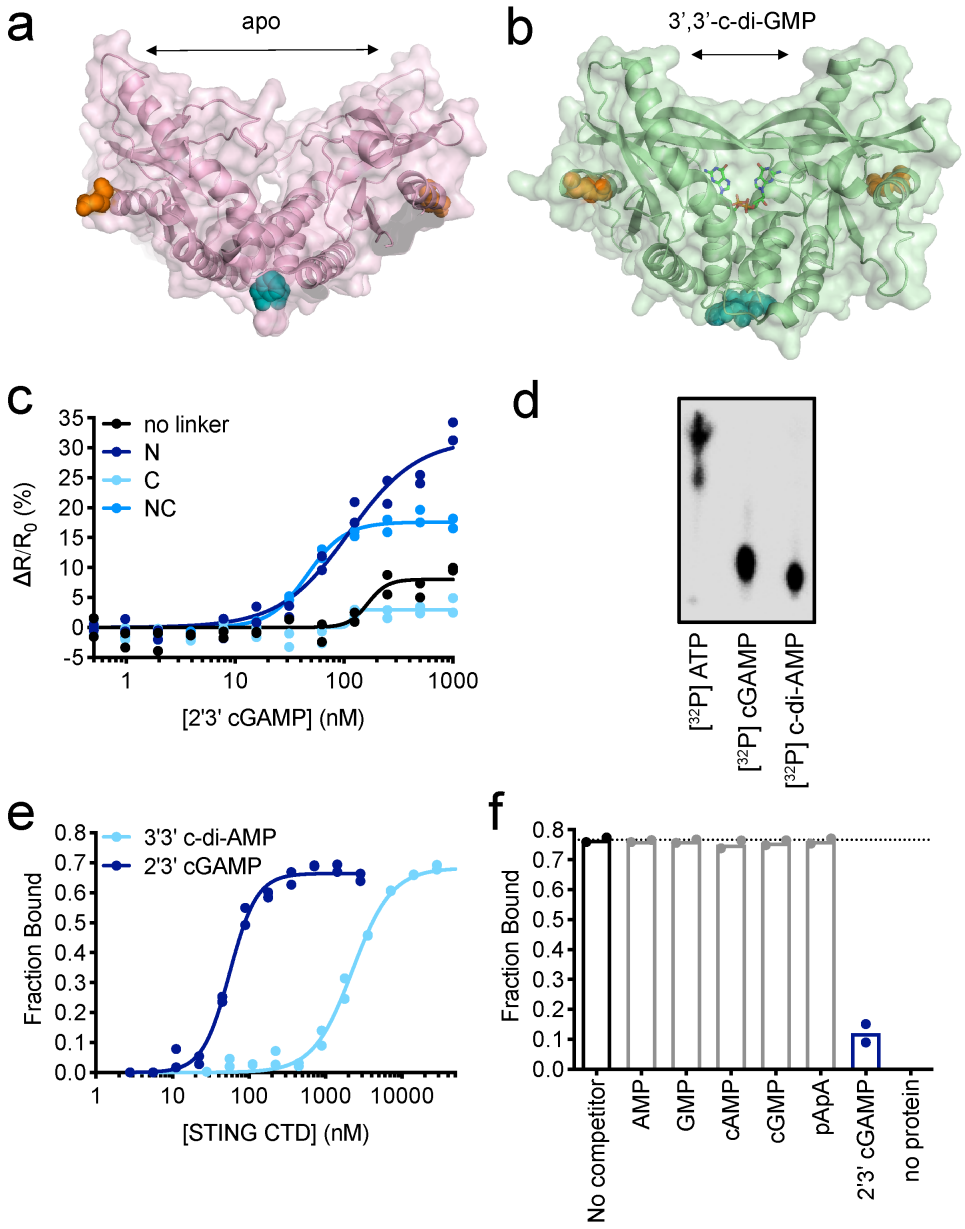

Figure 1.2: BioSTING development and characterization

(a-b) STING crystal structures [40] with N terminus highlighted in Teal and C terminus highlighted in Orange where mTFP and mKO2 fluorophores were respectively attached (a) STING Apo structure (pink) (PDB 4F5E) and (b) STING bound to 3′3′-c-di-GMP (green) (PDB 4F5D) **(c)** FRET response in the presence of increasing 2′3′-cGAMP of prototype biosensor (black) and biosensors with GGSGG linkers on the N (dark blue), C (light blue), or both (medium blue) termini of STING-CTD **(d)** TLC analysis of enzymatically synthesized [^{32}P] labeled 2′3′-cGAMP and 3′3′-c-di-AMP and [^{32}P] ATP standard. Data are representative of two independent experiments **(e)** DRaCALA binding analysis of STING-CTD using ~1 nM [^{32}P] labeled 2′3′-cGAMP and 3′3′-c-di-AMP. **(f)** DRaCALA binding analysis of recombinant STING-CTD using ~1 nM [^{32}P] labeled 2′3′-cGAMP in the presence of excess (500 µM) unlabeled nucleotides. In all panels, individual data points of n=2 biological replicates are shown.

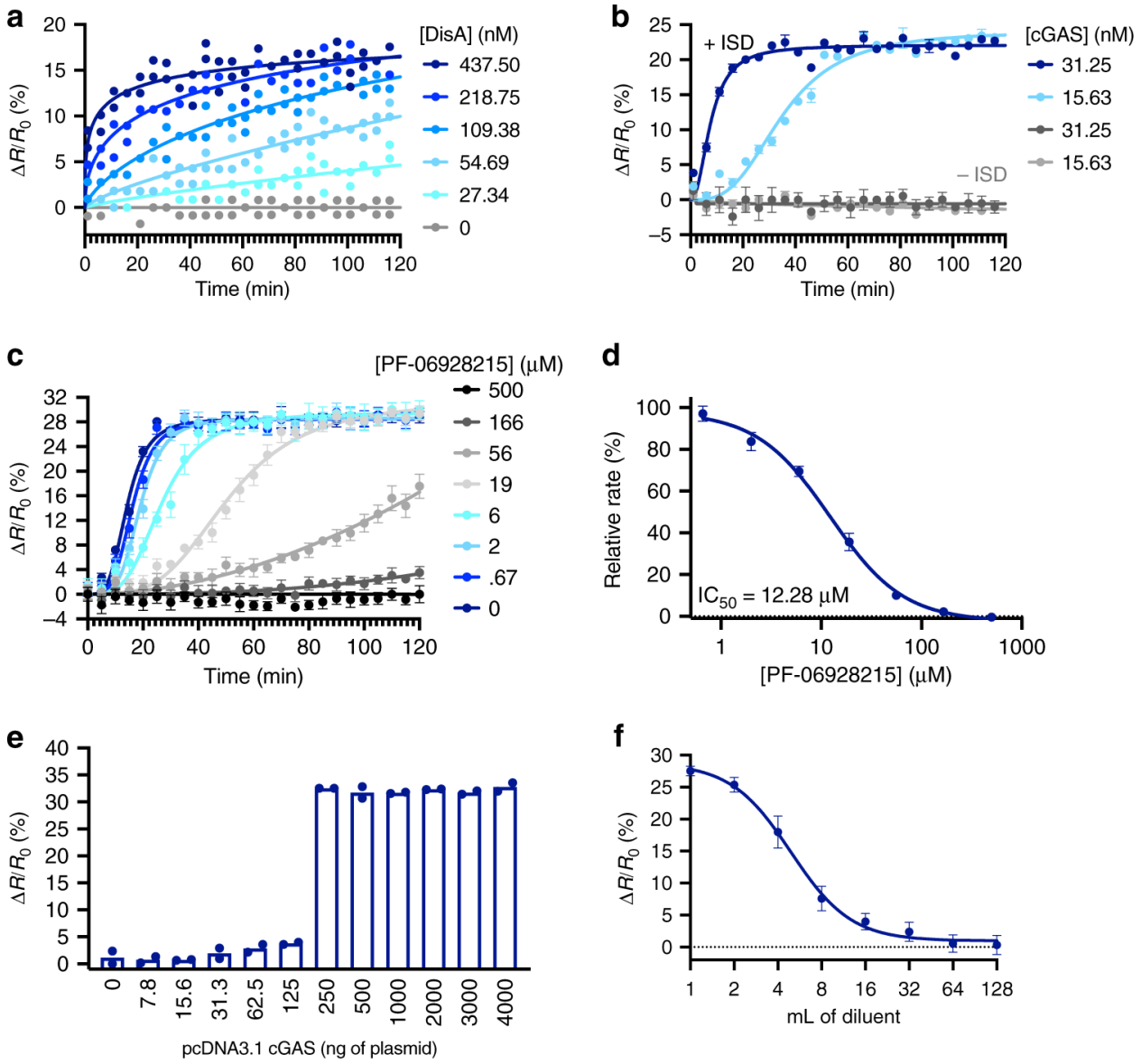

Figure 1.3: Real-time measurement of CDN synthesis and determination of CDN levels from cellular extracts.

(a) DisA enzyme activity assay time course in the presence of increasing concentrations of the 3′3′-c-di-AMP cyclase DisA using BioSTING. **(b)** cGAS activity assay in the presence of indicated concentrations of recombinant cGAS with or without Interferon Stimulatory DNA (ISD) using BioSTING. **(c)** cGAS activity assay measuring 2′3′-cGAMP production in the presence of fixed cGAS and ISD concentrations with increasing concentrations of the cGAS inhibitor PF-06928215 using BioSTING. **(d)** Reaction linear rates calculated from panel **c** plotted versus PF-06928215 concentration and fit to IC50 curve (Prism 8). € BioSTING FRET response in the presence of methanol extracted cGAMP from HEK293T cells transfected with increasing concentrations of pCDNA3.1-cGAS. **(f)** BioSTING FRET response over two-fold serial dilutions of cGAMP methanol extracts from HEK293T cells transfected with 5 µg of pCDNA3.1-cGAS. In panels a and e, individual data points of $n = 2$ biological replicates are shown. In panels b–d and f, data are presented as mean ± s.d. of $n = 3$ (b, f) or $n = 8$ (c–d) biological replicates.

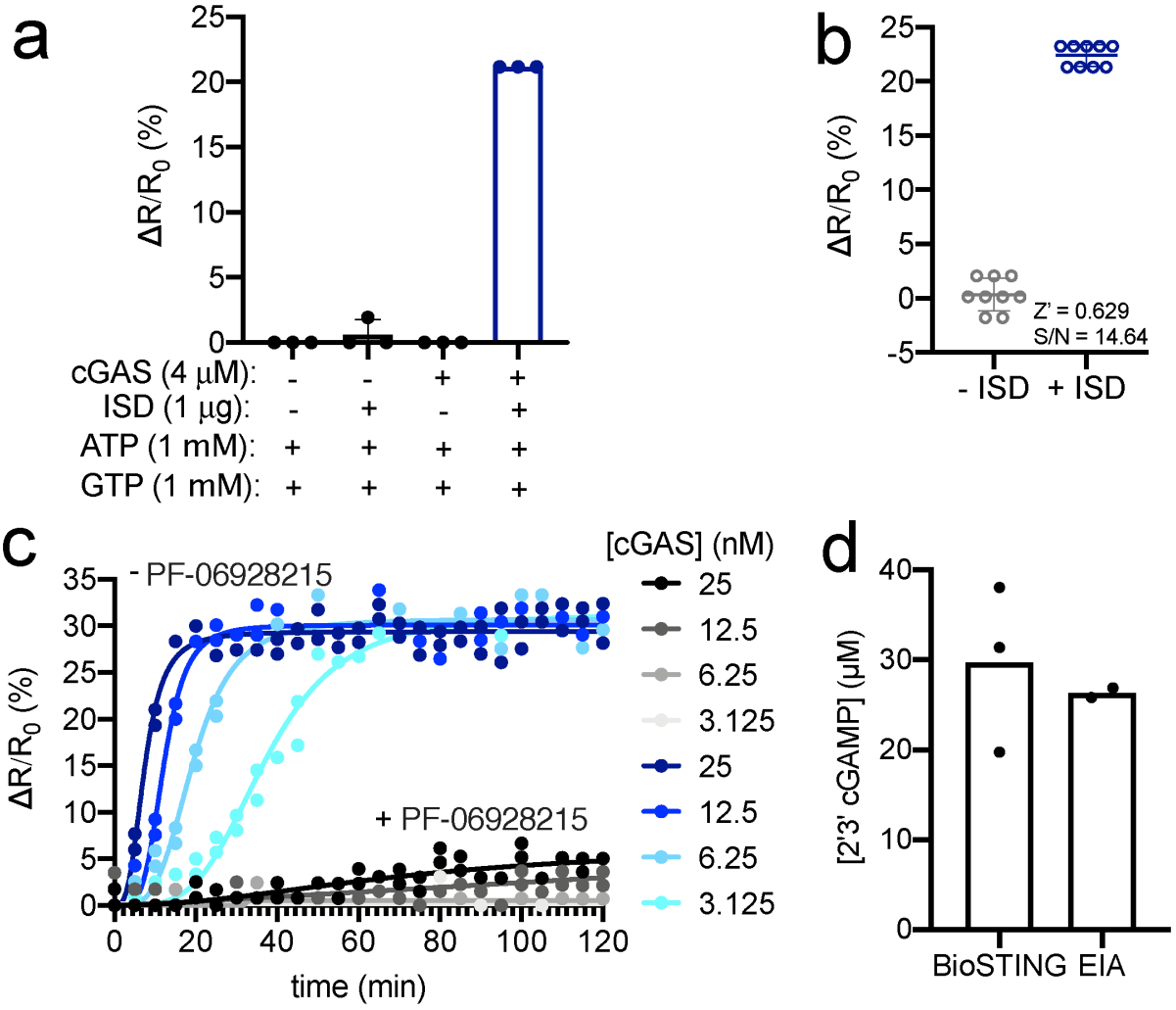

Figure 1.4: BioSTING detection of CDNs in vitro.

(a) cGAS activity assay in the presence and absence of indicated concentrations of recombinant cGAS, ISD, ATP, and GTP using BioSTING. (**b)** Determination of Z′ factor and signal to noise (S/N) ratio for BioSTING using recombinant cGAS in the presence and absence of ISD in a 96-well format. $0.5 < Z' < 1$ is considered excellent statistical reliability for high throughput screening applications. (**c)** cGAS activity assay measuring 2′3′-cGAMP production in the presence of a fixed concentration of PF-06928215 (500 μM) with increasing concentrations of cGAS using BioSTING. (**d)** Quantification of 2′3′-cGAMP levels from HEK293T cells transfected with 5 μg of pcDNA3.1-cGAS using BioSTING or EIA. Data are presented as mean ± s.d. of n=3 (a) or n=9 (b) biological replicates. In panels c and d, individual data points of n=2 (c, d) or n=3 (d) biological replicates are shown.

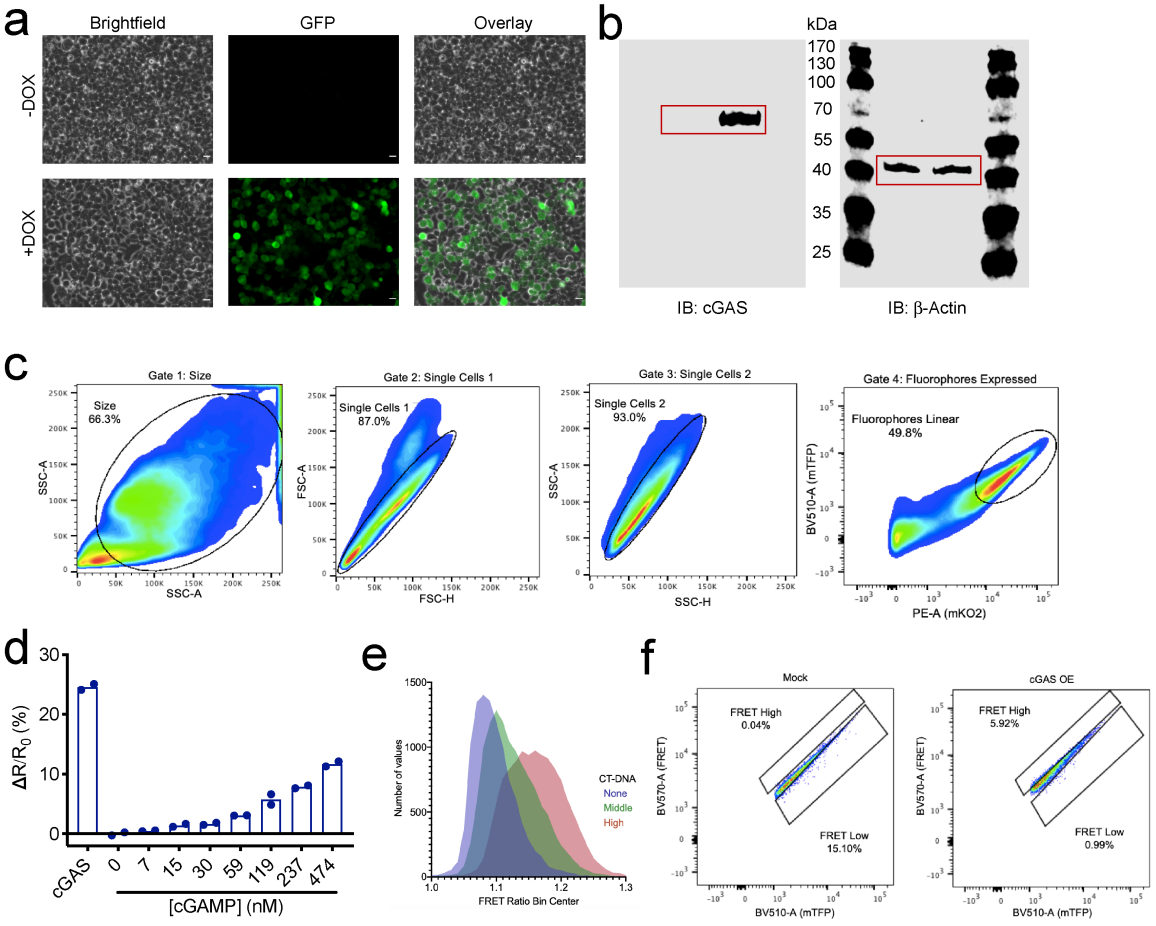

Figure 1.5: BioSTING can detect cGAMP in cells.
(a) BioSTING expression was induced in HEK293T cells transduced with pSLIK-BioSTING for 24 hours after the addition of doxycycline or vehicle control. Biosensor expression was analyzed using a BZ-X710 microscope (Keyence), GFP filter cube (EX 470/40, DM 495, and BA 525/50), and 40X objective. Scale bars, 15 µm. Data are representative of two independent experiments. **(b)** Uncropped blots for Figure 3.6a of HEK293T cells stably expressing BioSTING transfected with either 1 µg of empty-pCDNA3.1 vector or pCDNA3.1-cGAS vector. Data are representative of two independent experiments. **(c)** Flow analysis method: Step 1 is to set a permissive size gate, Step 2 and 3 are sorting for single cells using FSC and SSC A by H plots, and step 4 is to plot BV510 (mTFP) by PE (mKO2) and gate on cells with appropriate expression. These cells are then analyzed for BV570 (FRET)/BV510 (CFP) ratio. **(d)** HEK293T cells stably expressing BioSTING were transfected with either pCDNA3.1-cGAS or increasing concentrations of purified 2′3′-cGAMP using Lipofectamine 2000 transfection reagent according to the manufacturer's protocol and analyzed for FRET response by flow cytometry. Individual data points of n=2 biological replicates are shown. **(e)** Single cell analysis of HEK293T cells stably expressing BioSTING transfected with 10 ng of pCDNA3.1-cGAS and then transfected with a mock (0 ng), medium (156 ng), or high (1250 ng) amounts of cGAS-activating CT-DNA for 4 hours and analyzed by flow cytometry. **(f)** FRET high and low gates made on cells gated by above method (c) used to demonstrate flow selection potential. (Left) cells transfected with empty vector (Right) cells transfected with pCDNA3.1-cGAS.

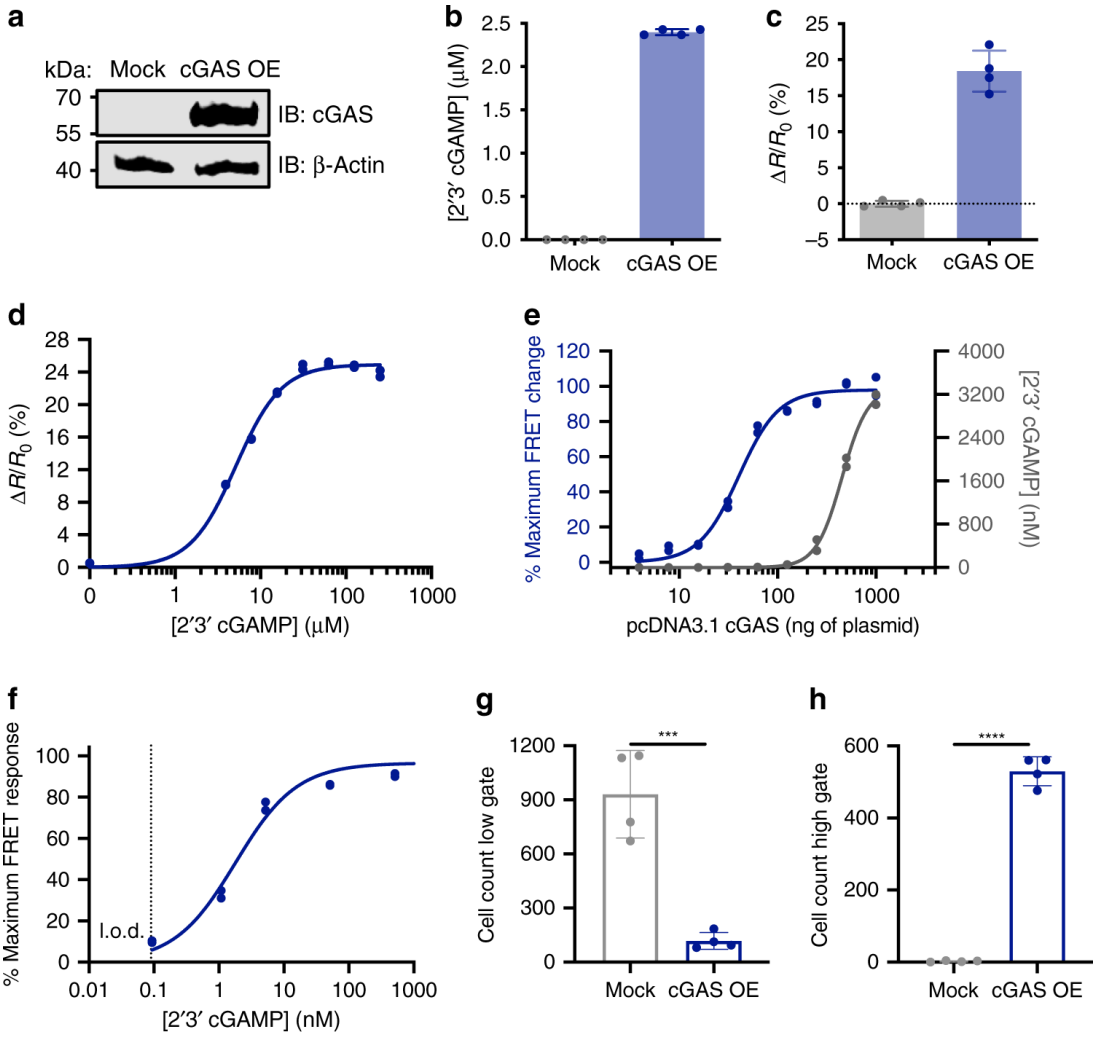

Figure 1.6: BioSTING quantitates cGAMP in single cells in a manner compatible with flow screening.

HEK293T cells stably expressing BioSTING transfected with 1 μg of either empty pCDNA3.1 vector or pCDNA3.1-cGAS vector and analyzed for **(a)** cGAS expression by western blot (data are representative of two independent experiments), **(b)** cGAMP production by EIA analysis, and **(c)** BioSTING FRET response by flow cytometry. **(d)** HEK293T cells stably expressing BioSTING were electroporated using AMAXA (Lonza) with increasing concentrations of purified 2′3′-cGAMP and analyzed for FRET response by flow cytometry. **(e)** HEK293T cells stably expressing BioSTING were transfected with increasing concentrations of pCDNA3.1-cGAS and analyzed for FRET response by flow cytometry or for 2′3′-cGAMP production by EIA. **(f)** BioSTING FRET response from (e) graphed as a function of intracellular 2′3′-cGAMP concentration measured by EIA. **(g–h)** HEK293T cells stably expressing BioSTING transfected with either empty-pCDNA3.1 vector or pCDNA3.1-cGAS vector and analyzed by the alternative gating method in S2d for (g) cells in the low gate and (h) cells in the high gate. Statistical analyses were performed using two-tailed *t*-tests: *** denotes $P = 0.0006$ (g) and **** denotes $P = 0.0000002$ (h) (Prism 8). In panels b–c and g–h, data are presented as mean ± s.d. of $n = 4$ biological replicates. In panels d–f, individual data points of $n = 2$ biological replicates are shown.

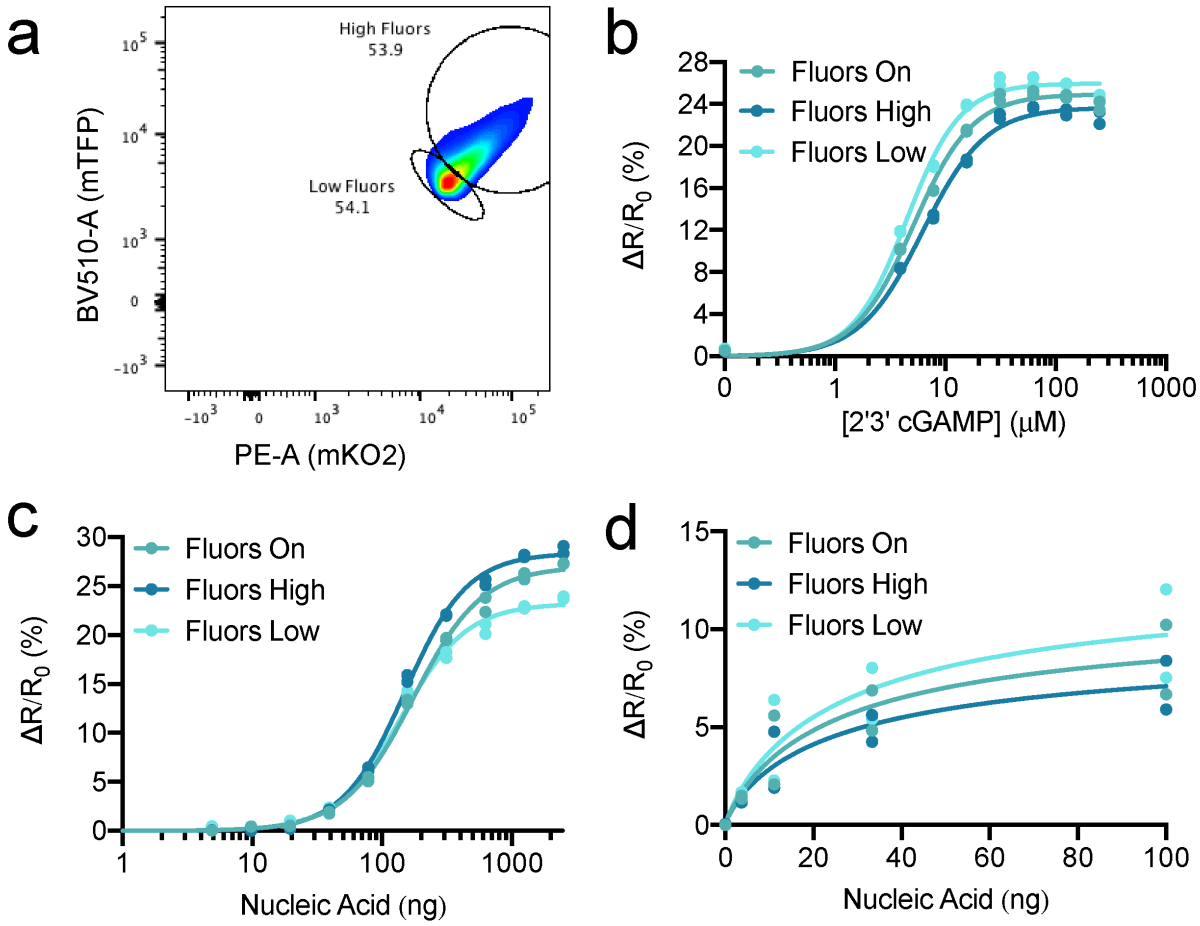

Figure 1.7: Effects of BioSTING expression levels on FRET responses.
(a) Representative flow plot demonstrating the gating method for separation of high and low BioSTING expressing populations. Cells were first analyzed as in Figure 3.5c and then separated as shown. This method was used to collect data for all figures in this panel. **(b)** Data from Figure 3.6d was reanalyzed to compare FRET responses from populations of cells expressing high and low levels of BioSTING **(c)** Data from Figure 3.10a was reanalyzed to compare FRET responses from populations of cells expressing high and low levels of BioSTING. **(d)** Data from Figure 3.10c was reanalyzed to compare FRET responses from populations of cells expressing high and low levels of BioSTING. In all panels, individual data points of n=2 biological replicates are shown.

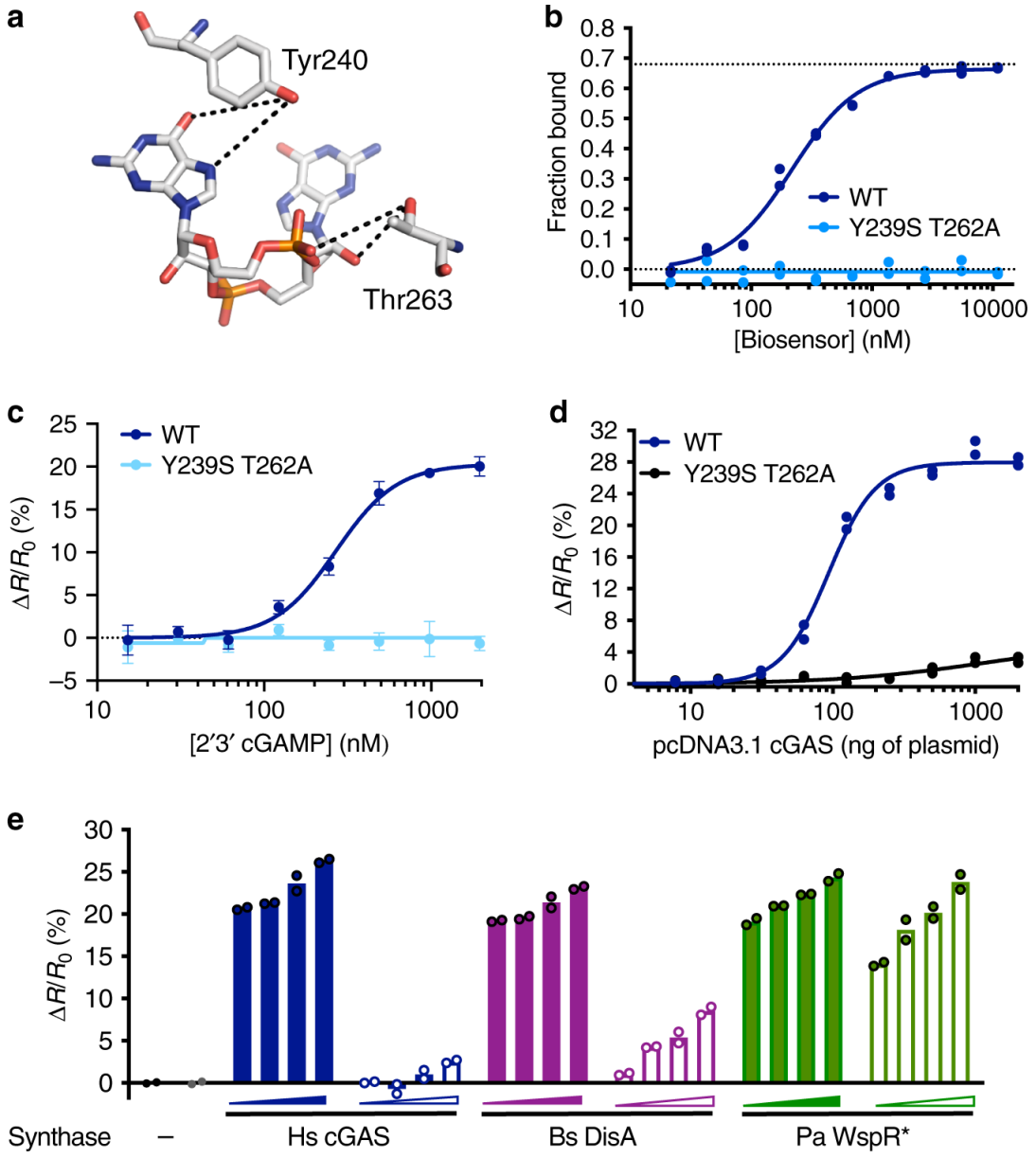

Figure 1.8: BioSTING variants exhibit distinct specificity for metazoan and bacterial CDNs. **(a)** Interactions made by human STING residues Y240 (mouse Y239) and T263 (mouse T262) hypothesized to stabilize CDN binding in PDB 4F5D visualized in PyMol. **(b)** DRaCALA binding analysis of WT and Y239S T262A BioSTING using [^{32}P] labeled 2′3′-cGAMP. **(c)** Recombinant WT and Y239S T262A BioSTING FRET response in the presence of increasing concentrations of 2′3′-cGAMP. Data are presented as mean ± s.d. of $n = 4$ biological replicates. **(d)** HEK293T cells stably expressing WT or Y239S T262A BioSTING were transfected with increasing concentrations of pCDNA3.1-cGAS and analyzed for FRET response by flow cytometry. **(e)** HEK293T cells stably expressing WT (solid bars) or Y239S T262A (open bars) BioSTING were transfected with increasing concentrations (125, 250, 500, or 1000 ng) of expression vectors for cGAS, DisA, WspR*, or empty vector and analyzed for FRET response by flow cytometry. Data in panels b, d and e are presented as individual data points of $n = 2$ biological replicates are shown.

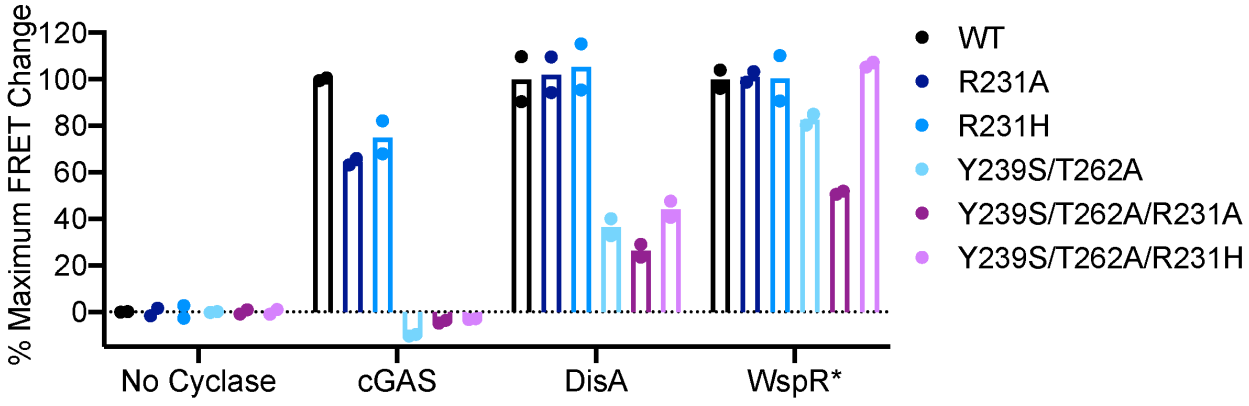

Figure 1.9: BioSTING R231 Mutations.

HEK293T cells stably expressing WT, R231A, R231H, Y239S/T262A, R231A/Y239S/T262A, or R231H/Y239S/T262A BioSTING were transfected with expression vectors for cGAS, DisA, WspR*, or empty vector and analyzed for FRET response by flow cytometry. Individual data points of n=2 biological replicates are shown.

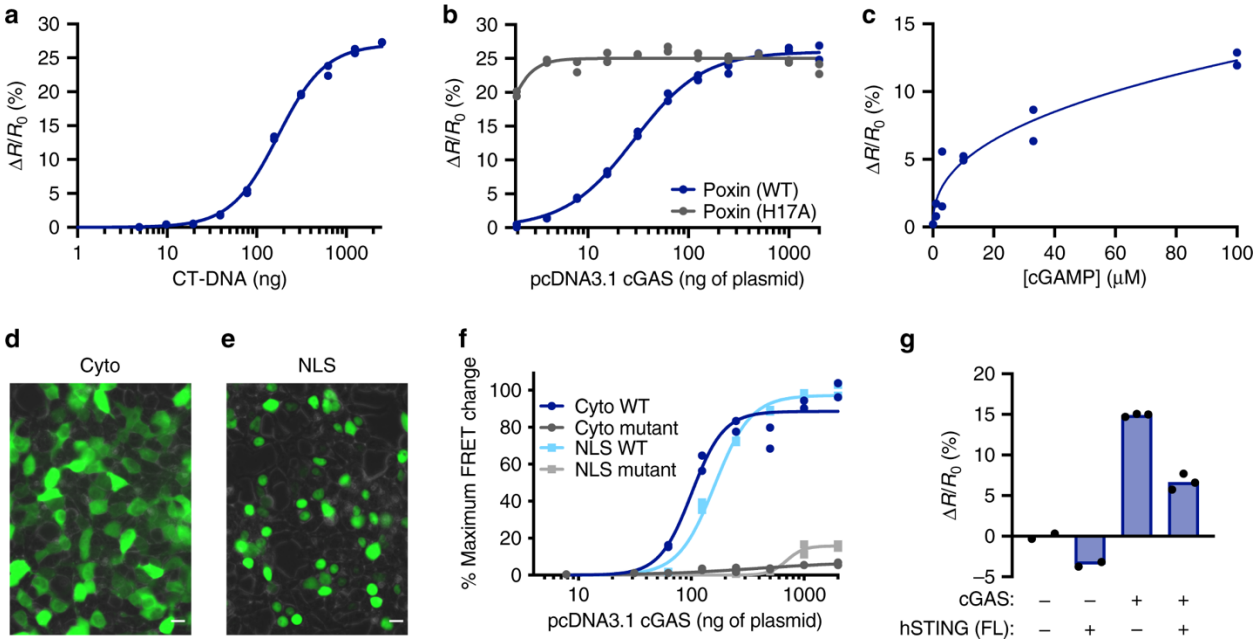

Figure 1.10: BioSTING exhibits broad utility for monitoring diverse aspects of cGAMP signaling.

(a) HEK293T cells stably expressing BioSTING were transfected with 10 ng of pCDNA3.1-cGAS for 16-20 h then transfected again with an increasing concentration of activating CT-DNA for 4 h and analyzed by flow cytometry. (**b)** HEK293T cells stably expressing BioSTING were transfected with 3 μg of WT or H17A Poxin and increasing concentrations of pCDNA3.1-cGAS and analyzed for FRET response by flow cytometry. (**c**) Increasing concentrations of 2′3′-cGAMP were added to the media of HEK293T cells stably expressing BioSTING for 6 h and analyzed for FRET response by flow cytometry. **(d–e)** BioSTING expression was induced in HEK293T cells transduced with pSLIK-BioSTING or pSLIK-NLS-BioSTING for 24 h by the addition of doxycycline and biosensor expression was analyzed using a BZ-X710 microscope (Keyence) using brightfield and a GFP filter cube (EX 470/40, DM 495, and BA 525/50) with a 40X objective. Scale bars, 15 μm. Data are representative of two independent experiments. (**f**) HEK293T cells stably expressing untagged or NLS-tagged WT or Y239S T262A BioSTING were transfected with increasing concentrations of pCDNA3.1-cGAS and analyzed for FRET response by flow cytometry. (**g**) HEK293T cells stably expressing untagged WT BioSTING were transfected with 100 ng of cGAS expression plasmid or empty vector alone with either 100 ng of empty vector or vector expressing full-length (FL) human STING and analyzed by flow cytometry. In all panels, individual data points of $n = 2$ (a–c, f–g) or $n = 3$ (g) biological replicates are shown.

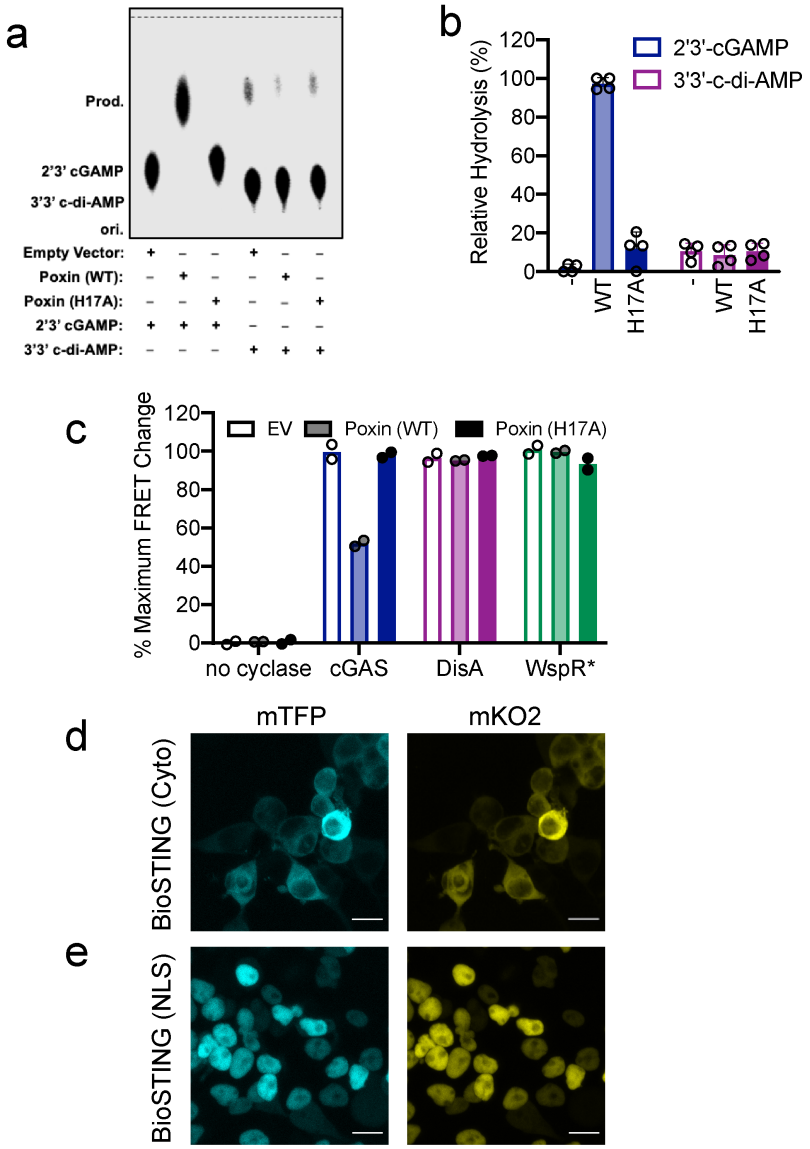

Figure 1.11: Poxin Activity Assays and BioSTING localization.

(a) TLC analysis of [^{32}P] labeled 2′3′-cGAMP and 3′3′-c-di-AMP degradation following 1h incubation in lysates from HEK293T cells transfected with 3 µg of empty vector or plasmid expressing wildtype (WT) or catalytically-dead (H17A) Poxin. Data are representative of four independent experiments. Relative hydrolysis from four biologically, independent samples is quantified on the right in panel (**b**). Data are presented as mean ± s.d. of n=4 biological replicates. (**c**) HEK293T cells stably expressing BioSTING were transfected with 3 µg of empty vector or plasmid expressing WT or H17A Poxin along with 40 ng of plasmid expressing cGAS, DisA, or WspR* and analyzed for FRET response by flow cytometry. Individual data points of n=2 biological replicates are shown. (**d-e**) BioSTING expression was induced in HEK293T cells transduced with pSLIK-BioSTING (d) or pSLIK-NLS-BioSTING (e) for 24 hours by the addition of doxycycline and biosensor expression was analyzed by confocal microscopy using a Leica SP8X confocal microscope (Leica). Scale bars, 15 µm. Data are representative of two independent experiments.

Table 1.1: BioSTING Parameters

BioSTING Parameters	
Kd (nM)	56
EC50 (nM)	77.4
L.O.D (nM)	12.6
L.O.Q. (nM)	38.2
Dynamic Range (nM)	12-125
ΔFRET Ratio (%)	~25

Table 1.2: Primers used in this study

Primer	Use	Sequence
1	Forward Amplify STING CTD no linker	GAGGAGACTAGTTTAAATGTTGCCCACGGGCTG
2	Reverse Amplify STING CTD no linker	GAGGAGGGTACCTTCCTGACGAATGTGCCGGAG
3	Forward Amplify STING CTD GGSGG linker	GAGGAGACTAGTGGCGGATCCGGGGGCTTAAATGTTGCCCACGGGCTG
4	Reverse Amplify STING CTD GGSGG linker	GAGGAGGGTACCGCCCCCGGATCCGCCTTCCTGACGAATGTGCCGGAG
5	Forward Y239S QuickChange	GGCATCAAGAATCGGGTTTCTTCCAACAGCGTCTACGAG
6	Reverse Y239S QuickChange	CTCGTAGACGCTGTTGGAAGAAACCCGATTCTTGATGCC
7	Forward T262A QuickChange	CTGTATCCTGGAGTACGCCGCCCCCTTGCAGACCC
8	Reverse T262A QuickChange	GGGTCTGCAAGGGGGCGGCGTACTCCAGGATACAG
9	Forward R231H QuickChange	CCCAGCAAAACATCGACCATGCTGGCATCAAGAATCGG
10	Reverse R231H QuickChange	CCGATTCTTGATGCCAGCATGGTCGATGTTTTGCTGGG
11	Forward R231A QuickChange	CCCCAGCAAAACATCGACGCTGCTGGCATCAAGAATCGG
12	Reverse R231A QuickChange	CCGATTCTTGATGCCAGCAGCGTCGATGTTTTGCTGGGG
13	Forward Amplify BioSTING for pSLIK	TGATCACTAGCGTACGACCATGGGCAGCAGCCATCATCATC
14	Reverse Amplify BioSTING for pSLIK	TCTTCCAATTCGTACGTCATCCGCCAAAACAGCCAAG
15	Reverse Amplify BioSTING for pSLIK with NLS tag	TCTTCCAATTCGTACGTCAGTCCAACTTGACCCTCTTGGCAGCAGGTCCGCCAAAACAGCCAAGC

Table 1.3: Plasmids used in this study

Number	Name	Use	Source
1	pET15b-mKO2-12AA-mTFP	Contained FRET fluorophores	Gift from Samuel Miller
2	pET15b-BioSTING	Bacterial expression vector	This study
3	pET15b-BioSTING (Y239S T262A)	Bacterial expression vector	This study
4	pSLIK-Empty Vector	Eukaryotic expression vector	Gift from Andrew Oberst
5	pSLIK-BioSTING	Eukaryotic expression vector	This study
6	pSLIK-BioSTING (R231A)	Eukaryotic expression vector	This study
7	pSLIK-BioSTING (R231H)	Eukaryotic expression vector	This study
8	pSLIK-BioSTING (Y239S T262A)	Eukaryotic expression vector	This study
9	pSLIK-BioSTING (R231A Y239S T262A)	Eukaryotic expression vector	This study
10	pSLIK-BioSTING (R231H Y239S T262A)	Eukaryotic expression vector	This study
11	pSLIK-NLS BioSTING	Expresses nuclear localized BioSTING	This study
12	pSLIK-NLS BioSTING (Y239S T262A)	Expresses nuclear localized BioSTING (Y239S T262A)	This study
13	pcDNA3-empty vector	Vector Control in Eukaryotic cells	Gift from Genhong Cheng
14	pcDNA3-cGAS	Expresses full-length human cGAS in Eukaryotic cells	Gift from Genhong Cheng
15	pcDNA4-DisA	Expresses DisA in Eukaryotic cells	Gift from Philip Kranzusch
16	pcDNA4-WspR*	Expresses WspR* in Eukaryotic cells	Gift from Philip Kranzusch
17	pcDNA4-Poxin (WT)	Expresses Poxin (WT) in Eukaryotic cells	Gift from Philip Kranzusch
18	pcDNA4-Poxin (H17A)	Expresses Poxin (H17A) in Eukaryotic cells	Gift from Philip Kranzusch
19	pcDNA3-hSTING (FL)	Expresses hSTING in Eukaryotic cells	Gift from Genhong Cheng
20	pSPEEDET-mRECON	Bacterial expression vector	[106]

21	pet28-mSTING-CTD	Bacterial expression vector	Gift from Russell Vance
22	pet20b-DisA	Bacterial expression vector	[103,104]
23	pET28a-His6-SUMO-mcGAS	Bacterial expression vector	Gift from Russell Vance

Chapter 2

A luminescence based coupled enzyme assay enables high throughput quantification of the bacterial second messenger 3′3′-cyclic-di-AMP

The majority of this chapter has been published in:

Zaver, S.A., Pollock, A. J., Boradia, V.M. & Woodward, J.J. A luminescence based coupled enzyme assay enables high throughput quantification of the bacterial second messenger 3′3′-cyclic-di-AMP. *ChemBioChem.* doi: 10.1002/cbic.202000667.

Summary

Cyclic dinucleotide signaling systems are found ubiquitously throughout nature allowing organisms to rapidly and dynamically sense and respond to alterations in their environments. In recent years, the secondary messenger, cyclic di-(3′,5′)-adenosine monophosphate (c-di-AMP), has been identified as an essential signaling molecule in a diverse array of bacterial genera. We and others have shown that defects in c-di-AMP homeostasis result in severe physiological defects and virulence attenuation in many bacterial species. Despite significant advancements in the field, there is still a major gap in the understanding of the environmental and cellular factors that influence c-di-AMP dynamics due to a lack of tools to sensitively and rapidly monitor changes in c-di-AMP levels. To address this limitation, we describe in this chapter the development of a luciferase-based coupled enzyme assay that leverages the cyclic nucleotide phosphodiesterase, CnpB, for the sensitive and high throughput quantification of 3′3′-c-di-AMP. We also demonstrate the utility of this approach for the quantification of the cyclic oligonucleotide-based anti-phage signaling system (CBASS) effector, 3′3′-cGAMP. These findings establish CDA-Luc as a more affordable and sensitive alternative to conventional c-di-AMP detection tools with broad utility for the study of bacterial cyclic dinucleotide physiology.

Introduction

Cyclic dinucleotide (CDN) second messengers have emerged as conserved signaling molecules across all domains of life. In response to altered environmental cues, CDN levels dynamically fluctuate through regulated synthesis by cyclic dinucleotide synthases and degradation by phosphodiesterases (PDEs)[71,72]. In bacteria, cyclic dinucleotides regulate a myriad of biological processes including central metabolism, cell wall homeostasis, osmoregulation, biofilm formation, motility, virulence and anti-phage immunity by modulating the activity of a diverse suite of protein and riboswitch effectors, which collectively coordinate a cellular response[71-82]. Additionally, bacterial cyclic dinucleotides have also been shown to interface with receptors of the metazoan innate immune system where they activate pro-inflammatory cytokine and autophagy pathways to sterilize the host of offending microorganisms[83-89].

Among these nucleotide small molecules, cyclic di-(3′,5′)-adenosine monophosphate (3′3′-c-di-AMP, c-di-AMP or CDA) has been shown to play an essential role in regulating the lifestyles of a diverse range of clinically significant bacterial genera[80,90]. Within these bacterial species, cyclic di-AMP production is mediated by a conserved family of diadenylate cyclase (DAC) domain containing proteins, of which, five classes have been characterized to date[80]. Degradation of CDA is catalyzed by dedicated phosphodiesterase enzymes, which fall into two major classes: DHH-DHHA1 (aspartate-histidine-histidine) domain or HD (histidine-aspartate) domain containing proteins[80,91]. Although the mechanisms of CDA synthesis and degradation are quite conserved, the arsenal of c-di-AMP receptors appears to vary among bacterial species[80]. This may allow the output of c-di-AMP signaling systems to be tailored to the individual needs of specific bacteria.

Despite significant advancements in the understanding of the components of bacterial c-di-AMP signaling networks, a detailed understanding of the environmental and cellular cues that regulate CDA homeostasis are lacking. A few studies have attempted to answer this question, mostly through the use of genetic approaches[74,78,79,92,93]. These studies revealed a role for potassium and

glutamate availability in the regulation of c-di-AMP synthesis, underscoring the importance of this molecule in maintaining osmotic balance[78,79,93]. Additionally, both DHH-DHHA1-type and HD-type phosphodiesterases have been shown to be inhibited by the alarmone (p)ppGpp, suggesting a link between amino acid starvation and cyclic di-AMP signaling[91,94]. Nevertheless, understanding of c-di-AMP regulation is still rudimentary and high-throughput, unbiased genetic and phenotypic screens to identify the factors that regulate CDA dynamics have not been performed.

Such studies are currently intractable due to the lack of tools to sensitively, affordably and rapidly quantify c-di-AMP levels. A sensitive liquid chromatography mass-spectrometry (LC-MS) based assay for CDA detection and quantification was previously described; however, mass-spectrometry based approaches are low throughput and require technical knowledge as well as access to expensive machinery[83,91]. RNA-aptamer based biosensors for c-di-AMP as well as other CDNs have been developed; unfortunately, these sensors typically have low affinities for their cognate CDNs (~3-30 μM for c-di-AMP)[95.] More recently, commercial enzyme immunoassays (EIAs) have become available for the quantification of several cyclic dinucleotide species. While these assays have reasonable throughput, they can be quite costly and have narrow dynamic ranges, which limits their utility in high-throughput screening campaigns. To address these limitations, we describe the development of a luciferase-based coupled-enzyme assay termed CDA-Luc to quantify 3′3′-c-di-AMP. This assay can be paired with conventional ATP detection assays to sensitively and affordably quantify c-di-AMP over a broad dynamic range and is likely to enable fundamental discoveries relating to c-di-AMP physiology.

Results

Selection of a suitable 3′3′-c-di-AMP phosphodiesterase

Recently, a luciferase based coupled enzyme assay for quantification of the metazoan CDN 2′3′-cGAMP (cGAMP-Luc) was described[108]. This assay takes advantage of the mammalian phosphodiesterase ectonucleotide pyrophosphatase (ENPP1), which hydrolyzes 2′3′-cGAMP to GMP and AMP. Following cleavage, AMP is subsequently phosphorylated to ADP by the enzyme polyphosphate:AMP phosphotransferase (PAP). Next, the enzyme myokinase is utilized to phosphorylate ADP to ATP. Finally, the ATP produced by the coupled-enzyme assay can be quantified using a conventional ATP detection kit. We hypothesized that a similar approach could be utilized to develop a sensitive assay to quantitate 3′3′-c-di-AMP. Several classes of CDA phosphodiesterase have been identified to date; however, many of these enzymes are incompatible with this approach as they linearize c-di-AMP to 5′-pApA rather than separating the two fused nucleotides. In addition, many of these enzymes are integral membrane proteins, making them challenging to work with and difficult to produce in large quantities (Figure 2.1)[80]. Fortunately, a small group of soluble, AMP-producing CDA phosphodiesterases have been identified, of which the *Mycobacterium tuberculosis* PDE, cyclic nucleotide phosphodiesterase B (CnpB), has been best characterized[97-102]. Thus, we hypothesized that Mtb CnpB would be an optimal candidate for a coupled enzyme-based c-di-AMP quantification assay.

Optimization of CnpB hydrolytic activity

We began by optimizing the *in vitro* reaction conditions in order to maximize CnpB hydrolytic activity. Recombinant hexahistidine-tagged CnpB was produced in *E. coli* and purified to apparent homogeneity in a single-step using Ni^{2+} affinity chromatography (Figure 2.2a). We next monitored the activity of CnpB towards bis-*p*-nitrophenyl phosphate (BNPP) a non-specific, colorimetric reporter substrate for phosphatase and phosphodiesterase enzymes. Consistent with previous reports, we observed no enzymatic activity in the absence of added metal cations (Figure 2.2b, c)[97-100]. We next tested CnpB activity against a panel of divalent metal ions. Among this array, CnpB activity was highest in the presence of Mn^{2+} and completely absent in the presence of Mg^{2+} (Figure 2.2b, c). Minor activity was observed with other metal cations including Co^{2+}; however, as Mn^{2+} resulted in the highest activity, it was selected for all future assays. As some metal ions have been shown to interfere with downstream steps in the AMP detection assay, we next titrated $MnCl_2$ in order to determine the minimal concentration required for full CnpB activity[96]. Based on these assays, we concluded that a minimum concentration of approximately 30 μM $MnCl_2$ is required for optimal activity (Figure 2.2d). Finally, as phosphodiesterase activity is highly sensitive to pH, CnpB activity was monitored across a pH gradient (Figure 2.2e). Consistent with previous reports, CnpB activity was highest at alkaline pH with a pH optimum of approximately 8.5 (Figure 2.2e)[97-100]. Taken together, a buffer formulation of [Tris-Cl pH 8.5, 0.1 mM MnCl2, 100 mM NaCl] was selected for all future assays.

Analysis of CnpB 3′3′-c-di-AMP binding and hydrolysis

Having optimized the activity of CnpB using the mock-substrate BNPP, we next sought to directly monitor CnpB hydrolytic activity against 3′3′-c-di-AMP under these assay conditions. To that end, [^{32}P]-labeled 3′3′-c-di-AMP was enzymatically synthesized and affinity purified to near homogeneity (Figure 2.3a). CnpB binding to 3′3′-c-di-AMP was confirmed by differential radial capillary action of ligand assay (DRaCALA). As a positive control, the mammalian c-di-AMP binding protein reductase controlling NF-κb (RECON) was employed, yielding a Kd of 68 nM[84]. In the absence of $MnCl_2$, binding of 3′3′-c-di-AMP to CnpB was weak and non-saturating with a Kd > 17 μM (Figure 2.3b). Interestingly, addition of $MnCl_2$ to the binding buffer appeared to enhance the affinity of CnpB towards CDA by five-fold with a Kd of approximately 3 μM (Figure 2.3b). These results were in agreement with the previously reported low micromolar Km of CnpB for 3′3′-c-di-AMP[97-100]. Additionally, these results support a role for Mn^{2+} in enhancing substrate binding in addition to increasing catalytic activity.

We next monitored the hydrolytic activity of CnpB by thin layer chromatography (TLC) analysis. We began by testing whether CnpB could cleave nanomolar concentrations of 3′3′-c-di-AMP to AMP, its previously reported product. Trace concentrations (~1 nM) of [^{32}P] labeled c-di-AMP were incubated with CnpB in the presence and absence of $MnCl_2$. After 2 hours, we observed complete hydrolysis of c-di-AMP to a product that migrated slightly slower than the [α-^{32}P] ATP standard (Figure 2.3c). Interestingly, we also observed complete hydrolysis of CDA in the absence of $MnCl_2$ under these assay conditions, perhaps because only trace quantities of substrate were used (Figure 2.3c). Addition of alkaline phosphatase completely converted the CnpB product to inorganic phosphate confirming that AMP and not 5′-pApA is indeed the reaction product (Figure 2.3c). Finally, in order for this approach to be suitable for quantification of 3′3′-c-di-AMP, CnpB

must also be capable of completely hydrolyzing low micromolar concentrations of CDA. To test this, we incubated CnpB with 1 μM 3′3′-c-di-AMP spiked with 1 nM [^{32}P] labeled c-di-AMP. After 24 hours, we observed complete hydrolysis of c-di-AMP to AMP with minimal degradation of AMP to adenosine and free inorganic phosphate (Figure 2.3d). Taken together, these data show that CnpB is capable of completely converting low nanomolar to low micromolar concentrations of CDA to AMP and suggest that this could be a viable approach for a c-di-AMP quantification assay.

Coupling of CnpB with commercially available AMP detection assays

Over the years, several commercial AMP detection assays have been formulated. Of these, the AMP-GloTM assay is one of the most commonly used. In the first reaction, AMP is converted to ADP by the enzyme PAP using polyphosphate as a substrate. In the next and final step, myokinase is coupled to luciferase. Thus, as ATP is produced by myokinase, it is subsequently utilized by luciferase to oxidize the luciferin substrate producing a luminescence signal (Figure 2.4a)[96]. Luciferase activity is proportional to the amount of ATP in the sample, enabling quantification. Thus, we began by coupling CnpB to the commercially available AMP-Glo™ assay. Promisingly, we were able to detect AMP produced by CnpB using this assay; however, consistent with previous findings, luciferase activity was not linear when plotted on a standard linear-linear plot greatly limiting the quantitative capabilities of this approach (Figure 2.4b)[96]. We observed similar non-linearity using purified AMP as the substrate suggesting that this problem is inherent to the assay itself and not the CnpB digestion step (Figure 2.4c). Interestingly, re-analysis of the data using a log-log plot resulted in a much more linear standard curve for both 3′3′-c-di-AMP and AMP with quantification limits of approximately 7.8 nM (Figure 2.5a, b). In contrast, commercially available luciferase-based ATP detection kits displayed linear standard curves under both analysis methods (Figures 2.4d, e and 2.5c, d). These results suggest that it is indeed possible to sensitively quantify 3′3′-c-di-AMP using commercially available AMP detection kits with this alternative analysis method; however, the high costs associated with these kits greatly diminishes their utility for high throughput screening campaigns.

Development of CDA-Luciferase (CDA-Luc) Assay

Recently, a revised method for AMP-detection, termed AMP-Luc, was described and successfully employed for quantification of 2′3′-cGAMP[96]. Here, the reaction components remained the same as in the AMP-GloTM assay, but the coupled steps in the assay were rearranged to allow complete conversion of AMP to ATP prior to ATP detection using a conventional luciferase-based ATP detection kit (Figure 2.6a). This is accomplished by coupling myokinase to PAP instead of luciferase as in the conventional assay. Second, the PAP and myokinase coupled step is allowed to proceed longer (up to three hours) to ensure complete conversion of the AMP to ATP. Simply, rearranging the steps in the assay in this way was shown to dramatically improve the quantitative capabilities of the assay. Encouraged by these findings, we hypothesized that we could couple CnpB with AMP-Luc to generate a robust and affordable method for 3′3′-c-di-AMP quantification. To that end, the enzyme PAP was expressed in *E. coli* and purified to near homogeneity using a single Ni^{2+} affinity purification step (Figure 2.6b and 2.7a). The activity of the purified PAP was confirmed by coupling the enzyme to commercially available myokinase and monitoring ATP production using the Kinase Glo® assay (Figure 2.6c). We next tested the ability of AMP-Luc to

detect CnpB-digested 3′3′-c-di-AMP. Incubation of 3′3′-c-di-AMP with CnpB followed by detection with AMP-Luc resulted in a robust luciferase response that was abolished in the absence of either CDA or CnpB (Figure 2.6d). Notably, the resulting luminescence signal was stable for at least one hour after addition of the Kinase Glo® reagent, allowing for flexibility in assay design (Figure 2.7b). Thus, these data suggest that the reconfigured AMP-Luc assay could be used to detect 3′3′-c-di-AMP using CnpB.

We next examined the ability of this assay to quantify AMP. As expected, the AMP-Luc assay yielded a robust standard curve for both AMP and 3′3-c-di-AMP with quantification limits of 31.2 or 7.8 nM, depending on the analysis method (linear-linear vs log-log) (Figure 2.6e, f and 2.7c, d). Next, we compared the standard curve of 3′3′-c-di-AMP generated using CDA-Luc to the standard curve of pure ATP using Kinase-Glo®. This yielded largely overlapping standard curves with low nanomolar limits of quantification, suggesting that there is no further room for optimization of the CDA-Luc assay (Figure 2.8a). Taken together, these data suggest that this approach is robustly quantitative for 3′3′-c-di-AMP. To be consistent with the nomenclature of preceding literature, we named this assay CDA-Luc[96].

Having optimized the CDA-Luc assay, we next sought to further characterize the limitations of the assay. As this assay relies on ATP-mediated oxidation of luciferin, we hypothesized that there would be an upper limit for c-di-AMP quantification based on the availability of luciferin substrate. To that end, we performed an extended c-di-AMP titration which yielded a standard curve that was linear up to 5 μM (Figure 2.8b). CDA concentrations greater than 5 μM resulted in a departure from linearity. Because each cleaved c-di-AMP molecule yields two AMP molecules, these results were consistent with the 10 μM specification for ATP quantification by the Kinase Glo® reagent.

In addition to cleaving 3′3′-c-di-AMP, CnpB has also been shown to possess some hydrolytic activity towards 3′3′-c-di-GMP, albeit with markedly reduced affinity[96-99]. Many c-di-AMP producing bacteria also encode catalytic machinery for the production and degradation of c-di-GMP. Thus, we wanted to make sure that any GMP produced by hydrolysis of CDG would not interfere with CDA quantification by the CDA-Luc assay. To that end, we generated CDA standard curves in the presence and absence of a fixed (1 μM) concentration of GMP. This yielded overlapping standard curves with similar limits of quantification (Figure 2.8c). Thus, although CnpB is capable of degrading c-di-GMP, its product GMP will not interfere with c-di-AMP quantification by the CDA-Luc assay.

Finally, we wanted to determine whether the CDA-Luc assay could successfully be employed under different buffer conditions. To do this, we previously described chemically defined minimal media for growth of *Listeria monocytogenes*[83-91]. Growth of *L. monocytogenes* in this medium enabled the identification of 3′3′-c-di-AMP by mass spectrometry analysis and has since been used by our lab and others to monitor the regulation of c-di-AMP homeostasis[83,91,92]. Thus, known concentrations of 3′3′-c-di-AMP were titrated into *L. monocytogenes* minimal media supplemented with streptomycin and subjected to digestion with CnpB followed by quantification by AMP-Luc. We observed robust linearity of the CDA-Luc assay in chemically defined media with a quantification limit of 7.8 nM, similar to the standard assay (Figure 2.9a, b). In contrast, conditioned, defined minimal media from Δ*dacA*Δ*oppA L. monocytogenes* deficient for endogenous c-di-AMP synthesis demonstrated only minor luminescence differences upon titration

of pure 3′3′-c-di-AMP suggesting the presence of interferents in the sample (Figure 2.9c). We also tested the performance of CDA-Luc in a commonly used lysis buffer, RIPA buffer. This yielded a mostly linear standard curve with a reduced quantification limit of approximately 62.5 nM, likely due to the presence of detergents in the lysis buffer (Figure 2.9d). These results suggest that CDA-Luc can be employed under a variety of buffer conditions but that interferents can be present in complex biological samples.

RECON enables affinity purification of c-di-AMP from biological samples in a manner compatible with CDA-Luc quantification

Although CDA-Luc is capable of monitoring c-di-AMP levels in chemically defined buffers, quantification of c-di-AMP from complex biological samples is hindered by biological interferents and large quantities of AMP, ADP, and ATP (ANPs), which would interfere with the CDA-Luc assay. We and others have previously utilized CDN binding proteins for the purification of cyclic dinucleotides from complex mixtures[75,84,96,103,104]. Most bacterial and host c-di-AMP binding proteins have low micromolar affinities for CDA, limiting their utility for affinity purification as large quantities of recombinant protein would be required[75,80,87,89]. We recently identified a host 3′3′-c-di-AMP binding protein, RECON, with high affinity for c-di-AMP (Kd of 68 nM) (Figure 2.3b)[84]. We have also previously utilized RECON affinity purification (RECAP) to specifically capture [32P] labeled c-di-AMP from crude reaction mixtures containing ANPs and free inorganic phosphates (Figures 2.3a and 2.10a, b)[103,104]. Thus, we hypothesized that RECON could be employed as an upstream step to purify 3′3′-c-di-AMP prior to quantification using the CDA-Luc assay.

Recombinant hexahistidine-tagged RECON was immobilized onto NiNTA agarose beads and incubated with samples containing known concentrations of 3′3′-c-di-AMP. Following washing, the RECON-CDA complexes were eluted from the beads using imidazole. The resulting supernatant was then boiled to remove the bound c-di-AMP, which was then quantified using CDA-Luc. Quantification of RECON-purified CDA by CDA-Luc resulted in a linear standard curve with a quantification limit of approximately 31.2 nM and a detection limit of 1.2 nM (Figure 2.10c). We hypothesize that the quantification limit could be improved further by reducing the volume of elution buffer. We performed a similar analysis using c-di-AMP dissolved in *L. monocytogenes* chemically defined media. This approach yielded a standard curve with a quantification limit of 39 nM and a dynamic range of 5 nM – 5 μM (Figure 2.10d). We next sought to determine whether RECAP is able to extract c-di-AMP away from interferents generated from biological samples. Implementing RECAP on conditioned media doped with known concentrations of 3′3′-c-di-AMP as in figure 2.9c allowed for high fidelity recovery and detection of c-di-AMP (Figure 2.10e). Thus, RECAP allows for c-di-AMP quantification in a wide array of samples, even when interferents which disrupt the CDA-Luc assay are present.

Having established the utility of RECON affinity purification for CDA quantification, we next sought to monitor the intracellular and secreted levels of c-di-AMP from various *L. monocytogenes* strains with altered levels of c-di-AMP production, degradation, and/or secretion. As expected, we observed no c-di-AMP in a *L.m.* strain deficient for CDA production (Δ*dacA*Δ*oppA*) (Figure 2.10f, g). Consistent with our previous findings, deficiency of both CDA phosphodiesterases (Δ*pgpH*Δ*pdeA*) resulted in an approximately four-fold enhancement in both the intracellular and

extracellular levels of c-di-AMP as compared to the wildtype (WT) strain (Figure 2.10f, g)[91]. Finally, depletion of TetR (*tetR::Tn917*), a negative regulator of multidrug resistant transporters that export c-di-AMP, augmented the levels of c-di-AMP secreted into the bacterial growth medium (Figure 2.10f, g). Interestingly, depletion of TetR did not affect intracellular levels of 3′3′-c-di-AMP. We believe that this is due to compensation for enhanced export by increased production and/or decreased degradation of CDA. Taken together, these data demonstrate that pairing of RECON affinity purification (RECAP) with the CDA-Luc assay can enable detection of c-di-AMP from complex biological samples.

Comparison of CDA-Luc to LC-MS

Having optimized and established the utility of CDA-Luc for quantification of 3′3′-c-di-AMP, we next wanted to compare it to the established gold standard for c-di-AMP quantification, LC-MS. To that end, we generated standard curves of known concentrations of c-di-AMP doped with an isotopically labeled internal standard and subjected them to LC-MS analysis. This yielded a robustly linear standard curve with a quantification limit of 50 nM and a dynamic range from 5 nM – 5 μM (Figure 2.11a, c). Consistent with our previous results, CDA-Luc performed similarly with a limit of quantification of 39 nM (Figure 2.11b, c). Collectively, these data establish CDA-Luc as a high throughput and affordable alternative to LC-MS based quantification of 3′3′-c-di-AMP without loss of sensitivity.

Quantification of 3′3′-cGAMP using CDA-Luc

Recently, cyclic oligonucleotides have been shown to play an important signaling role in bacterial, innate anti-phage immunity. In this context, cyclic oligonucleotide second messengers are synthesized by cGAS/DncV-like nucleotidyltransferases (CD-NTases) upon infection with bacteriophage[72,81,82]. The resulting second messenger then activates a cognate effector protein culminating in abortive phage infection through the death of the infected cell, thereby protecting the greater bacterial community[72,81,82]. Among the cyclic oligonucleotide-based anti-phage signaling systems (CBASS), 3′3′-cGAMP synthesized by DncV has been the most well studied; nevertheless, the mechanisms that trigger 3′3′-cGAMP production remain poorly elucidated. Such studies would benefit from sensitive and affordable quantification tools. Interestingly, CnpB has been shown to possess hydrolytic activity against 3′3′-cGAMP[99]. Thus, we hypothesized that the CnpB-based CDA-Luc assay could also be utilized to quantify 3′3′-cGAMP. To that end, we first confirmed that CnpB could utilize 3′3′-cGAMP using a competitive BNPP hydrolysis assay. CnpB was incubated with BNPP in the presence of increasing concentrations of 3′3′-cGAMP and production of *p*-nitrophenol was monitored (Figure 2.12a). Consistently, we observed a dose-dependent decrease in the rate of BNPP hydrolysis in the presence of 3′3′-cGAMP (Figure 2.12a). Having confirmed utilization of 3′3′-cGAMP by CnpB, we next tested the ability of the CDA-Luc assay to quantify purified 3′3′-cGAMP. This analysis yielded a linear standard curve with a quantification limit of 62.5 nM and a detection limit of approximately 3 nM, in line with the limits of the ENPP1-based cGAMP-Luc assay (Figure 2.12b)[96]. Taken together, these data demonstrate the utility of CDA-Luc for the quantification of the CBASS second messenger 3′3′-cGAMP.

Concluding Remarks

In this study, we have developed a robustly quantitative, high throughput luminescence-based c-di-AMP detection method. We show that the unique ability of the *M. tuberculosis* phosphodiesterase CnpB to cleave CDA to AMP can be leveraged for the design of a highly sensitive and precise c-di-AMP quantification assay. CnpB can easily be paired with commercially available AMP detection kits to yield a moderately quantitative c-di-AMP detection method; however, rearrangement of the coupled steps greatly improved the quantitative capabilities of the assay yielding a dynamic range spanning four orders of magnitude while maintaining the general accessibility of this approach. We also show that the high affinity mammalian c-di-AMP binding protein, RECON, can be leveraged to purify c-di-AMP from complex biological mixtures, allowing this method to be used in diverse investigations. Thus, we anticipate that CDA-Luc can be readily employed to replace mass-spectrometry based measurements of c-di-AMP.

Over the last decade, cyclic di-AMP has emerged as a widespread secondary messenger among both environmental and pathogenic microbes[74-77,80]. In bacteria, c-di-AMP has been shown to regulate a number of diverse processes including central metabolism, cell wall homeostasis, osmoregulation, genome integrity, antibiotic resistance, biofilm formation, sporulation, and virulence[73-80,93]. These pleiotropic functions of cyclic di-AMP are mediated by a diverse suite of protein and ribonucleotide effectors. Because of these critical functions, c-di-AMP is unique amongst all other cyclic dinucleotides as it is both essential for many bacterial species as well as toxic at elevated concentrations; however, the molecular mechanisms involved in regulation of c-di-AMP synthesis and degradation are still poorly understood[80,90].

Several classes of cyclic di-AMP synthases have been identified to date with the DacA or CdaA family of diadenylate cyclases being the largest[80]. Structurally DacA consists of an N-terminal transmembrane domain and a catalytic C-terminal DAC domain. In many bacterial species, DacA is encoded in a three gene operon consisting of an extracytoplasmic regulatory protein, CdaR or YbbR, and the phosphoglucosamine mutase, GlmM, an enzyme involved in peptidoglycan biosynthesis, both of which have been shown to modulate the activity of DacA—providing evidence for crosstalk between cell wall biosynthesis and c-di-AMP signaling networks[80,104,105]. In addition to synthesis, degradation of c-di-AMP must be dynamically regulated in order to allow bacteria to sense and respond to alterations in their environment. In *L. monocytogenes*, two phosphodiesterases that cleave c-di-AMP to the linear dinucleotide pApA have been identified, PdeA and PgpH[73,91]. Structurally, PdeA is comprised of a membrane spanning N-terminus followed by a PAS domain, GGDEF domain, and catalytically active DHH-DHHA1 domain[73]. PgpH consists of an N-terminal extracellular domain followed by a seven-pass transmembrane domain reminiscent of G-protein coupled receptors and a C-terminal catalytic HD domain[91]. While these enzymes have somewhat redundant functions, biochemical studies revealed that PdeA is the dominant c-di-AMP hydrolase during intracellular bacterial growth; whereas, PgpH is the dominant hydrolase during broth culture[91]. It is likely that these enzymes, through their regulatory domains, respond to specific environmental or cellular cues as *L. monocytogenes* transitions from its environmental, saprophytic lifestyle to its pathogenic lifecycle. Thus, a detailed understanding of the factors that regulate c-di-AMP dynamics is of fundamental importance to the field.

Development of the first sensitive, high throughput c-di-AMP quantification tool will make these fundamental lines of inquiry tractable. We expect that pairing unbiased genomic and chemical screens with CDA-Luc measurements will uncover the key cellular and environmental factors that regulate c-di-AMP dynamics during infection and environmental growth. As cyclic di-AMP is both essential and toxic, high throughput drug screens using CDA-Luc to identify compounds that either target c-di-AMP cyclases or phosphodiesterases would have promising potential for the development of novel antimicrobial agents. Because CDA is also a potent inducer of host innate immune responses, PDE inhibitors could be especially promising as they would induce bacterial cell death while simultaneously boosting host, antibacterial inflammatory responses. Additionally, we also provide evidence that CDA-Luc can be used for the quantification of other bacterial CDN species, namely 3′3′-cGAMP. Although not tested here, we also expect that CDA-Luc could be used to quantify other AMP-containing 3′3′-CDNs including 3′3′-cUAMP. We anticipate that this will make CDA-Luc not only useful to the study of c-di-AMP signaling but also the newly discovered CBASS field. One caveat to CDA-Luc based measurements is that this approach, like mass-spectrometry and EIA, only allows population level measurements of c-di-AMP at a single time point following destruction of the biological sample. Thus, there is still a need for the development of reversible, continuous, single cell methods for in vivo quantification of c-di-AMP. Nevertheless, we anticipate that CDA-Luc will facilitate fundamental discoveries relating to c-di-AMP dynamics and physiology for years to come.

Materials and Methods

Materials

ATP, [α-^{32}P], 3000Ci/mmol 10mCi/ml, 250 µCi was obtained from PerkinElmer (cat. no. BLU003H250UC). 3′3′-c-di-AMP and 3′3′-cGAMP were obtained from Invivogen (cat. no. tlrl-nacda and cat. no. tlrl-nacga, respectively). AMP-Glo™ (cat. no. V5011), Cell Titer Glo® (cat. no. G7570), and Kinase Glo® (cat. no. V6712) reagents were obtained from Promega Corporation. Sodium Hexametaphosphate (polyphosphate) was obtained from Sigma-Aldrich (cat. no. 71600). Myokinase from rabbit muscle was obtained from Sigma-Aldrich (cat. no. M3003). RIPA buffer was purchased from ThermoFisher Scientific (cat. no. 89900).

Cloning

M. tuberculosis CnpB gene (Rv2837c) was amplified by PCR from Mtb H37Rv genomic DNA using the forward primer 5′-GAAATACCATATGACGACGATCGACCCAAGG and reverse primer 5′-GAATATCAAGCTTCTAACCAAGCGCCGCGC. The resulting PCR product was cloned into the NdeI /HindIII site of pET28b vector to generate an N-terminal His-tagged polypeptide. The resulting CnpB expression vector was confirmed by sequencing using the T7 and T7 Term universal primers (GENEWIZ).

Codon optimized PAP gene from *A. johnsonii* 210A (GenBank accession no. AB092983) was chemically synthesized (Integrated DNA Technologies). The gBlock™ was then PCR amplified using the forward primer 5′-GAGGAGCATATGGATACAGAGACTATCGCAAGTGC and reverse primer 5′-GAGGAGAAGCTTATCAGTGTCGCGGTCGGC. The resulting PCR product was cloned into the NdeI/HindIII site of pET20b vector to generate a C-terminal His-tagged polypeptide. The resulting PAP expression vector was confirmed by sequencing using the T7 and T7 Term universal primers (GENEWIZ).

Protein Expression and Purification

For expression of Mtb CnpB, plasmid encoding CnpB was transformed into LOBSTR (low background strain) BL21 (DE3) chemically competent *E. coli*. Overnight cultures of the resulting bacterial strains were used to inoculate 1.5 L of LB broth at a 1:100 dilution. Bacterial cultures were grown to OD_{600} 0.6 at 37°C. The cultures were then cooled down to room temperature and protein expression was induced by the addition of 0.5 mM isopropyl β-D-1-thiogalactopyranoside (IPTG) for 18 hours at 16°C. Bacteria were harvested by centrifugation at 9000 x g for 5 minutes, and the cell pellets were resuspending into 30 mL of Buffer A [50 mM Tris pH = 8.0, 500 mM NaCl, 20 mM Imidazole, 5 mM β-Mercaptoethanol (BME), and 1 mM phenylmethylsulfonyl fluoride (PMSF)] and cooled on ice for 30 minutes. Bacteria were lysed by sonication on ice and clarified by centrifugation at 40,000 x g for 30 minutes at 4°C. The resulting clarified lysate was bound to HisPur NiNTA Resin (Thermo Scientific). The resin was washed with 100 column volumes of buffer A and bound proteins were eluted in Buffer B [50 mM Tris-Cl pH = 8.0, 500 mM NaCl, 300 mM Imidazole, 5 mM β-Mercaptoethanol (BME), and 1 mM phenylmethylsulfonyl fluoride (PMSF)]. Eluates were assessed for purity by SDS-PAGE analysis. Proteins were concentrated using Vivaspin 6 (5000 MWCO) centrifugal concentrators and then buffer exchanged

into storage buffer [50 mM Tris-Cl pH = 8.5, 100 mM NaCl] using PD-10 desalting columns (GE Healthcare). The desalted proteins were concentrated again using Vivaspin 6 (5000 MWCO) centrifugal concentrators, supplemented with glycerol (25%), snap frozen using liquid nitrogen, and stored at -80°C until use.

For expression of PAP, plasmid encoding PAP was transformed into LOBSTR (low background strain) BL21 (DE3) chemically competent *E. coli*. Overnight cultures of the resulting bacterial strains were used to inoculate 1.5 L of LB broth at a 1:100 dilution. Bacterial cultures were grown to OD_{600} 0.4 at 37°C. The cultures were then cooled down to room temperature and protein expression was induced by the addition of 0.5 mM isopropyl β-D-1-thiogalactopyranoside (IPTG) for 18 hours at 16°C. Bacteria were harvested by centrifugation at 9000 x g for 5 minutes, and the cell pellets were resuspending into 30 mL of Buffer A [50 mM Tris pH = 8.0, 500 mM NaCl, 20 mM Imidazole, 5 mM β-Mercaptoethanol (BME), and 1 mM phenylmethylsulfonyl fluoride (PMSF)] supplemented with 0.2 mg mL-1 Lysozyme and cooled on ice for 30 minutes. Bacteria were lysed by sonication on ice and clarified by centrifugation at 40,000 x g for 30 minutes at 4°C. The resulting clarified lysate was bound to HisPur NiNTA Resin (Thermo Scientific). The resin was washed with 100 column volumes of buffer A and bound proteins were eluted in Buffer B [50 mM Tris-Cl pH = 8.0, 500 mM NaCl, 300 mM Imidazole, 5 mM β-Mercaptoethanol (BME), and 1 mM phenylmethylsulfonyl fluoride (PMSF)]. Eluates were assessed for purity by SDS-PAGE analysis. Proteins were concentrated using Vivaspin 6 (5000 MWCO) centrifugal concentrators and then buffer exchanged into storage buffer [50 mM Tris-Cl pH = 8.5, 100 mM NaCl] using PD-10 desalting columns (GE Healthcare). The desalted proteins were concentrated again using Vivaspin 6 (5000 MWCO) centrifugal concentrators, aliquoted into PCR strip tubes, snap frozen using liquid nitrogen, and stored at -80°C until use.

For expression of RECON, plasmid encoding mRECON was transformed into Rosetta (DE3)pLysS chemically competent *E. coli*. Overnight cultures of the resulting bacterial strains were used to inoculate 1.5 L of LB broth at a 1:100 dilution. Bacterial cultures were grown to OD_{600} 0.5 at 37°C. The cultures were then cooled down to room temperature and protein expression was induced by the addition of 0.5 mM isopropyl β-D-1-thiogalactopyranoside (IPTG) for 18 hours at 16°C. Bacteria were harvested by centrifugation at 9000 x g for 5 minutes, and the cell pellets were resuspending into 30 mL of Buffer A [50 mM Tris pH = 8.0, 500 mM NaCl, 20 mM Imidazole, 5 mM β-Mercaptoethanol (BME), and 1 mM phenylmethylsulfonyl fluoride (PMSF)] and cooled on ice for 30 minutes. Bacteria were lysed by sonication on ice and clarified by centrifugation at 40,000 x g for 30 minutes at 4°C. The resulting clarified lysate was bound to HisPur NiNTA Resin (Thermo Scientific). The resin was washed with 100 column volumes of buffer A and bound proteins were eluted in Buffer B [50 mM Tris-Cl pH = 8.0, 500 mM NaCl, 300 mM Imidazole, 5 mM β-Mercaptoethanol (BME), and 1 mM phenylmethylsulfonyl fluoride (PMSF)]. Eluates were assessed for purity by SDS-PAGE analysis. Proteins were concentrated using Vivaspin 6 (5000 MWCO) centrifugal concentrators and then buffer exchanged into storage buffer [40 mM Tris pH 7.5, 100 mM NaCl, 20 mM MgCl2] using PD-10 desalting columns (GE Healthcare). The desalted proteins were concentrated again using Vivaspin 6 (5000 MWCO) centrifugal concentrators, supplemented with glycerol (25%), snap frozen using liquid nitrogen, and stored at -80°C until use.

BNPP Cleavage Assays

Unless otherwise noted, CnpB activity assays were carried out in clear polystyrene 96-well plates using assay buffer [50 mM Tris-Cl pH = 8.5, 100 mM NaCl] in 100 µL of assay buffer at 37°C. Indicated concentrations of CnpB and specified metal ions were diluted into assay buffer and reactions were initiated by the addition 0.2 mM BNPP. CnpB reaction rates were monitored by measuring the absorbance at 405 nm (OD_{405}) using a plate reader (Synergy HTX multimode reader, BioTek Instruments).

Synthesis of [^{32}P] 3′3′-c-di-AMP

Briefly, 1 µM of *B. subtilis* DisA and 1 µM α-[^{32}P] ATP (Perkin-Elmer) (100 µL total reaction volume) was incubated in buffer [40 mM Tris pH 7.5, 100 mM NaCl, 20 mM MgCl2] at 37°C overnight. The following day, the reaction was spiked with an additional 1 µM DisA enzyme and incubated at 37°C for four hours. The reaction was terminated by boiling for 10 min at 95°C. The resulting crude [^{32}P] 3′3′-c-di-AMP mixture was further purified using RECON affinity purification: 100 µM His-tagged mRECON was immobilized on HisPur Ni-NTA resin for 30 min on ice. The resin was washed twice with buffer and held on ice until use. The RECON resin was incubated with the crude [^{32}P] 3′3′-c-di-AMP mixture for 30 minutes at room temperature. Following removal of the supernatant, the Ni-NTA resin was washed five times with ice cold buffer. 500 uL of buffer was added to the resin and the sample was incubated at 95°C for 10 minutes. The slurry was transferred to a minispin column and [^{32}P] 3′3′-c-di-AMP was eluted by centrifugation. [^{32}P] 3′3′-c-di-AMP was analyzed for purity by Thin Layer Chromatography (TLC) analysis using Polygram CEL300 PEI TLC plates (Machery-Nagel) in running buffer containing 1:1.5 (vol/vol) saturated (NH4)2SO4 and 1.5 M NaH2PO4 pH 3.6.

DRaCALA Binding Assays

Two-fold serial dilutions of CnpB in buffer [50 mM Tris-Cl pH = 8.5, 100 mM NaCl] with and without 0.1 mM $MnCl_2$ were incubated with ~1 nM [^{32}P] 3′3′-c-di-AMP for 10 minutes at 4°C. Samples were blotted onto nitrocellulose membranes and air dried for 15 minutes. Membranes were then exposed onto PhosphorImager screens (GE Healthcare) and developed using a Sapphire Biomolecular Imager (Azure Biosystems). Data were analyzed using Fiji/ImageJ software as previously described and graphed using GraphPad Prism 8 software.

[^{32}P] 3′3′-c-di-AMP Hydrolysis Assays

Briefly, recombinant CnpB was incubated with radiolabeled 3′3′-c-di-AMP in buffer [50 mM Tris-Cl pH = 8.5, 100 mM NaCl] at 37°C. After indicated times, samples were dotted onto TLC plates and allowed to air dry for 5-10 minutes and then separated in TLC running buffer. TLC plates were then air dried for 30-60 minutes, exposed onto PhosphorImager screens (GE Healthcare) and developed using a Sapphire Biomolecular Imager (Azure Biosystems).

Quantification of 3′3′-c-di-AMP Using AMP-Glo™ Assay

3′3′-c-di-AMP standards were prepared by performing two-fold serial dilutions in buffer [50 mM Tris-Cl pH = 8.5, 100 mM NaCl]. 3′3′-c-di-AMP samples were supplemented with 0.1 mg mL^{-1} Bovine Serum Albumin, 1 mM DTT, 0.1 mM $MnCl_2$, and 1 μM CnpB (final concentration) (100 μL total reaction volume). Samples were incubated overnight at 37°C. 24 hours later, 100 μL of AMP-Glo™ reagent I was added to each sample and incubated at room temperature for 2 hours. 50 μL of the resulting sample was transferred to a solid white 96-well plate (BioRad) and then incubated with 50 μL of AMP Detection Solution (equilibrated at room temperature for at least one hour) for one hour at room temperature. Luminescence was quantified using a plate reader (Synergy HTX multimode reader, BioTek Instruments) with an integration time of one second. Relative luminescence units (RLU) for each sample were background corrected by subtracting the RLU of the no 3′3′-c-di-AMP control. Standard curves were generated using default settings in GraphPad Prism software. Quantification and detection limits were calculated as previously described[26].

Quantification of 3′3′-c-di-AMP Using AMP-Luciferase Assay (CDA-Luc)

3′3′-c-di-AMP standards were prepared by performing two-fold serial dilutions in buffer [50 mM Tris-Cl pH = 8.5, 100 mM NaCl]. 3′3′-c-di-AMP samples dissolved in buffer [50 mM Tris-Cl pH = 8.5, 100 mM NaCl] were supplemented with 0.1 mg mL^{-1} Bovine Serum Albumin, 1 mM DTT, 0.1 mM $MnCl_2$, and 1 μM CnpB (final concentration) (100 μL total reaction volume). Samples were incubated overnight at 37°C. 24 hours later, 100 μL of ATP generation solution [50 mM Tris-Cl pH = 8.5, 100 mM NaCl, 2 μM PAP, 50 μg mL^{-1} sodium hexametaphosphate, 2U myokinase, 0.1 mg mL^{-1} Bovine Serum Albumin, 1 mM DTT, 0.1 mM $MgCl_2$] was added to each sample and incubated at room temperature for 3 hours. 50 μL of the resulting sample was transferred to a solid white 96-well plate (BioRad) and then incubated with 50 μL of Kinase Glo® reagent (equilibrated at room temperature for at least one hour). The plates were briefly centrifuged and incubated for at least ten minutes at room temperature. Luminescence was quantified using a plate reader (Synergy HTX multimode reader, BioTek Instruments) with an integration time of one second. Relative luminescence units (RLU) for each sample were background corrected by subtracting the RLU of the no 3′3′-c-di-AMP control. Standard curves were generated using default settings in GraphPad Prism 8 software. Concentrations of 3′3′-c-di-AMP in unknown samples was determined by interpolating into standard curves using GraphPad Prism 8 software. Quantification and detection limits were calculated as previously described[26].

RECON Affinity Purification

Listeria monocytogenes was back diluted into *Listeria* defined media[3,103] at an OD 0.1 and grown for 24 hours shaking at 37°C. The following day, 1 mL of overnight culture was spun at max speed in a microcentrifuge for 1 minute and supernatant and cell pellet were separated and saved for processing. The cell pellet was resuspended in 200 μL ice cold pulldown buffer [100uM Tris pH = 7.5 20mM MgCl2 50mM NaCl] and lysed by sonication for 5 seconds at 25% power. Next, 800 μL of pulldown buffer and 1.3 μM (final concentration) of RECON bound to 20 μL of Ni-NTA beads were added to the sample and agitated for 15 minutes at room temperature to allow binding. The beads were then spun down and washed 3X with pulldown buffer. Subsequently, 150 μL of

pulldown buffer with 500mM Imidazole was added to the beads and agitated for 15 minutes at room temperature to release RECON. (Note: We have found that directly boiling the RECON-bead complexes can release interferents that affect downstream quantification. We recommend eluting the RECON-CDA complexes first, followed by boiling to release CDA.) Beads were spun down at max speed and supernatant added to a clean microcentrifuge tube. The supernatant was heated to 95°C for 10 minutes to denature RECON and release c-di-AMP then spun down at maximum speed to pellet the denatured protein. The supernatant was then processed to determine c-di-AMP concentration using the CDA-Luc protocol, as detailed above. Supernatant samples were processed identically except that 500 µL of supernatant was added to 500 µL of 2X pulldown buffer and 1.3 µM (final concentration) of RECON bound to 20 µL of Ni-NTA beads was used to bind c-di-AMP.

Figures

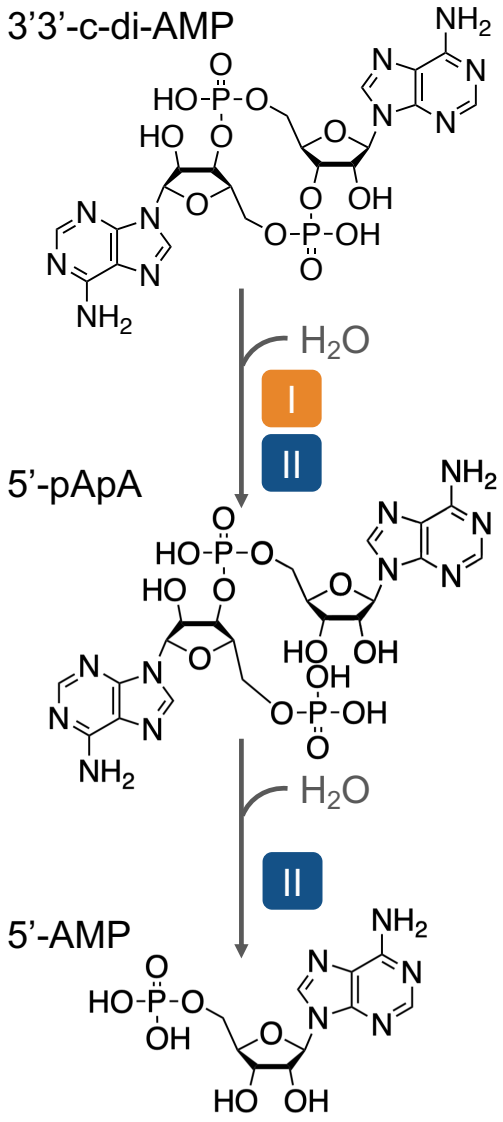

Group I Phosphodiesterases

PdeA – *Listeria monocytogenes*
PgpH – *Listeria monocytogenes*
GdpP – *Bacillus subtilis*
GdpP – *Lactococcus lactis*
GdpP – *Staphylococcus aureus*
GdpP – *Streptococcus pyogenes*
GdpP – *Streptococcus suis*
GdpP – *Lactococcus lactis*
Pde1 – *Streptococcus pneumoniae*
DhhP – *Borrelia burgdorferi*

Group II Phosphodiesterases

Pde2 – *Streptococcus pneumoniae*
CnpB – *Mycobacterium tuberculosis*
PDE – *Mycobacterium smegmatis*
AtaC – *Streptomyces venezuelae*
CdnP – *Streptococcus agalactiae*

Figure 2.1: Mechanisms of 3′3′-c-di-AMP hydrolysis
Overview of 3′3′-c-di-AMP hydrolysis by phosphodiesterases (PDEs). Group I PDEs hydrolyze 3′3′-c-di-AMP to the linear dinucleotide 5′-pApA. Group II PDEs hydrolyze 3′3′-c-di-AMP to 5′-AMP. Group II PDEs can also hydrolyze 5′-pApA to 5′-AMP.

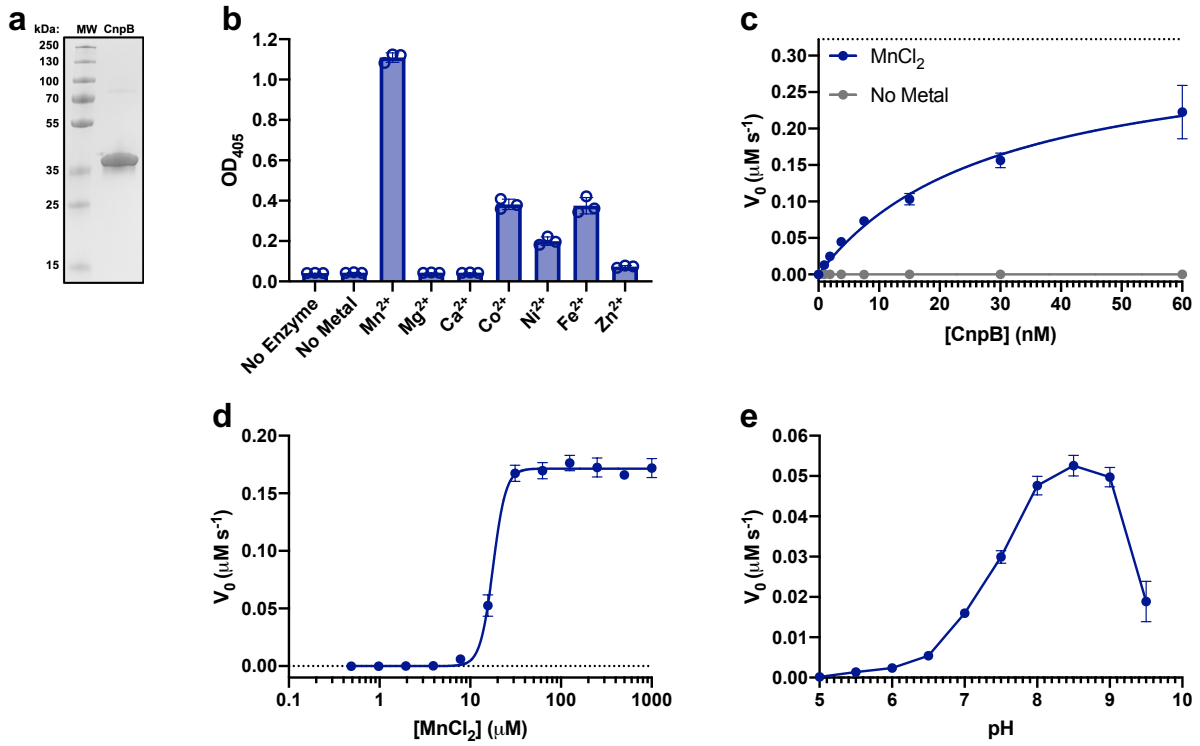

Figure 2.2: Optimization of CnpB hydrolytic activity

(a) SDS-PAGE analysis of NiNTA purified *M. tuberculosis* CnpB. **(b-e)** BNPP hydrolysis activity of CnpB. (b) 500 nM CnpB was incubated with 0.2 mM BNPP in the presence and absence of 0.1 mM indicated metal ions for 5 minutes at 37°C and absorbance at 405 nm was recorded. **(c)** Increasing concentrations of CnpB were incubated with 0.2 mM BNPP in the presence and absence of 0.1 mM $MnCl_2$ at 37°C and absorbance at 405 nm was monitored. **(d)** 15 nM CnpB was incubated with 0.2 mM BNPP and increasing concentrations of $MnCl_2$ at at 37°C and absorbance at 405 nM was monitored. **(e)** 15 nM CnpB was incubated with 0.2 mM BNPP and 0.1 mM $MnCl_2$ in pH 5-9.5 reaction buffer at 37°C and absorbance at 405 nm was monitored. In all panels, data are presented as mean ± standard deviation of n=3 replicates.

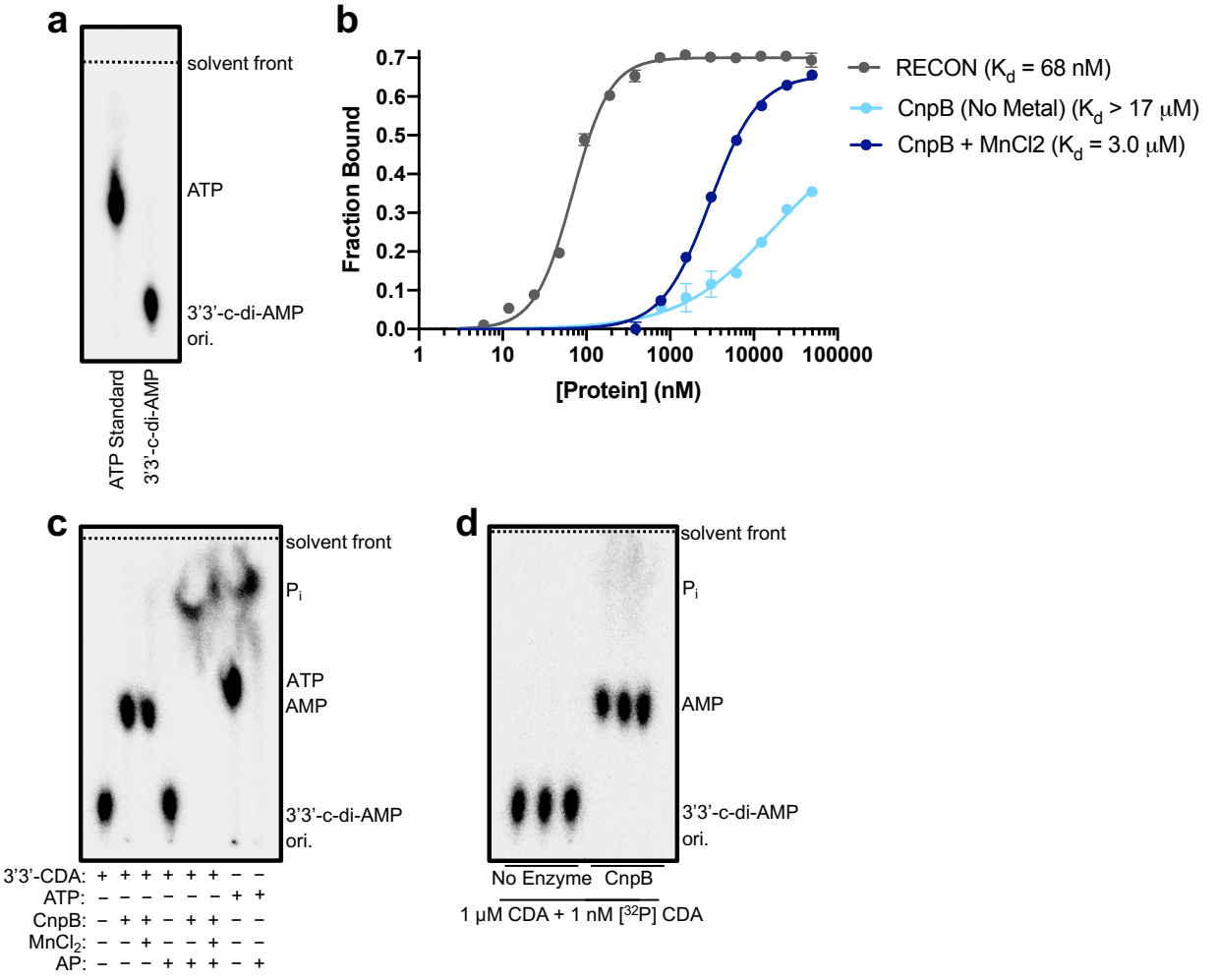

Figure 2.3: Analysis of CnpB 3′3′-c-di-AMP binding and hydrolysis
(a) Thin layer chromatography (TLC) analysis of enzymatically synthesized [^{32}P] 3′3′-c-di-AMP and [^{32}P] ATP standard. Data are representative of several independent experiments. **(b)** DRaCALA analysis of 3′3′-c-di-AMP binding to RECON and CnpB in presence and absence of 0.1 mM $MnCl_2$. data are presented as mean ± standard deviation of n=3 replicates. (c-d) TLC analysis of 3′3′-c-di-AMP hydrolysis by CnpB. **(c)** ~1 nM [^{32}P] 3′3′-c-di-AMP was incubated with or without 25 μM CnpB in the presence and absence of 0.1 mM $MnCl_2$ for 2 hours at 37°C. Samples were then treated with or without 0.1 U of Alkaline Phosphatase for 1 hour. Samples were then spotted onto TLC plates and separated. Data are representative of n=3 experiments. **(d)** 1 μM unlabeled 3′3′-c-di-AMP spiked with ~1 nM [^{32}P] 3′3′-c-di-AMP was treated with or without 1 μM CnpB overnight at 37°C. Samples were then spotted onto TLC plates and separated. N=3 replicates are shown.

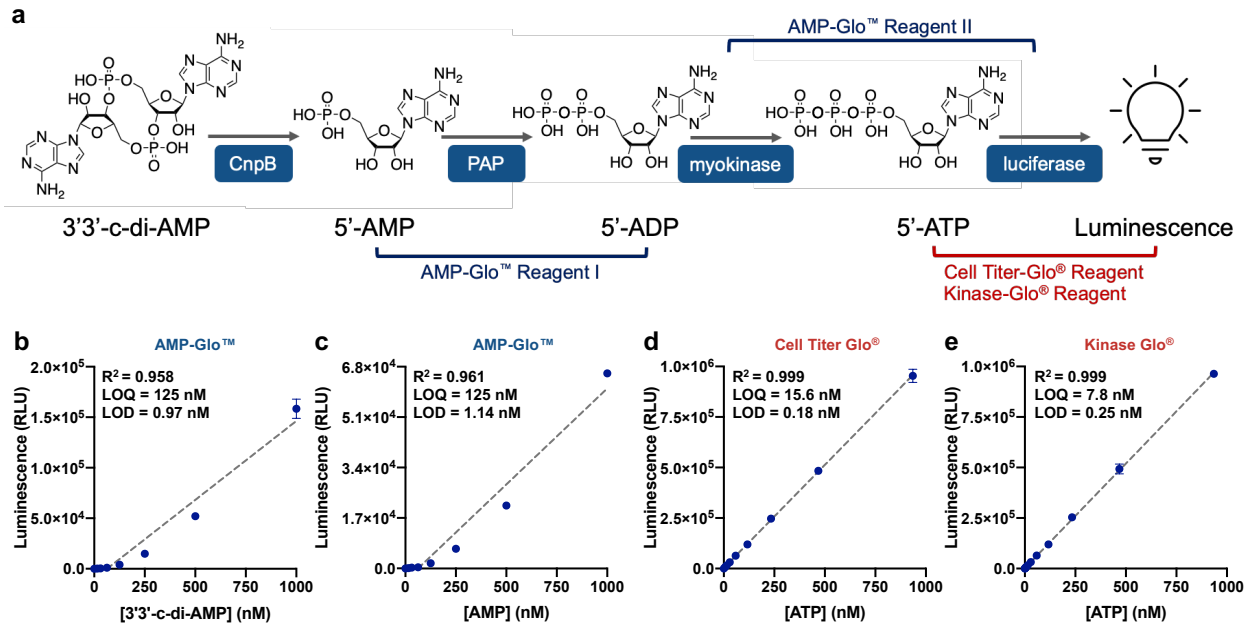

Figure 2.4: Detection of 3′3′-c-di-AMP using conventional AMP-Glo assay
(a) Schematic overview of AMP and ATP detection methods. **(b)** Standard curve of CnpB hydrolyzed 3′3′-c-di-AMP using AMP-Glo™ assay. **(c)** Standard curve of AMP using AMP-Glo™ assay. **(d)** Standard curve of ATP using Cell Titer Glo® reagent. **(e)** Standard curve of ATP using Kinase Glo® reagent. In all panels, data are presented as mean ± standard deviation of n=3 replicates.

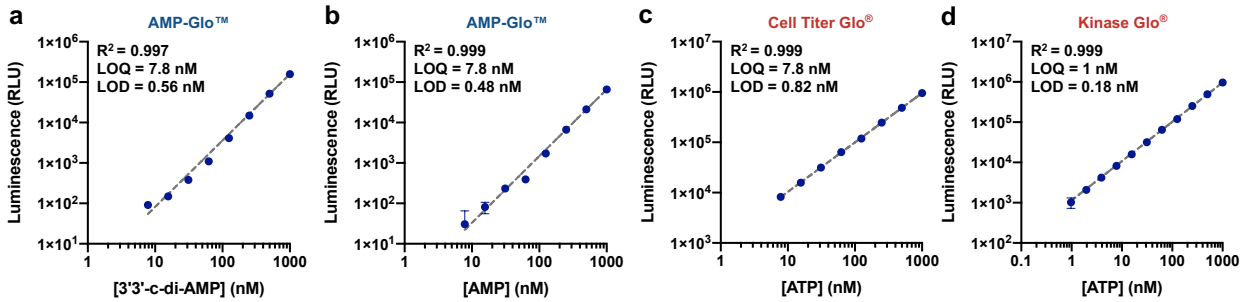

Figure 2.5: Reanalysis of AMP and ATP detection methods

Data from Figure 2.4 b-e were reanalyzed using log-log plots. **(a)** Standard curve of CnpB hydrolyzed 3′3′-c-di-AMP using AMP-Glo™ assay. **(b)** Standard curve of AMP using AMP-Glo™ assay. **(c)** Standard curve of ATP using Cell Titer Glo® reagent. **(d)** Standard curve of ATP using Kinase Glo® reagent. In all panels, data are presented as mean ± standard deviation of n=3 replicates.

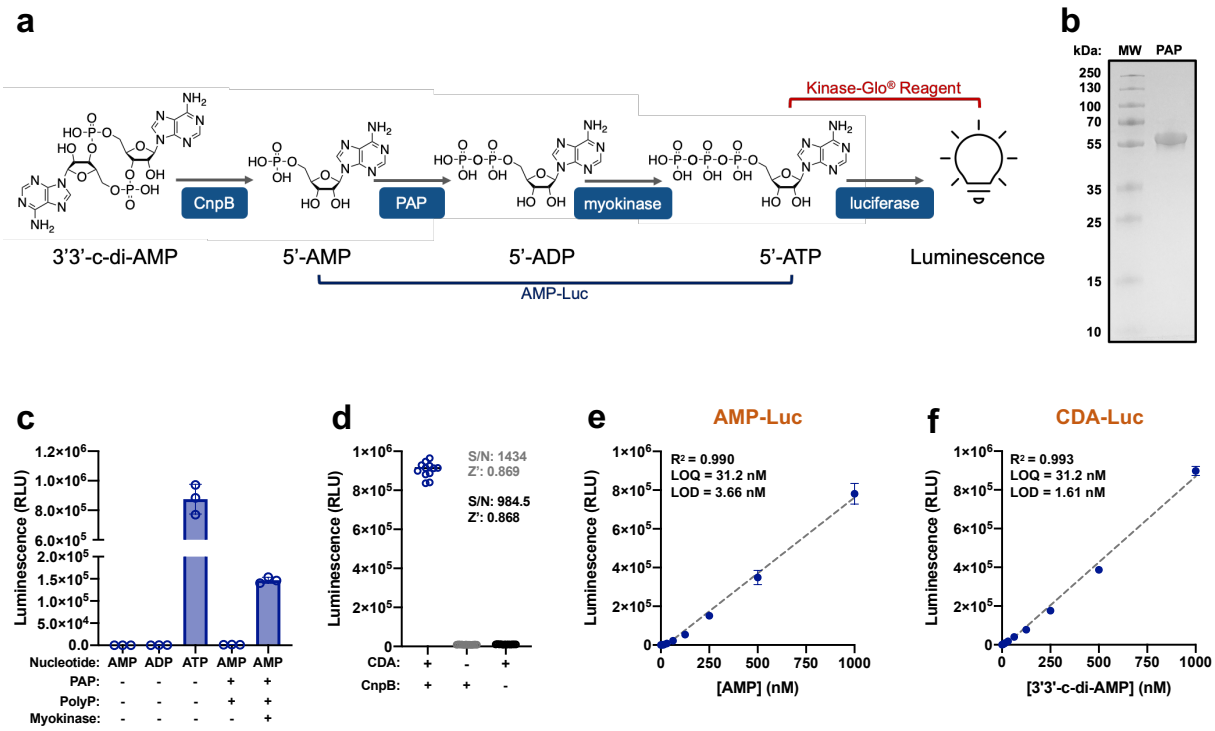

Figure 2.6: Quantification of 3′3′-c-di-AMP using CDA-Luc Assay

(a) Schematic overview of CDA-Luc assay. **(b)** SDS-PAGE analysis of NiNTA purified *A. johnsonii* PAP. **(c)** Optimization of AMP-Luc assay. AMP was incubated with 2 µM PAP and 50 µg mL^{-1} of sodium hexametaphosphate (PolyP) with or without 1U myokinase for 3 hours followed by incubated with Kinase Glo® reagent for 10 minutes. **(d)** Z′ factor analysis of CDA-Luc Assay. 1 µM 3′3′-c-di-AMP was treated with or without CnpB overnight and AMP was detected using AMP-Luc assay. **(e)** Standard curve of AMP using AMP-Luc assay. **(f)** Standard curve of CnpB hydrolyzed 3′3′-c-di-AMP using AMP-Luc assay. In all panels, data are presented as mean ± standard deviation of n=3 (c, e-f) or n=12 (d) replicates.

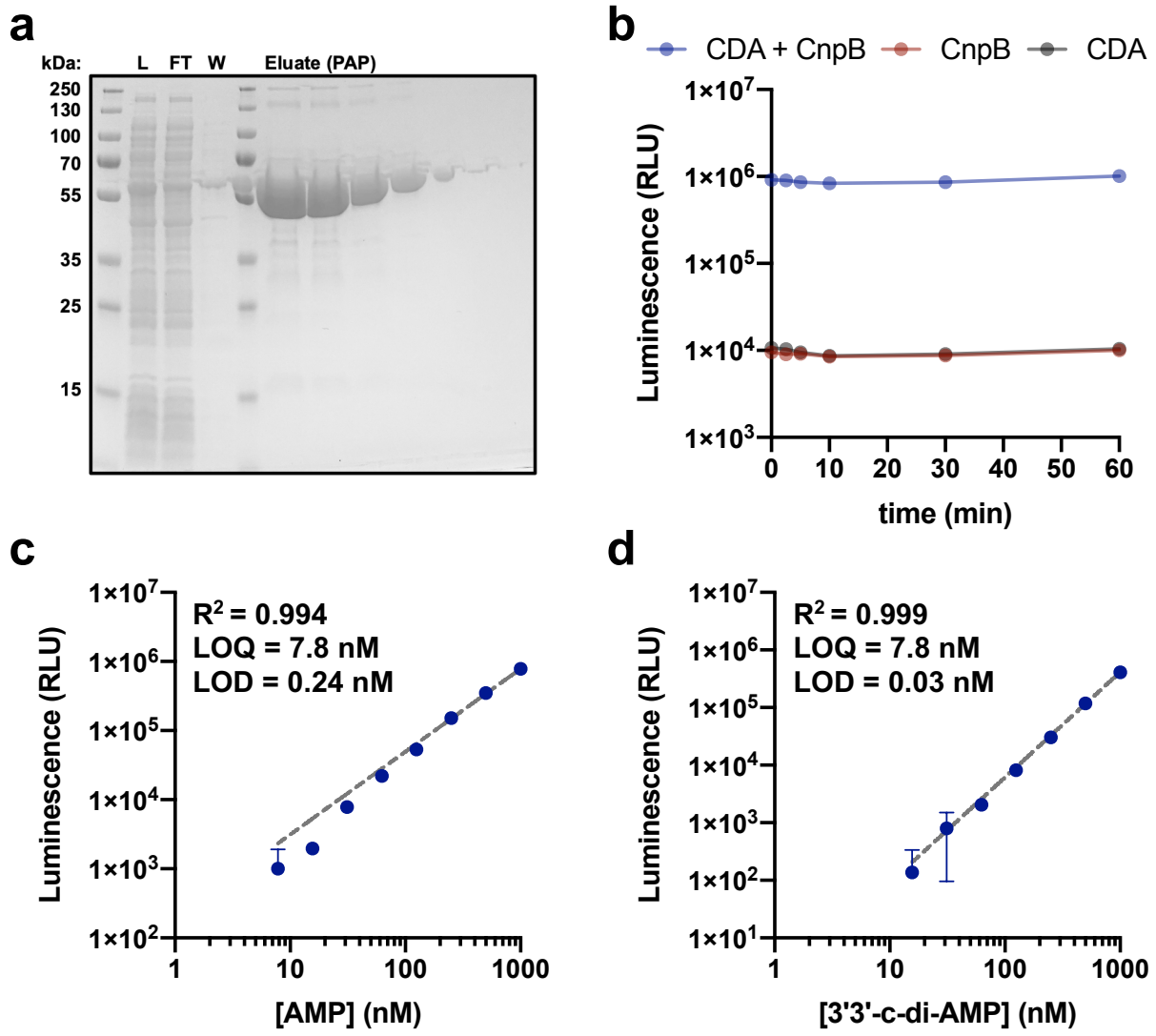

Figure 2.7: Development of CDA-Luc assay

(a) SDS-PAGE analysis of NiNTA purified PAP. L = lysate; FT = flow through; W = wash. Samples were pooled, desalted, and reanalyzed by SDS-PAGE on the right. **(b)** Stability of CDA-Luc Assay. 1 µM 3′3′-c-di-AMP was treated with or without CnpB overnight and AMP was detected using AMP-Luc assay. Luminescence was monitored over one hour. **(c-d)** Reanalysis of AMP-Luc assay using log-log plot. (c) Standard curve of AMP using AMP-Luc assay. (d) Standard curve of CnpB hydrolyzed 3′3′-c-di-AMP using AMP-Luc assay. In all panels, data are presented as mean ± standard deviation of n =12 (b) or n=3 (c-d) replicates.

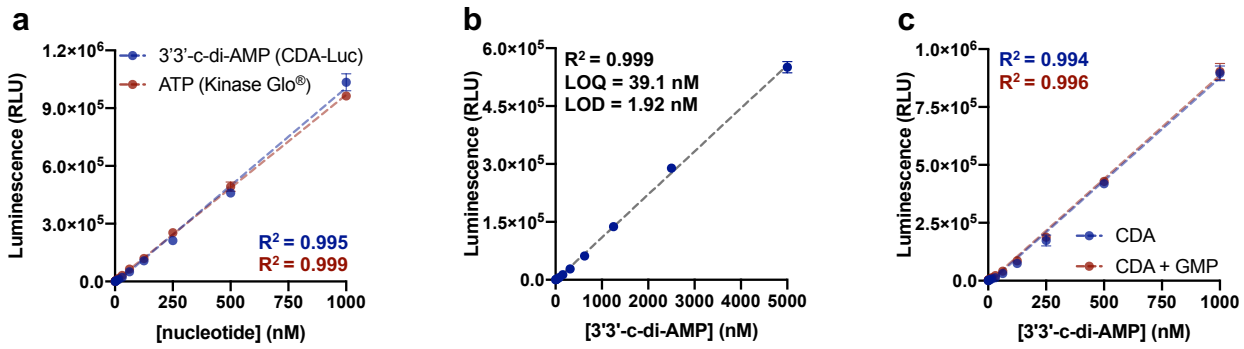

Figure 2.8: Characterization of CDA-Luc Assay
(a) Overlay of 3′3′-c-di-AMP standard curve generated using AMP-Luc and ATP standard curve generated using Kinase-Glo®. Limit of quantification for 3′3′-c-di-AMP is 31.2 nM and ATP is 7.8 nM. **(b)** Extended standard curve of CDA-Luc assay. **(c)** CDA-Luc standard curve in the presence and absence of 1 μM GMP. In all panels, data are presented as mean ± standard deviation of n=3 replicates.

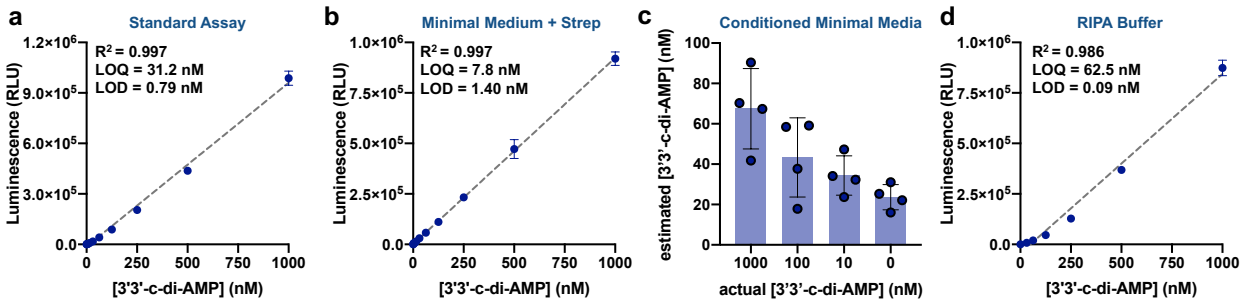

Figure 2.9: Performance of CDA-Luc in different buffers

(a) CDA-Luc standard curve using standard assay conditions. **(b)** CDA-Luc standard curve in *Listeria monocytogenes* minimal media supplemented with streptomycin. **(c)** Conditioned minimal media derived from Δ*dacA*Δ*oppA L. monocytogenes* was doped with known concentrations of pure 3′3′-c-di-AMP and subjected to CDA-Luc analysis. **(d)** CDA-Luc standard curve in RIPA buffer. In all panels, data are presented as mean ± standard deviation of n=3 (a, b, and d) or n=4 (c) replicates.

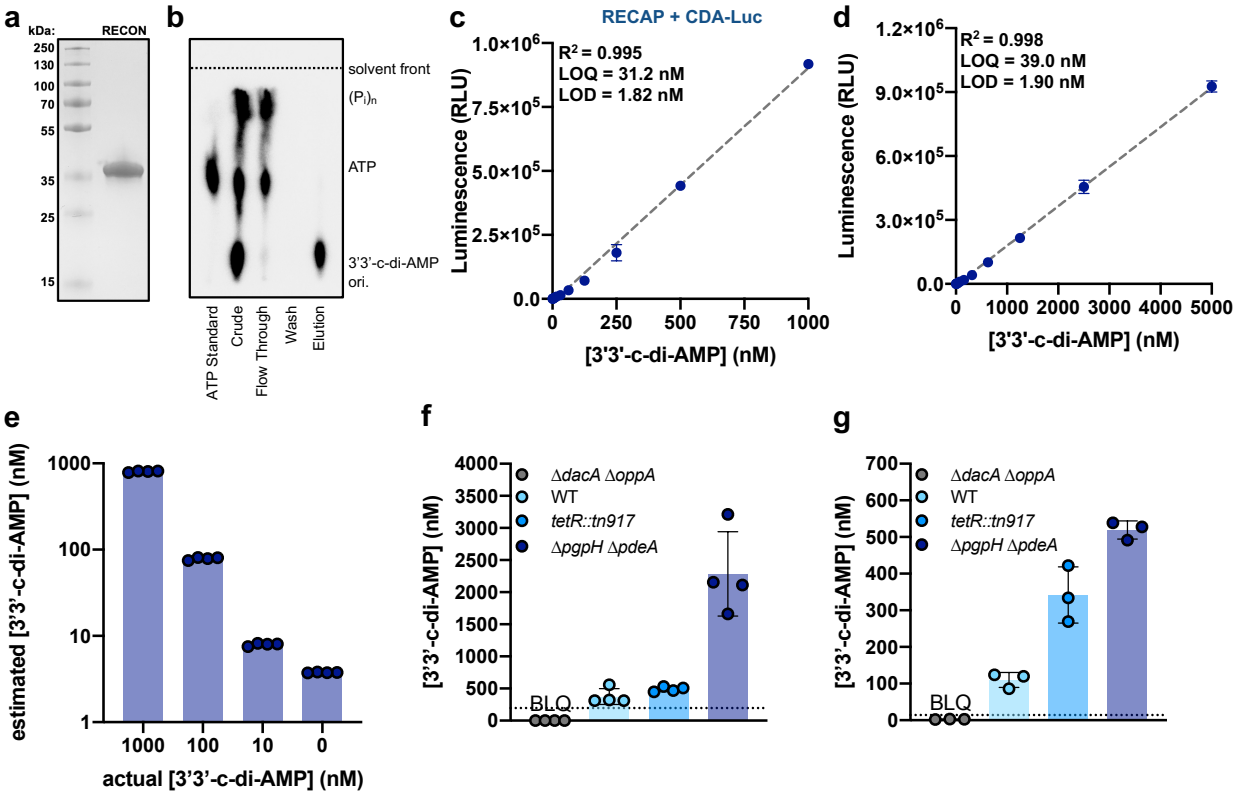

Figure 2.10: RECON enables affinity purification of c-di-AMP from biological samples
(a) SDS-PAGE analysis of NiNTA purified murine RECON. **(b)** TLC analysis of 3′3′-c-di-AMP using RECON affinity purification. **(c)** CDA-Luc standard curve of 3′3′-c-di-AMP affinity purified using 2 µM RECON. Data are presented as mean ± standard deviation of n=3 replicates. **(d)** CDA-Luc standard curve of 3′3′-c-di-AMP affinity purified from *L. monocytogenes* minimal media using 10 µM RECON. Data are presented as mean ± standard deviation of n=3 replicates. **(e)** Conditioned minimal media derived from Δ*dacA*Δ*oppA L. monocytogenes* was doped with known concentrations of pure 3′3′-c-di-AMP and subjected to RECAP prior to CDA-Luc analysis. Limit of quantification was determined to be 7.8 nM. Data are presented as mean ± standard deviation of n=4 replicates. **(f)** Quantification of intracellular 3′3′-c-di-AMP from lysates of various *L. monocytogenes* strains using RECON affinity purification and CDA-Luc. Dashed lines indicate the limit of quantification (BLQ denotes below the limit of quantification). Data are presented as mean ± standard deviation of n=4 replicates. **(g)** Quantification of secreted 3′3′-c-di-AMP from the growth medium of various *L. monocytogenes* strains using RECON affinity purification and CDA-Luc. Dashed lines indicate the limit of quantification (BLQ denotes below the limit of quantification). Data are presented as mean ± standard deviation of n=3 replicates.

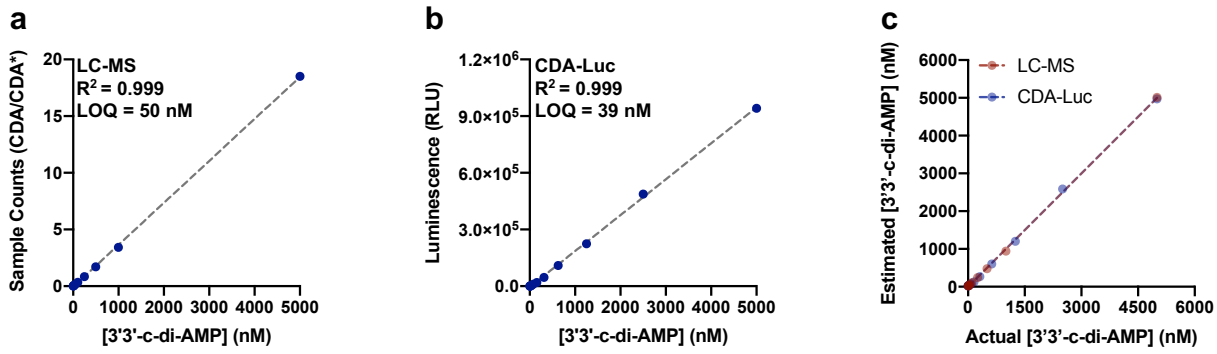

Figure 2.11: Comparison of CDA-Luc to Mass Spectrometry (LC-MS)
(a) LC-MS standard curve of 3′3′-c-di-AMP. Known concentrations of c-di-AMP were mixed with 500 nM of (C^{13} N^{15}) isotopically labeled c-di-AMP (CDA*) and subjected to LC-MS analysis. One representative standard curve of n=1 replicates is shown. **(b)** CDA-Luc standard curve of 3′3′-c-di-AMP. Data are presented as mean ± standard deviation of n=3 replicates. **(c)** Plot of estimated [3′3′-c-di-AMP] by interpolation into the standard curve vs the actual concentration for LC-MS from (a) and CDA-Luc from (b).

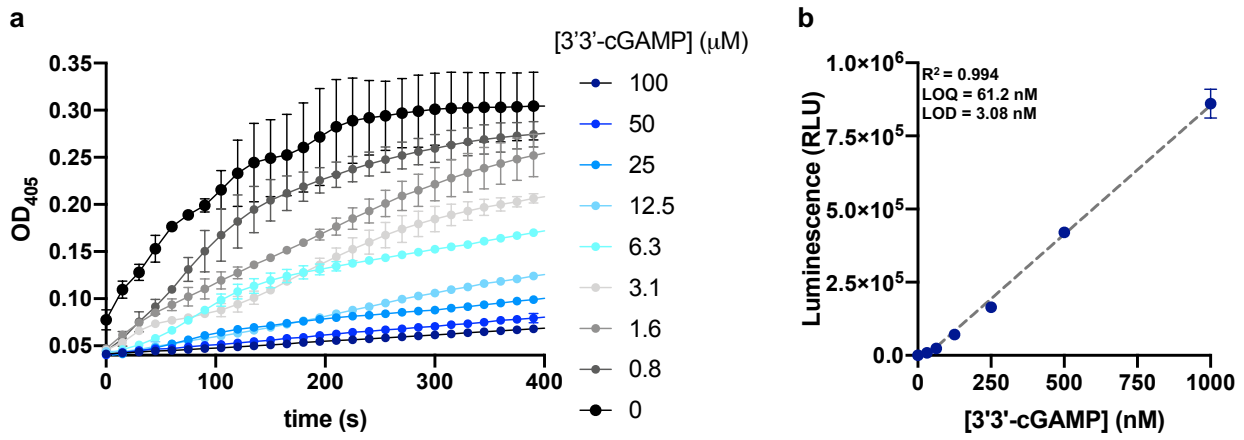

Figure 2.12: Quantification of 3′3′-cGAMP using CDA-Luc
(a) 15 nM CnpB was incubated with 0.1 mM BNPP and 0.1 mM $MnCl_2$ in pH 8.5 reaction buffer in the presence of increasing concentrations of 3′3′-cGAMP and absorbance at 405 nm was monitored. Data are presented as mean ± standard deviation of n=2 replicates. **(b)** Standard curve of CnpB hydrolyzed 3′3′-cGAMP using AMP-Luc assay. Data are presented as mean ± standard deviation of n=3 replicates.

Chapter 3

A rationally designed c-di-AMP FRET biosensor to monitor nucleotide dynamics to environmental changes

The majority of this chapter is expected to be published as:

Pollock A.J., Choi P.H., Laporta L.G., Zaver S.A., Süel G.M., Tong L., & Woodward J.J.
A rationally designed c-di-AMP FRET biosensor to monitor nucleotide dynamics to environmental changes.

Summary

3′3′-cyclic di-adenosine monophosphate (c-di-AMP) is an important nucleotide second messenger found throughout the bacterial domain of life. C-di-AMP is essential in many bacteria and regulates a diverse array of effector proteins controlling pathogenesis, cell wall homeostasis, osmoregulation, and central metabolism. Despite the ubiquity and importance of c-di-AMP, methods to detect this signaling molecule are limited, particularly at single cell resolution. In this work, crystallization of the *Listeria monocytogenes* c-di-AMP effector protein Lmo0553 enabled structure guided design of a Förster resonance energy transfer (FRET) based biosensor, which we have named CDA5. CDA5 is a fully genetically encodable, specific, and reversible biosensor which allows for the detection of c-di-AMP dynamics both *in vitro* and within live single cells in a nondestructive manner. Our initial studies identify a unimodal distribution of c-di-AMP in *Bacillus subtilis* which decreases rapidly when cells are grown in diluted Luria Broth. Furthermore, we find that when *B. subtilis* cells are grown in similar media with supplemental potassium they retain a higher intracellular concentration of c-di-AMP, again in a unimodal manner. These findings provide novel insight into c-di-AMP distribution within bacterial populations and establish CDA5 as a powerful platform for characterizing new aspects of c-di-AMP regulation.

Introduction

Bacterial growth, reproduction, and survival demand rapid, accurate, and coordinated responses to internal and environmental cues. These responses are commonly relayed by nucleotide second messengers which dynamically change concentration through rapid synthesis and degradation[106-110]. The nucleotide second messenger 3′3′-cyclic di-adenosine monophosphate (c-di-AMP) is unique in that it is essential in diverse bacterial genera and regulates clinically and industrially relevant processes such as osmotic stress responses, cell wall metabolism, and metabolic homeostasis[106,111-131]. C-di-AMP is known to be produced by five classes of di-adenylate cyclases, although most bacteria contain only one of two main cyclases: the membrane associated CdaA and DNA binding DisA[106,114,115]. *Bacillus subtilis*, the model organism used in this study, interestingly encodes *cdaA*, *disA*, and a spore restricted cyclase, *cdaS*. Due to redundancy, it is possible to delete individual cyclases in *B. subtilis* without dramatic phenotypic consequences. C-di-AMP is degraded by 4 classes of phosphodiesterase although most bacteria only encode one or two of these enzymes[106,109,114,115]. *Bacillus subtilis* encodes both *gdpP* and *pgpH*, which again, due to redundancy, allows for deletion of single phosphodiesterases without significant physiological defects.

Despite being a second messenger of growing interest, only a small handful of studies have explored the internal and external signals which regulate the activity of c-di-AMP cyclases and phosphodiesterases. Multi-hour exposure to glutamine, potassium, and light have been reported to impact signal levels but the mechanisms by which nucleotide levels change have either not been defined or have been linked to altered phosphodiesterase expression[106,117,119,124,129-131]. Additionally, investigations of protein-protein interactions influencing intracellular c-di-AMP levels have been performed elucidating DacA regulation by the cistronic GlmM and YbbR proteins[132-134]. To our knowledge, the only studies which clearly identified post-translational c-di-AMP responses to environmental conditions have been: first, that a wide array of bacteria when non-growing but energized quickly accumulate more c-di-AMP in low osmotic conditions relative

to high osmotic conditions, and second, that (p)ppGpp, which accumulates during amino acid starvation, inhibits c-di-AMP phosphodiesterases[119,121,122]. Such foundational studies remain largely elusive because detection methods are underdeveloped.

C-di-AMP is currently quantified using either mass spectrometry or an enzyme immunoassay which are both relatively low throughput and expensive methods providing only a snapshot of the population average at a single time point[135,136]. Additionally, an RNA-aptamer based biosensor has also been developed to detect c-di-AMP[137]. Unfortunately, this biosensor has not been able to be utilized because it has a long k_{off} which obscures c-di-AMP decreases, suffers from stochasticity in fluorescent ligand uptake, and lacks an internal control. To partially remedy this dearth, we recently developed the CDA-Luc assay which is an inexpensive and higher throughput method for quantifying c-di-AMP[138]. Although we anticipate this method being invaluable to many investigations, it is still limited to destructive snapshots of the population average.

Thus, an intramolecular FRET biosensor for c-di-AMP is an ideal tool to complement existing techniques as it would allow for nondestructive and rapid resampling of c-di-AMP in single cells. Intramolecular FRET biosensors have been central to diverse investigations of nucleotide second messenger regulation in both eukaryotic and bacterial cells[139-151]. Most similarly to c-di-AMP, FRET biosensors have been used extensively to study the bacterial nucleotide second messenger 3′3′-cyclic di-guanosine monophosphate (c-di-GMP)[139-148]. These investigations have interrogated important phenomena which are currently intractable using current c-di-AMP detection methods including: sub-population responses to environmental conditions, mother/daughter cell heterogeneity, and regulation during infection.

Intramolecular FRET biosensors are fusion proteins which combine compatible fluorophores with a native binding protein for the ligand of interest[152-158]. The locations of these fluorophores are engineered such that ligand binding induces a conformational change which moves the donor fluorophore either closer to or further from the acceptor fluorophore generating altered energy transfer. This shift in energy transfer causes a change in the fluorescent signal quantified as the ratio of: energy transferred to and released by the acceptor fluorophore divided by energy released by the donor fluorophore. The FRET ratio reports on the binding state of the biosensor allowing for back calculation of the free ligand concentration within the solution or cell. Thus, FRET biosensors are powerful, entirely genetically encodable, internally controlled, and, due to their native effector protein scaffold, have physiologically relevant binding parameters.

In this work, we engineer and utilize CDA5: a FRET biosensor designed around the *Listeria monocytogenes* c-di-AMP binding protein, Lmo0553[118]. We demonstrate that CDA5 retains relevant native binding characteristics, produces a robust FRET response upon the addition of c-di-AMP, and successfully reports on the concentration of c-di-AMP in individual bacterial cells. Furthermore, we report that *B. subtilis* grown in diluted LB media rapidly decreases its intracellular c-di-AMP concentration and that supplementation of potassium lessens this effect. Additionally, we report that, in all conditions tested and unlike c-di-GMP, c-di-AMP concentrations in single cells follow a unimodal distribution. Our investigations not only identify a new facet of c-di-AMP biology but also establish CDA5 as a versatile platform which will facilitate a wealth of basic and applied investigations of the essential bacterial signaling molecule c-di-AMP.

Results

Overall structure of Lmo0553 in complex with cyclic-di-AMP

We previously identified Lmo0553 as a *Listeria monocytogenes* protein of unknown function which binds c-di-AMP at physiologically relevant concentrations. Despite numerous attempts to investigate the function of Lmo0553, its physiology has remained elusive. Thus, we sought to determine its basis of recognition and molecular response to c-di-AMP. The crystal structure of Lmo0553 in complex with c-di-AMP was determined at 1.6 Å resolution, as well as the structure of free Lmo0553 at 2.48 Å resolution. The atomic models have good agreement with the crystallographic data and the expected bond lengths, bond angles, and other geometric parameters (Table 1).

Lmo0553 contains tandem CBS motifs (Bateman domain) followed by an ACT domain. We observed a dimer of Lmo0553 in the crystals in which the Bateman domains of the two monomers contact each other in a head-to-head fashion, forming a disc-like dimer (Figures 3.1A 3.1B). This dimer is similar to other structures of CBS motif-containing proteins. As predicted, the C-terminal ACT domain of Lmo0553 adopts a ferredoxin fold (βαββαβ). This domain also forms a dimer, producing a structure consisting of an 8-stranded β-sheet packed against four α-helices on one face. The Bateman domain dimer sits atop the β-sheet of the ACT dimer, forming an extensive interface. The Bateman and ACT domains are diagonally swapped in the dimer, such that the Bateman domain of monomer 1 packs against the ACT domain of monomer 2 (Figure 3.1A).

Two c-di-AMP molecules are bound in the central cavity of the Bateman domain dimer, one on each face of the disc (Figure 3.1B). The dinucleotide adopts a folded conformation, with both bases in the *anti* configuration. The adenine of the first nucleotide (labeled 1 in Figure 3.1C) is buried between the CBS1 and CBS2 motifs of a monomer. This adenine makes extensive interactions with the protein and is recognized specifically, with a hydrogen-bond to its N1 and N6 atoms. Tyr34 is p-stacked against one face of the adenine ring, while several hydrophobic residues flank the other face. In contrast, the adenine of the second nucleotide (labeled 2 in Figure 3.1C) makes few direct interactions with the protein. The most notable interaction of the second nucleotide is the 5-prime phosphate which interacts with the side chain of Arg35. In the free as compared to c-di-AMP bound Lmo0553 structure, the side chain of Arg35 assumes a different conformation and occupies the binding site of c-di-AMP (Figure 3.1D). In the c-di-AMP complex structure, residues that contact the adenine base of the first nucleotide show substantial conformational differences as well. These changes in the binding site are likely the trigger for the overall changes in the organization of the dimer upon c-di-AMP binding.

Large conformational changes upon c-di-AMP binding guide biosensor design

Although elucidating the native physiology of Lmo0553 remains a subject of investigation, our detailed understanding of the molecular consequences of c-di-AMP binding led us to hypothesize that Lmo0553 could serve as a scaffold for development of a Förster resonance energy transfer (FRET) biosensor. FRET is exquisitely sensitive to angstrom level changes, therefore we

compared the structure of free Lmo0553 to that of the c-di-AMP complex to identify conformational differences (Figure 3.2A and 3.2B). After the Bateman domain of one monomer is overlaid, the orientation of the Bateman domain in the other monomer differs by 13° (Figure 3.2B). In addition, the orientation of the ACT domain differs by 12° (Figure 3.2A).

To leverage these structural rearrangements, the FRET pair eCFP and eYFP were respectively fused to the N and C termini of full length Lmo0553. This construct was purified and found to be stable, but no FRET response was observed upon the addition of c-di-AMP suggesting that fluorophores were too distant or oriented such that structural rearrangements were not detected. Additional engineering may have allowed for the generation of a FRET biosensor utilizing full length Lmo0553, but without a response to optimize, these efforts would have been arduous and potentially unsuccessful.

Reanalyzing the crystal structures, we noted that truncation of the ACT domain might lead to a better biosensor scaffold. The N-terminal Bateman domain of Lmo0553 is distinct from the ACT domain, encompasses the entire binding domain, undergoes large structural changes upon c-di-AMP binding, and, if isolated, would bring fluorophores into close contact increasing the potential to detect FRET ratio changes (Figure 3.3). To generate this second iteration biosensor, Lmo0553 was truncated at N-127 and fused to eCFP and eYFP (Figure 3.2C) to best leverage expected large conformational shifts and avoid disruption of the globular domain. Additionally, removal of the expected active domain decreased the potential of heterologous biosensor expression to disrupt cellular function.

This second iteration c-di-AMP biosensor was recombinantly produced and found to be stable in solution. Excitingly, increasing concentrations of c-di-AMP caused a robust, 23% FRET increase with an EC50 of 0.38 μM (Figure 3.2D). Thus, when this biosensor binds c-di-AMP, the chromophores of the flanking fluorophores come in closer contact allowing for increased energy transfer producing an elevated FRET response (Figure 3.2E). Satisfied by the magnitude of FRET response, we named this biosensor CDA5 (cyclic-di-AMP biosensor based on Lmo0553) and sought to characterize it biochemically.

Affinity and specificity of CDA5

Although initial FRET response assays suggested that CDA5 retains physiologically relevant biochemical parameters, we sought to further validate this assumption by comparing it directly to full length Lmo0553. DRaCALA analysis[159] using [^{32}P]-labeled c-di-AMP was employed which revealed an apparent Kd of 2.83 μM and 5.87 μM for Lmo0553 and CDA5 respectively (Fig 3.4A). This result demonstrates unaltered affinity for c-di-AMP supporting our hypothesis that neither truncation nor fusion with eCFP or eYFP altered ligand binding thermodynamics. To ensure that CDA5 engineering did not alter the previously reported specificity of Lmo0553, the DRaCALA assay was again employed[159]. This was done by competing bound radiolabeled c-di-AMP with excess unlabeled nucleotides. CDA5 and Lmo0553 both demonstrated exquisite specificity for c-di-AMP, as only unlabeled c-di-AMP but no other nucleotide in a wide array of monophosphate, triphosphate, cyclic, and dicyclic purine containing nucleotides could compete off radioactive c-di-AMP (Fig 3.4B, 3.5). These data support our hypothesis that CDA5 engineering did not alter critical biochemical parameters.

To further interrogate CDA5 specificity, we utilized a complex cytosolic environment where an array of cyclic dinucleotide (CDN) cyclases could be reliably ectopically expressed. Specifically, we recently engineered a biosensor capable of broadly detecting CDNs, particularly 2′3′-cGAMP, in the eukaryotic cytosol and adapted this system for CDA5[149]. We observed a titratable FRET response to the c-di-AMP cyclase DisA and, as expected, no response to high levels of either WspR*, a 3′3′-c-di-GMP cyclase, or cGAS, a 2′3′-cGAMP cyclase, further validating the specificity of CDA5 for c-di-AMP (Fig 3.4C, 3.4D, and 3.6).

CDA5 Reversibility

To be a reliable reporter, CDA5 must rapidly respond to both increasing and decreasing concentrations of c-di-AMP. CDA5 relies on a native effector protein scaffold which we hypothesized would rapidly respond to nucleotide second messenger fluctuations in order to carry out post-translational responses. We found that FRET responses were stable immediately upon addition of c-di-AMP providing evidence of a k_{on} less than the sampling limit of 10 seconds. Similarly, the k_{off} rate was also unable to be quantitated due to sampling limitations. Utilizing the DRaCALA specificity assay, excess unlabelled c-di-AMP was added to both CDA5 and Lmo0553 pre-bound with [^{32}P]-labeled c-di-AMP and immediately sampled for binding. Unlabeled c-di-AMP competed off bound [^{32}P]-labeled c-di-AMP completely within two seconds providing evidence of a k_{off} less than this time interval (Fig 3.4D). Despite not being able to quantify k_{on} and k_{off} rates with these assays, our results suggest that CDA5 can rapidly report on c-di-AMP fluctuations.

To further investigate the ability of CDA5 to repetitively detect c-di-AMP increases and decreases, similar to what we hypothesize is occurring in bacterial cells, we cycled c-di-AMP in solution by increasing the concentration using a bolus of c-di-AMP and decreasing the concentration using the c-di-AMP phosphodiesterase, PdeA. As expected, we observed that: PdeA caused a FRET decrease proportional to enzyme concentration, addition of a bolus of c-di-AMP restored the FRET response, and finally, the FRET response decreased again proportional to the concentration of PdeA (Fig 3.4E). This assay provides evidence that CDA5 is responsive to dynamic c-di-AMP fluctuations and also that CDA5 is a useful platform for kinetic investigations *in vitro*.

Development of a c-di-AMP blind control

Characterization of CDA5 indicated that it can reliably quantitate c-di-AMP in simplified systems but, recognizing that complexities can occur in native systems, we sought to develop a point mutant control version of CDA5 that does not bind c-di-AMP. Such a control would provide the capacity to separate FRET signal due to bonafide changes in c-di-AMP from other phenomena such as fluorophore quenching and protein-protein interactions.

Analysis of the crystal structure of Lmo0553 identified tyrosine-34 coordination of c-di-AMP binding via p-stacking (Fig 3.1C). We hypothesized that by replacing the stabilizing tyrosine ring with an alanine (Y34A), c-di-AMP binding would be minimized in a manner unlikely to disrupt protein stability. Recombinant Y34A CDA5 was found to be stable in solution and analyzed for binding using the DRaCALA binding assay. As hypothesized, c-di-AMP bound to CDA5 but not

the Y34A CDA5 point mutant control (Fig 3.7A). Next, increasing concentrations of c-di-AMP were added to purified CDA5 and Y34A CDA5 and analyzed by plate reader assay for FRET response. CDA5 but not Y34A CDA5 produced a robust FRET increase upon the addition of c-di-AMP (Fig 3.7B). Together these results suggest that Y34A CDA5 remains unbound and in the apo conformation even in the presence of c-di-AMP.

We next sought to validate Y34A CDA5 in *Escherichia coli* which is a complex model bacterial organism that does not naturally produce c-di-AMP but can be made to ectopically express a c-di-AMP cyclase and synthesize c-di-AMP. Thus, *E. coli* was transformed with a plasmid to express WT CDA5 or Y34A CDA5 as well as a second plasmid encoding the soluble domain of the c-di-AMP cyclase, DacA or an empty vector and then analyzed for FRET response by flow cytometry (Fig 3.8). *E. coli* carrying WT CDA5 produced a robust FRET response while Y34A CDA5 had an, albeit minor, FRET decrease (Fig 3.7C). We hypothesize that the minor FRET response is due to altered levels of non specific protein-protein interactions. Regardless, these results reinforce the utility of a nonbinding control such as Y34A CDA5 control to provide confidence that observed FRET responses are due to changes in ligand concentration and not other phenomena. It is often useful to also calculate the ratio of WT CDA5 to Y34A CDA5 FRET responses into a ′Y/A Ratio′ (Fig 3.7D). This metric combines the control biosensor data and declutters data, making results more clear.

CDA5 detects unimodal Bacillus subtilis responses to media alteration

CDA5 was then expressed in *Bacillus subtilis* to study native c-di-AMP regulation. *B. subtilis* is a model organism encoding a large array of c-di-AMP cyclases and phosphodiesterases but not a homologue to Lmo0553 which could cause disruptive heterodimerization. We found that rich media like LB is necessary to attain robust CDA5 expression but, at the same time, it is also important to use media with low autofluoresce to clearly quantitate FRET ratios. Due to the necessity of rich media to express CDA5, back dilution into minimal media was not ideal due to the large metabolism changes required to transition to fully biosynthetic growth. We found that we could back dilute *B. subtilis* expressing CDA5 into 10% LB media which retains a complex nutrient content and also has low enough autofluorescence to clearly quantitate FRET by flow cytometry. Additionally, because c-di-AMP null *B. subtilis* requires low potassium minimal media to grow, we were unable to express CDA5 in this mutant to investigate FRET responses in the c-di-AMP present vs absent manner utilized in *E. coli*.

In this diluted LB media, we tracked FRET changes overtime and observed a steady FRET decrease during the entire 180 minutes of growth until the WT and Y34A sensor had nearly the same FRET ratio (Fig 3.9A and 3.10). To verify this unexpected result, we split our sample to simultaneously detect c-di-AMP using our flow-based FRET assay and the gold standard for c-di-AMP quantification, mass spectrometry. These results were plotted on XY plots graphing c-di-AMP measured by mass spectrometry versus either the WT CDA5 FRET ratio (Fig 3.9B) or the Y/A ratio combining WT CDA5 and Y34A CDA5 ratios (Fig 3.9C). Although both the WT CDA5 FRET ratio and the Y/A ratio both correlated with c-di-AMP as measured by mass spec, the Y/A ratio highly correlated with c-di-AMP highlighting the importance of both the Y34A CDA5 control and the Y/A metric.

Flow cytometry allows for the collection of an enormous amount of informative single cell data providing an excellent opportunity to understand more about c-di-AMP dynamics. To understand more about the mechanics of this population level c-di-AMP decrease, WT CDA5 and Y34A CDA5 single cell data was normalized by the control biosensor's population average and plotted as histograms (Fig 3.9D-G). This analysis revealed a progressive unimodal population shift as the WT biosensor more closely overlays Y34A CDA5 over time, tracking with population level results. These data also suggest that the vast majority, if not all, of the *B. subtilis* cells are responding in a coordinated fashion to readjust to media conditions.

CDA5 detects unimodal c-di-AMP differences between Bacillus subtilis mutants

To better contextualize the biologic meaning of the FRET ratios detected in WT *B. subtilis*, we next sought to detect c-di-AMP differences between mutants defective in either a c-di-AMP cyclase or phosphodiesterase. As expected, Δ*pgpH*, a mutant lacking the phosphodiesterase PgpH, had higher Y/A ratios due to elevated c-di-AMP; while a mutant lacking the cyclase DisA, Δ*disA*, had lower Y/A ratios due to reduced c-di-AMP production (Fig 3.11A). All three strains experienced different degrees of FRET ratio decreases. Δ*disA* decreased most quickly, followed by WT, and Δ*pgpH* decreased minimally and remained elevated throughout the experiment. At the single cell level Y/A ratios for all strains again decreased in a unimodal fashion following the population average (Fig 3.11B-C 3.12A-F). More experiments will be required to elucidate the mechanism by which Δ*pgpH* but not other strains retain elevated c-di-AMP in reduced LB media. Importantly, these data provide convincing evidence that CDA5 detects physiologically relevant differences in c-di-AMP in *B. subtilis*.

CDA5 detects unimodal, potassium dependent, regulation of c-di-AMP

Due to the intimate relationship between c-di-AMP and both osmotic regulation and potassium dependent essentiality, we hypothesized that potassium supplementation might influence the c-di-AMP response in *B. subtilis*. To both test this hypothesis and simulate future experiments utilizing CDA5 to investigate environmental regulation, we supplemented LB media with either NaCl, KCl, or Sorbitol and measured FRET by flow cytometry. Although results had some stochasticity, KCl slightly inhibited the previously observed c-di-AMP decrease (Fig 3.13A). As this response was mild we turned to microscopy which is a more sensitive technique to further investigate the role of potassium in c-di-AMP regulation.

We first established a method to investigate the FRET responses of single cells by creating cell masks based on the light field image and then taking the average FRET ratio of each cell (Fig 3.13B). To further investigate the generality and single cells responses of potassium regulated c-di-AMP regulation we chose to investigate the relationship between potassium and c-di-AMP in the defined media MSgg by microscopy. We obtained a clear signal via microscopy (Fig 3.13B) and increased the potassium concentration in the agar pad rather than liquid media. In this assay we observed an entire population shift to higher c-di-AMP levels in accordance with increasing c-di-AMP (Fig 3.13C-D). Thus our results suggest both that c-di-AMP is regulated by potassium availability in *B. subtilis* and that CDA5 is a useful tool to investigate bacterial c-di-AMP dynamics.

Concluding Remarks

In this work we describe the development of CDA5, a FRET based biosensor capable of detecting the essential signaling molecule c-di-AMP within individual bacterial cells. Through rational design based on the Lmo0553 crystal structure, we were able to generate a stable biosensor which retains relevant native binding characteristics as well as a nucleotide blind control which improves measurement accuracy. In live cells, CDA5 allowed for the detection of c-di-AMP differences between mutants of *B. subtilis* as well as for the identification of potassium-dependent environmental adaptation to diluted complex media. Interestingly, analysis at the single cell level revealed unimodal c-di-AMP shifts providing evidence that the entire bacterial population responds in a coordinated fashion. This is particularly notable because it is in contrast to the bacterial nucleotide second messenger c-di-GMP which is regulated in a largely bimodal manner[143-145,147].

In addition to its ability to monitor native c-di-AMP regulation, CDA5 is also capable of facilitating diverse investigations of c-di-AMP in other contexts. CDA5 is easy to produce, specific, and provides a kinetic readout making it a good platform to study c-di-AMP enzymology. For example, CDA5 can be used to detect protein-protein or small molecule-dependent activation or inhibition of c-di-AMP cyclases and phosphodiesterases *in vitro*. Such work may allow for the development of new antibiotics targeting this essential signaling molecule. Some interactions, especially those of membrane associated proteins, are difficult to model with recombinant protein and are better investigated in an ectopic cytosolic environment[132]. CDA5 expressed in such a model system would facilitate these investigations. For example, CDA5 expressed in *E. coli* would provide a platform for the interrogation of important protein-protein interactions controlling c-di-AMP synthesis and degradation. Additionally, c-di-AMP is known to be detected but not produced by eukaryotic cells during infection and perhaps also by certain bacteria like *Pseudomonas aeruginosa* in multicellular environments[135,160]. CDA5 expressed by these organisms may be able to detect accumulated c-di-AMP accelerating these interesting investigations.

Although alternative uses are promising, the primary motivation for the development of the CDA5 biosensor was to more thoroughly and efficiently investigate native c-di-AMP regulation. Current tools, including our recently developed CDA-Luc assay, are well suited for detecting c-di-AMP at the population level but the ability to measure c-di-AMP kinetically or at the single cell level is lacking. Thus, CDA5 is a major advance which allows for a wealth of new investigations.

A major finding using the c-di-GMP biosensor was mother-daughter cell heterogeneity which allows for different roles within a population[143,144]. Similarly we hypothesize that there will be replication phase dependent c-di-AMP fluctuations in bacteria that naturally produce c-di-AMP. However, rather than mother-daughter cell heterogeneity, we hypothesize that the intracellular concentration of c-di-AMP is linked to periods of rapid peptidoglycan synthesis during bacterial elongation due to the close link between c-di-AMP and cell wall homeostasis. Such insights could lead to greater understanding of morphology and virulence differences between c-di-AMP mutants.

Furthermore, the c-di-GMP biosensor was recently utilized to detect regulation of c-di-GMP signaling during macrophage infection[147]. Due to the avirulence of mutants which hyper- or hypo-

produce c-di-AMP, we hypothesize that similar, if not more profound, regulation is occurring during infection of eukaryotic cells. Such investigations will help elucidate the role of c-di-AMP during infection for a multitude of clinically important organisms including *Streptococcus pneumoniae, Listeria monocytogenes,* and *Mycobacteria tuberculosis*[118,121,124-126,161].

CDA5, similarly to previous c-di-GMP biosensor studies[145], will also facilitate the identification of diverse environmental stimuli that regulate c-di-AMP at the population and subpopulation level. In this study, we detected a unimodal c-di-AMP response to specific environmental conditions but CDA5 can elucidate a more thorough understanding of c-di-AMP regulation via use of an arrayed media library containing a wide variety of nutrients and stress conditions. In addition to advancing basic biology, such studies may also facilitate the development of clinical interventions which alter intracellular c-di-AMP concentrations.

CDA5 is highly functional in its current form but future development will further improve utility. One such improvement is the use and subsequent optimization of alternative fluorophores. For example, a far-red shifted FRET pair could be utilized allowing for simultaneous non-overlapping fluorescence with BFP-tagged proteins[157,158,162,163]. Similarly, a BRET pair could be developed for c-di-AMP detection within mammalian tissue or biofilms[148,164,165]. Another type of improvement is modification of the nucleotide binding pocket to increase affinity or alter specificity. For example, it may be possible to engineer additional hydrogen bonding interactions to increase the affinity for c-di-AMP allowing for detection of lower concentrations of nucleotides. Such a sensor would be able to detect low levels of c-di-AMP found within a mammalian cytosol during infection or within a non-c-di-AMP producing bacteria in a biofilm environment. Similarly, the binding pocket of CDA5 may be able to be modified to detect the growing class of CBASS cyclic di-nucleotides produced as part of the anti-bacteriophage response[166]. A final type of improvement would be modification of the dimerization domain. It may be possible to reverse polar interactions in the dimerization domain to avoid potentially obfuscating interactions with full length Lmo0553. This would mainly be useful for investigations in *Listeria monocytogenes* or *Enterococcus faecalis* which respectively encode *lmo0553* or a homologue. Alternatively, unless Lmo0553 is the protein of interest, such studies could also be done in a *lmo0553* null background as no phenotype has been identified for this protein to date.

CDA5 is a powerful tool which makes a large class of investigations now feasible. In addition to current capabilities, there are clear next steps to modify CDA5 and apply it to even more diverse studies. Thus, CDA5 holds exceptional promise for accelerating our understanding of the essential bacterial signaling molecule, c-di-AMP.

Materials and Methods

Cloning

Primers for CDA5 cloning are listed in Supplementary Table 2, plasmids in Supplementary Table 3, and strains in Supplementary Table 2. CDA5 was generated by subcloning *lmo0553* from the previously generated pET28a-*lmo0553* vector using Kapa HiFi polymerase (Kapa Biosystems) using primers 1 and 2. The resulting product was ligated into pET15b-eCFP-12AA-eYFP using Spe1/Kpn1 fast digest restriction endonuclease cloning (Thermo Fisher) and transformed into XL1-Blue chemically competent *E. coli*. To generate pSLIK-CDA5, pET15b-CDA5 was amplified using primers 3 and 4 and added to the BsiW1 (Thermo Fisher) site of pSLIK using InFusion (Takara) then transformed into Stbl3-OneShot competent cells (Thermo Fisher). pET15b-CDA5-Y34A was made using site directed mutagenesis by amplifying the generated pET15b-CDA5 construct using primers 5 and 6 using Kapa HiFi polymerase. PCR product was purified (Promega) and digested using DpnI (NEB) and then transformed into XL1-Blue chemically competent *E. coli*. To generate pHT264-Bs-CDA5, a gBlock codon optimized for *Bacillus subtilis* expression (IDT) was purchased and amplified using primers 7 and 8. The resulting product was ligated into pET15b using Not1 fast digest restriction endonuclease cloning (Thermo Fisher) and transformed into XL1-Blue chemically competent *E. coli* generating pET15b-Bs-CDA5. pET15b-Bs-CDA5-Y34A was generated as above using primers 9 and 10. Finally, pHT264-Bs-CDA5 and pHT264-Bs-CDA5-Y34A were generated by amplifying pET15b-Bs vectors with primers 11 and 12. The resulting product was ligated into pHT264 using BamH1/SmaI fast digest restriction endonuclease cloning (Thermo Fisher) and transformed into XL1-Blue chemically competent *E. coli.*

Protein expression

To obtain *L. monocytogenes* full-length Lmo0553, pET28a-*lmo0553* vector with an N-terminal hexa-histidine tag was transformed into BL21 Star (DE3) cells. The cells were cultured in LB medium with 35 mg/L kanamycin and were induced for 14 h at 20 °C with 1 mM IPTG. A selenomethionine-derivative of Lmo0553 was expressed using a methionine-auxotroph *E. coli* BL21 strain, and the defined medium was supplemented with selenomethionine[167]. The protein was purified through nickel-agarose affinity chromatography followed by gel filtration chromatography (S-300, GE Healthcare). The purified protein was concentrated to 30 mg/mL in a buffer containing 20 mM Tris (pH 8.0), 250 mM NaCl, 5% (v/v) glycerol, and 5 mM dithiothreitol, flash-frozen in liquid nitrogen and stored at −80 °C. The N-terminal hexa-histidine tag was not removed for crystallization.

To obtain CDA5, pET15b plasmids encoding CDA5 and CDA5-Y34A were transformed into BL21 Star (DE3) cells. An overnight culture of the transformed bacteria was inoculated into 1 L of LB broth and grown and grown at 37°C until an OD_{600} between 0.5-0.7 at which point protein expression was induced by the addition of 0.1 mM isopropyl β-D-1-thiogalactopyranoside (IPTG) for 16-20 hours at 18°C. The protein was purified using nickel-agarose affinity chromatography

(Thermo Scientific). The protein was subsequently buffer exchanged (Cytiva) into Buffer A (40 mM Tris pH 7.5, 100 mM NaCl, 20 mM $MgCl_2$, 1mM DTT). Protein samples were tested for purity by SDS-PAGE followed by Coomassie Brilliant Blue staining. Samples were then flash-frozen in liquid nitrogen and stored at −80°C until use in biochemical assays. DisA, RECON, and PdeA were purified the same as above with the exception that they were induced with 1 mM IPTG at 37°C for 4 hours.

Protein crystallization

Crystals of Lmo0553 in complex with c-di-AMP were grown by the sitting-drop vapor diffusion method at 20 °C. The protein at 15 mg/mL was first incubated with 2.5 mM c-di-AMP for 30 min, and then mixed with reservoir solution containing 23% (w/v) PEG3350, and 0.2 M calcium acetate. The crystals were cryo-protected with the reservoir solution supplemented by 12% (v/v) glycerol and flash-frozen in liquid nitrogen for data collection at 100 K. Crystals of free Lmo0553 were grown by the sitting-drop vapor diffusion method at 20 °C. The protein at 16 mg/mL was mixed with a reservoir solution containing 1.4 M ammonium sulfate, and 0.1 M sodium citrate (pH 5). The crystals were cryo-protected with 20% (v/v) glycerol and flash-frozen in liquid nitrogen for data collection at 100 K.

Data collection, structure determination and refinement

X-ray diffraction data for Lmo0553 were collected on the X29A beamline at the National Synchrotron Light Source. The diffraction images were processed using HKL2000[168]. The structure was solved using the single-wavelength anomalous dispersion (SAD) method with selenomethionine-derivatized crystals, using the program PHENIX[169]. Manual rebuilding was carried out in Coot[170] and refinement was done with the program Refmac[171]. Data collection and refinement statistics are summarized in Table 1.

Radioactive nucleotide binding assays

[^{32}P] 3′3′-cyclic di-AMP was synthesized identically as previously described[149]. This nucleotide was then used to perform DRaCALA assays2. Briefly, binding assays were performed in Buffer A at room temperature. To determine binding affinities, two-fold serial dilutions of proteins were incubated with ~1 nM of radioactive 3′3′-cyclic di-AMP for 10 minutes then blotted onto nitrocellulose membranes and allowed to air dry. To determine binding specificity, samples were pre-incubated with 500 μM excess unlabeled nucleotides for 10 minutes followed by incubation with ~1 nM of radioactive 3′3′-cyclic-di-AMP for 10 minutes then blotted onto nitrocellulose membranes and allowed to dry. Finally, to determine the time frame of competition, ~1 nM of radioactive 3′3′-cyclic di-AMP was preincubated with protein for 10 minutes at which point 500 μM of unlabeled 3′3′-cyclic-di-AMP was added, mixed, and blotted onto nitrocellulose membranes every two seconds and allowed to dry. [^{32}P] radioactivity was visualized by exposure onto Phosphor-Imager screens, which were developed using a Typhoon FLA 9000 biomolecular imager (GE Healthcare).

***In vitro* FRET measurements**

In all assays, 2 μM of CDA5 or CDA5-Y34A was incubated in black flat bottom half volume opaque 96-well plates (Greiner Bio-One). For nucleotide response assays, two fold dilutions of

3′3′-c-di-AMP (Invitrogen) were made in molecular grade water and added to the protein solution. eCFP and FRET fluorescence was monitored at room temperature using a fluorimeter (BioTek Synergy H1 Hybrid Reader, Biotek Instruments) at 425 nm excitation and read at 480nm and 535nm emission wavelengths for eCFP and FRET respectively. PdeA enzyme activity assay was performed as above with the exception that: Buffer A was supplemented 20 mM $MnCl_2$, two fold dilutions of PdeA rather than c-di-AMP were added to each well, samples were spiked with 2 μM c-di-AMP at t=0 and t=90 minutes, and the assay was monitored every 5 minutes.

Eukaryotic CDA5 specificity assays

Assays were performed similarly as previously described[149]. Briefly, Human Embryonic Kidney (HEK) 293T cells were grown in Glutamax Dulbecco's Modified Eagle Medium (DMEM) (Gibco) supplemented with 10% (v/v) heat-inactivated FBS (HyClone) and 100 U mL^{-1} penicillin and 100 μg mL^{-1} streptomycin and maintained at 37°C and 5% CO2 in a humidified incubator. Self-inactivating lentivirus was made via transfection of a semi-confluent 10 cm dish of HEK293T cells with 4 μg of psPAX2, 2 μg of pCMV-VSV-G, and 4 μg of pSLIK lentiviral vector using Poly(ethyleneimine) (PEI). Growth media was replaced 24 hours after transfection and supernatants collected at 48 and 72 hours, pooled, and filtered through a 0.45 μm filter. Lentivirus was then concentrated with a Lenti-X concentrator (Takara) and added to 4 million HEK293T cells seeded on a 10 cm plate and spinfected for 1 hour at 500X g. After a 24 hour recovery period, media was replaced and supplemented with 2 μg mL^{-1} puromycin (Gibco). Transduced cells were continually passaged and maintained in selection media containing puromycin. For FRET measurements, 750,000 HEK293T cells transduced with the doxycycline inducible pSLIK-CDA5 plasmid were plated in a 6-well culture dish. The subsequent day, cells were transfected with indicated concentrations of cyclase-encoding plasmids using PEI transfection reagent. One hour after transfection, biosensor expression was induced by the addition of Doxycycline Hydrochloride (Sigma-Aldrich) at 2 μg mL^{-1}. The next day, cells were harvested via resuspension in room temperature PBS and CDA5 FRET measurements were collected by FACS analysis. Cells were analyzed using a LSR II flow cytometer (BD) with the following voltages: FSC-350 SSC-240 V500-350 Pacific Blue-420 GFP-400. Data was analyzed using FlowJo software (Tree Star)

Bacterial FRET measurements

E. coli FRET measurements were obtained by transforming BL21 Star (DE3) cells with pET15b-CDA5 and pET15b-CDA5-Y34A in combination with either pBAVE-EV or pBAVE-DacA and plated on LB Carb 100 μg mL^{-1} Kan 50 μg mL^{-1} plates. An overnight culture of the transformed bacteria was inoculated into 1 L of LB broth and grown and grown at 37°C until an OD_{600} between 0.5-0.7 at which point protein expression was induced by the addition of 0.1 mM isopropyl β-D-1-thiogalactopyranoside (IPTG) for 16-20 hours at 18°C. At this point, cells were spun down and resuspended in room temperature PBS and CDA5 FRET measurements collected by FACS analysis. Cells were analyzed using a LSR II flow cytometer (BD) with the following voltages: FSC-400 SSC-200 V500-500 Pacific Blue-600 GFP-400. Data was analyzed using FlowJo software (Tree Star)

B. subtilis FRET measurements were obtained by transforming B. subtilis with pET264-CDA5 and pET264-CDA5-Y34A and plating cells on LB Carb 100 μg mL^{-1} plates and incubated at 37°C. Single colonies were then struck onto LB Carb 100 μg mL^{-1} IPTG 1 mM plates and incubated overnight at 30°C. The resulting single colonies were harvested in 10% LB media (FRET

detectable up to 30% LB media) and clumps dissociated by passing cells 2-3 times through a 27 gauge needle. Cells were then grown shaking at 37°C until desired time points at which CDA5 FRET measurements were collected by FACS analysis. Cells were analyzed using a LSR II flow cytometer (BD) with the following voltages: FSC-400 SSC-200 V500-450 Pacific Blue-550 GFP-375. Data was analyzed using FlowJo software (Tree Star).

Mass spectrometry

The OD_{600} of *B. subtilis* samples was taken. Then, half of the sample was analyzed by FACS analysis and the other half pelleted and frozen for c-di-AMP extraction. Cell pellets were resuspended in 50 µL of 0.5 µM heavy-labeled (C13 N15) c-di-AMP, then mixed with 500 µL of methanol and sonicated. The sample was pooled, centrifuged, and supernatant saved. The resulting pellet was resuspended in 50 µL water then mixed with 500 µL methanol and sonicated again. The solution was centrifuged and the second supernatant pooled with the first. The extract was then dried using a speed vacuum concentrator. The resulting film was resuspended in 50 µL of molecular grade water and measured by mass spectrometry as described[121].

Figures and Tables:

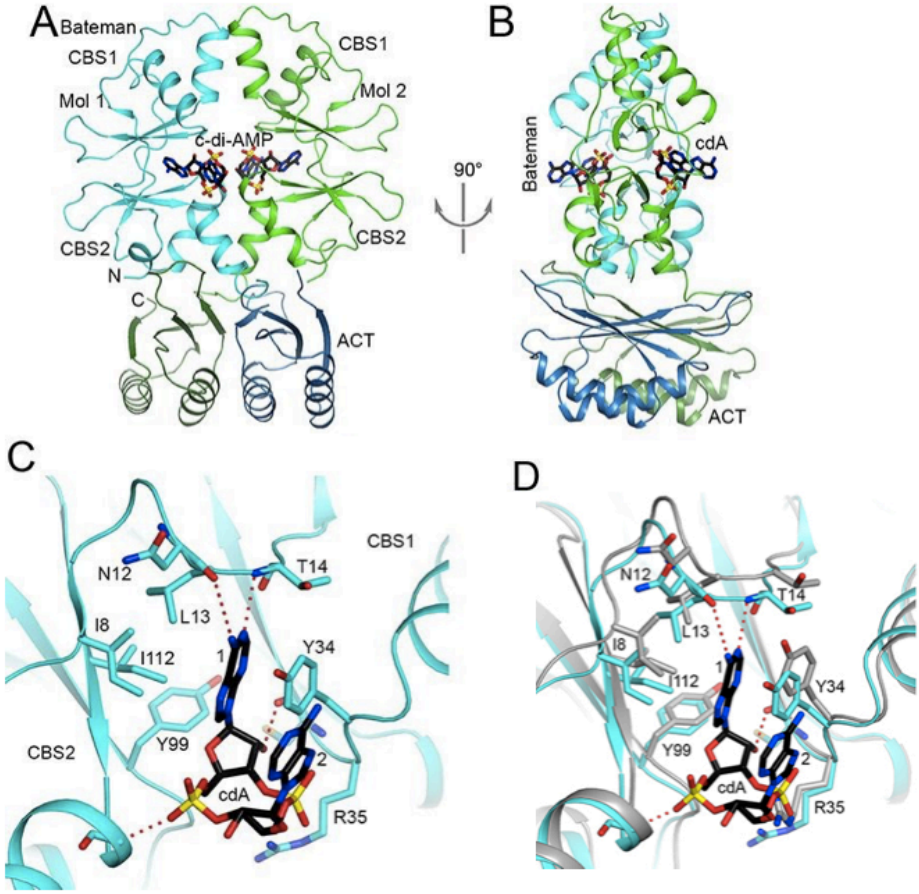

Figure 3.1: Crystal structure of Lmo0553 in complex with c-di-AMP
(A) Schematic drawing of the Lmo0553 dimer bound to two c-di-AMP (cdA) molecules. The CBS motifs and the ACT domain of one monomer are colored in cyan and dark blue, respectively, and those of the other monomer in green and dark green. **(B)** Schematic drawing of the Lmo0553 dimer bound to two c-di-AMP (cdA) molecules, viewed after a 90° rotation around the vertical axis. **(C)** Detailed interactions between Lmo0553 and c-di-AMP. The first and second nucleotides of c-di-AMP are labeled 1 and 2, respectively. Hydrogen-bonding interactions are shown as a dashed line (red). **(D)** Conformational changes in the c-di-AMP binding site. Overlay of the structure of Lmo0553 in complex with c-di-AMP (in color) with that of free Lmo0553 (in gray). All structure figures were produced with PyMOL (www.pymol.org).

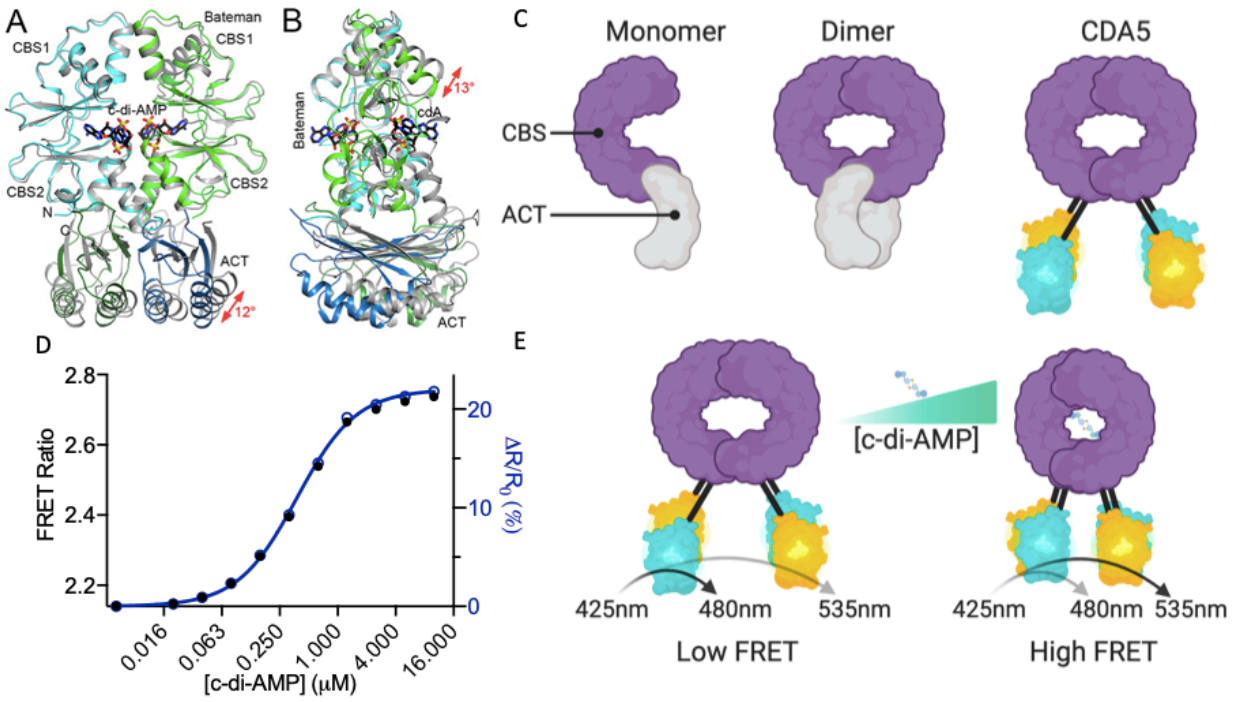

Figure 3.2: Binding c-di-AMP induces a large structural change in Lmo0553 guiding development of CDA5

(A) Overlay of the structure of Lmo0553 in complex with c-di-AMP (in color) with that of free Lmo0553 (in gray). The Bateman domain of one monomer (cyan) is overlaid, in order to visualize the changes in the position of the other domains in the dimer. The conformational change in the ACT domain is indicated by the red arrow. **(B)** Same as panel A, but viewed after a 90° rotation around the vertical axis. The conformation change in the CBS domain is indicated by the red arrow. **(C)** Model of the restructuring used to generate the CDA5 biosensor **(D)** Recombinant CDA5 FRET response to increasing concentrations of c-di-AMP using 425nm excitation and 480nm and 535nm emission wavelengths. Data presented as individual n=1 data points. **(E)** Schematic of CDA5 FRET increase upon c-di-AMP binding. Panels **A** and **B** were produced with PyMOL (www.pymol.org). Panels **C** and **E** were produced using RioRender (www.biorender.com)

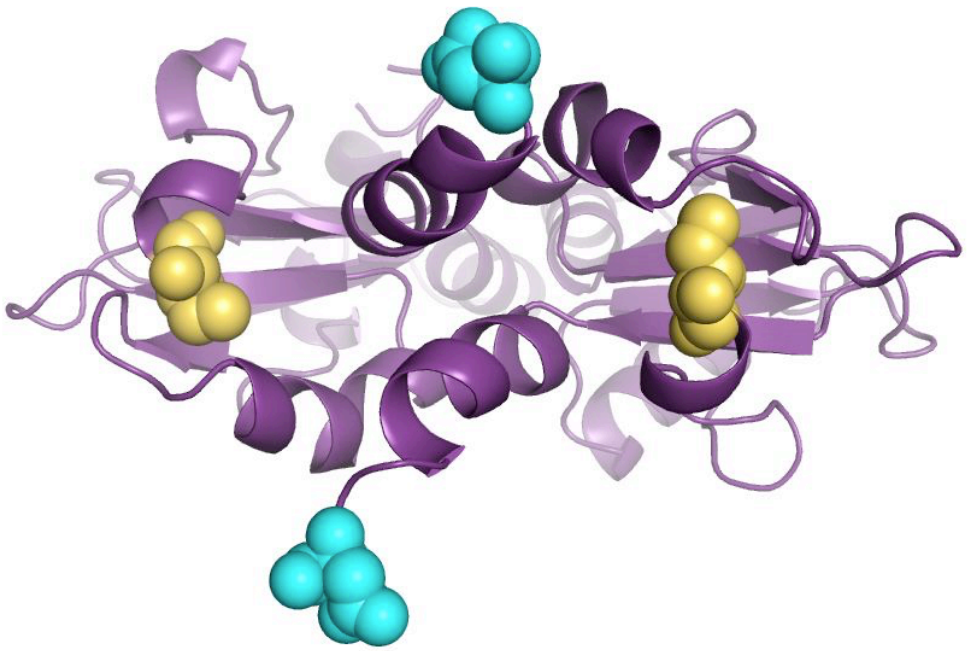

Fig 3.3: CBS domain structural rearrangement upon c-di-AMP binding
Movie models the rearrangement of Lmo0553 upon c-di-AMP binding. Yellow and Cyan denote location of eYFP and eCFP fusion respectively. Made using PyMol (www.PyMol.com)

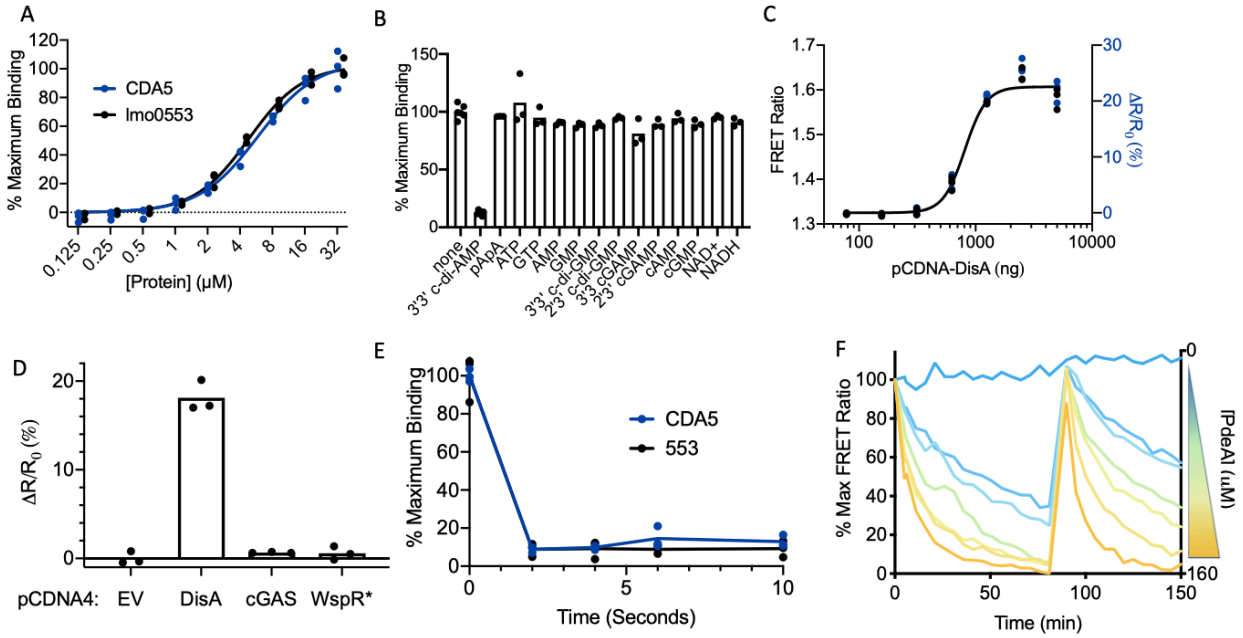

Figure 3.4: CDA5 retains native and physiologically relevant binding characteristics
(A) DRaCALA radioactive nucleotide binding assay of CDA5 (blue) and full length Lmo0553 (black) using ~1nM [^{32}P] labeled 3′3′-c-di-AMP. Data fit to a nonlinear curve. Radioactive c-di-AMP bound Lmo0553 and CDA5 at 2.83 μM and 5.87 μM respectively. **(B)** DRaCALA radioactive nucleotide binding assay of CDA5 using ~1nM [^{32}P] labeled 3′3′-c-di-AMP in the presence of excess (500 μM) unlabeled nucleotides. Corresponding full length Lmo0553 competition assay is Fig S3B. **(C)** HEK293T cells stably expressing CDA5 were transfected with increasing concentrations of pCDNA4-DisA and analyzed for FRET response by flow cytometry. **(D)** HEK293T cells stably expressing CDA5 were transfected with 2000 ng of expression vectors for DisA, cGAS, WspR*, or empty vector and analyzed for FRET response by flow cytometry. **(E)** DRaCALA radioactive nucleotide binding assay time course of CDA5 (blue) and full length Lmo0553 (black) using ~1nM [^{32}P] labeled 3′3′-c-di-AMP in the presence of excess (500 μM) unlabeled c-di-AMP. **(F)** PdeA phosphodiesterase activity assay time course in the presence of decreasing concentrations of recombinant PdeA (2 fold dilutions from 160μM) monitored using CDA5. 2 μM c-di-AMP was re-spiked into the solution at 90 minutes. In panels **A-E** data are presented as n=3 biological replicates. Panel **F** is presented as individual n=1 data points connected by a line.

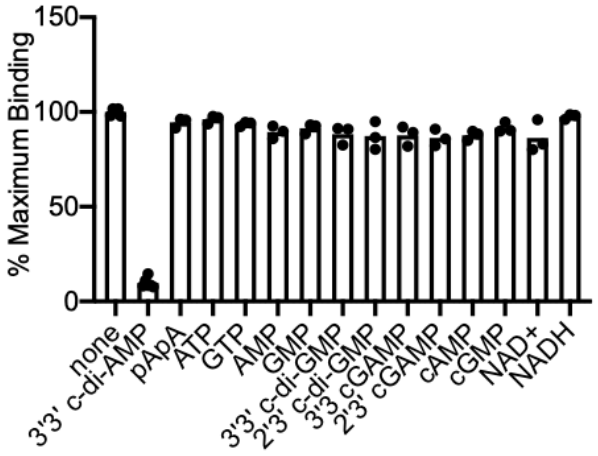

Fig 3.5: Lmo0553 DRaCALA specificity assay
DRaCALA radioactive nucleotide binding assay of full length Lmo0553 using ~1nM [^{32}P] labeled 3′3′-c-di-AMP in the presence of excess (500 μM) unlabeled nucleotides. Data are presented as n=3 biological replicates.

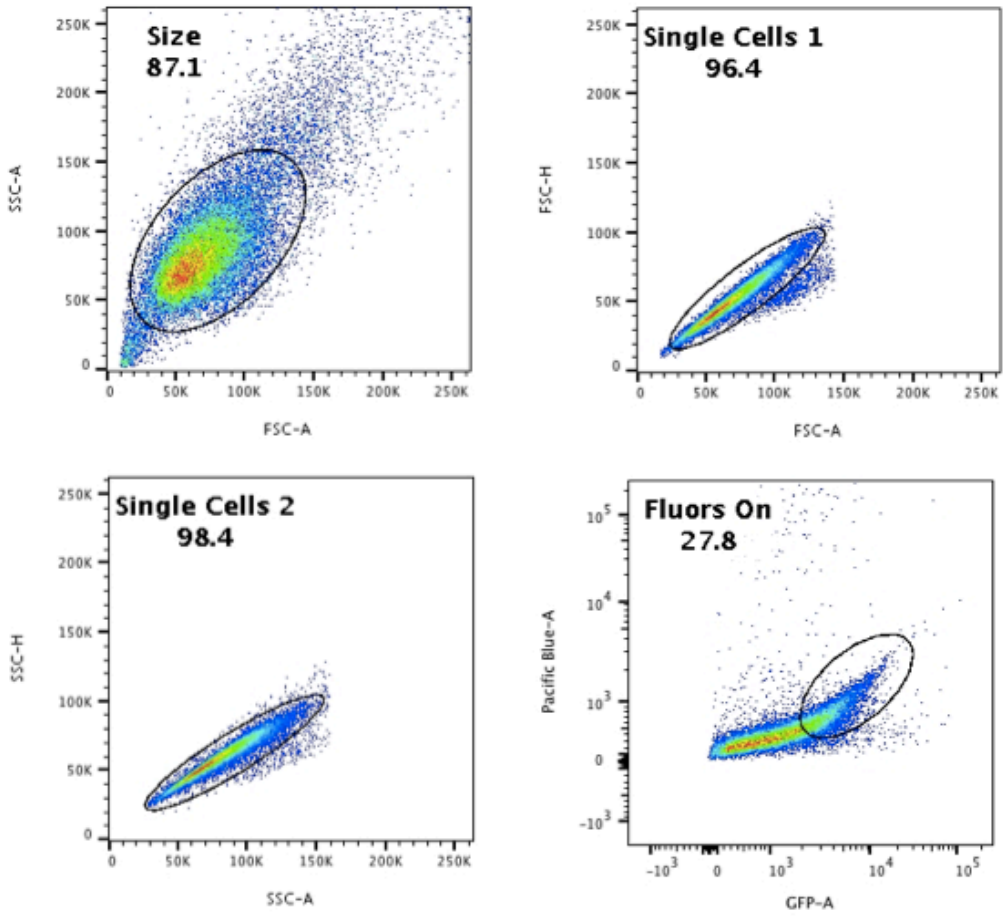

Fig 3.6: Flow sort method for HEK 293T cells.
Cells were sorted using the following gating strategy. All cells in the 'Fluors On' gate were analyzed.

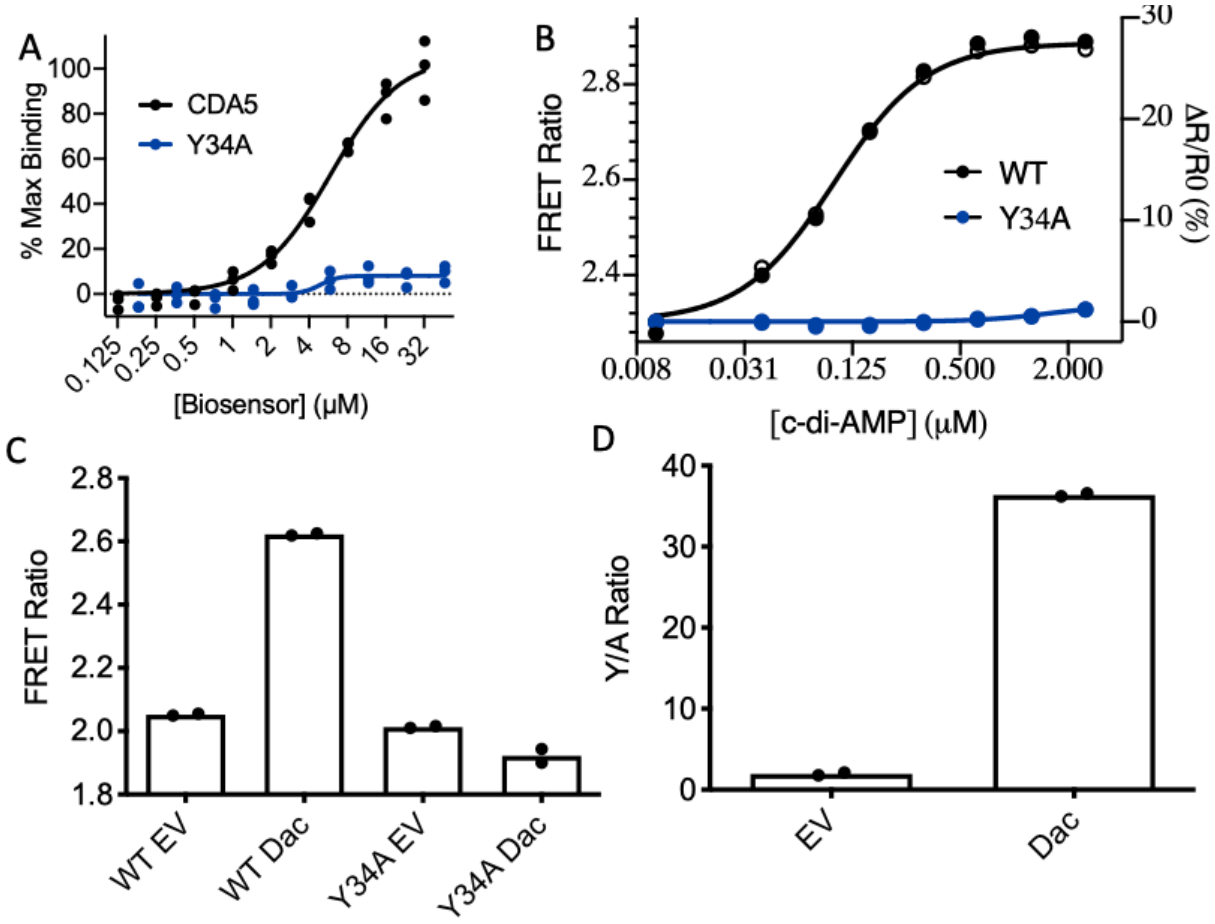

Figure 3.7: CDA5 Y34A is an important c-di-AMP blind control
(A) DRaCALA radioactive nucleotide binding assay of CDA5 WT (black) and Y34A (blue) using ~1nM [^{32}P] labeled 3′3′-c-di-AMP. **(B)** Recombinant CDA5 WT (black) and Y34A (blue) FRET response to increasing concentrations of c-di-AMP. **(C)** BL21 (DE3) E. coli transformed with pET15b-CDA5 (WT or Y34A) and pBAV-dacA or empty vector then analyzed by flow cytometry. **(D)** Data in panel C converted into Y/A ratio. Data in panel A is presented as n=3 biological replicates. Panel **B** is presented as individual n=1 data points. Data in panels **C** and **D** are presented as n=2 biological replicates.

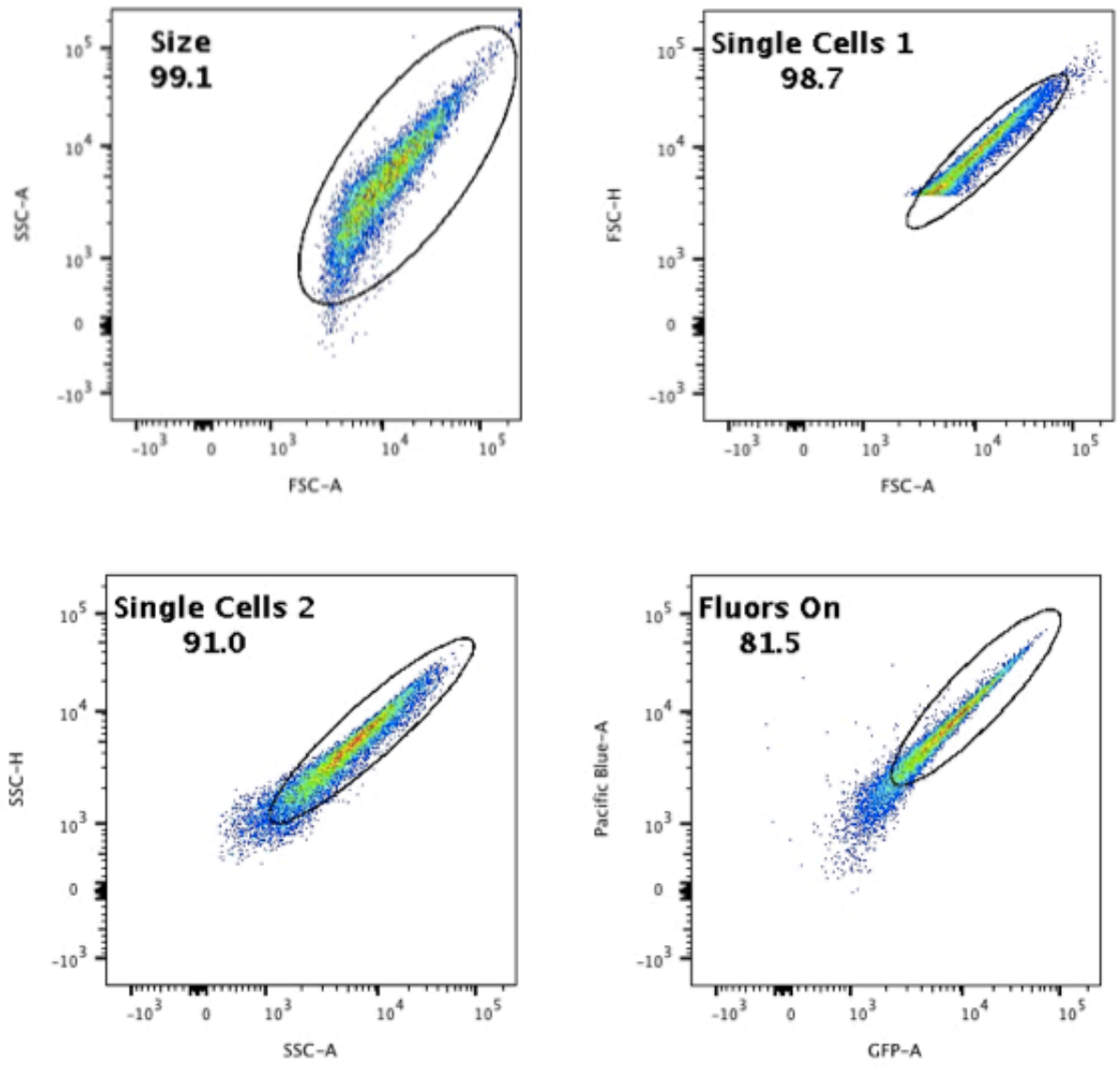

Fig 3.8: Flow sort method for *E. coli*.
Cells were sorted using the following gating strategy. All cells in the 'Fluors On' gate were analyzed.

Figure 5. CDA5 allows for the detection of native c-di-AMP dynamics in single cells

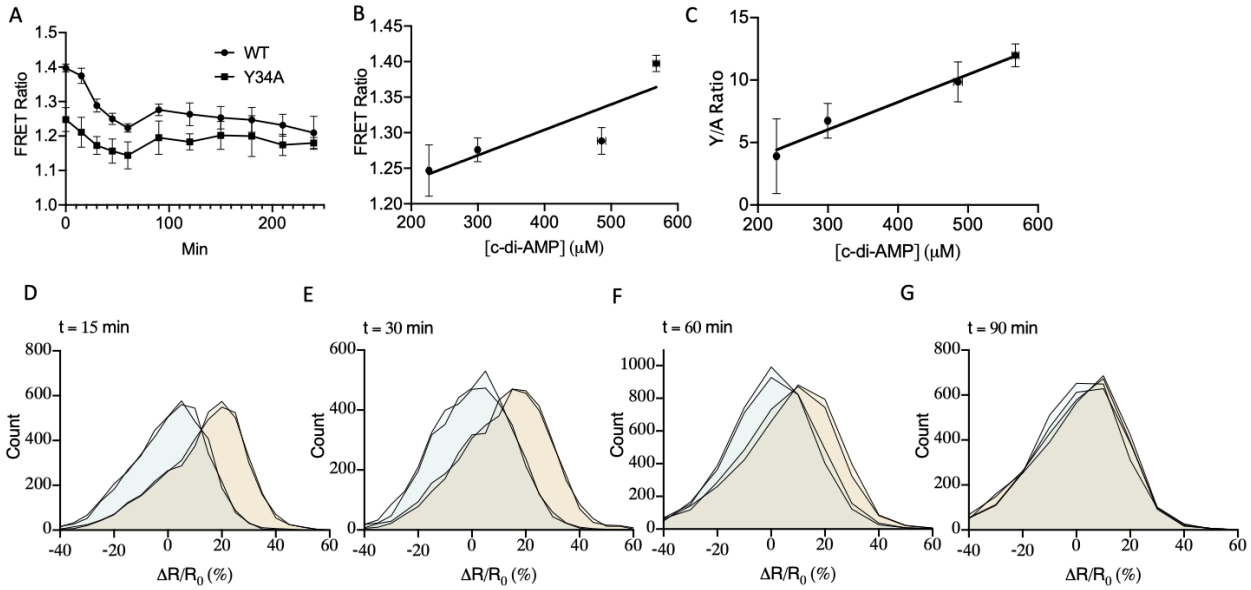

Figure 3.9: CDA5 allows for the detection of native c-di-AMP dynamics in single cells
(A) B. subtilis expressing CDA5 WT (black) and Y34A (blue) back diluted into 10% LB media and grown at 37°C and analyzed for FRET response by flow cytometry **(B)** CDA5 WT FRET ratio in panel A plotted versus c-di-AMP quantitated by mass spectrometry. **(C)** CDA5 Y/A ratio in panel A plotted versus c-di-AMP quantitated by mass spectrometry. **(D-G)** CDA5 WT FRET ratio of single cells divided by the average CDA5 Y34A FRET ratio plotted as histograms at indicated time points. Data in panels **A-C** are presented as mean and standard deviation of n=3 biological replicates. Data in panels **D-G** are presented as histograms consisting of individual data points of n=2 replicates. Blue and orange histograms respectively represent CDA5 Y34A and CDA5 WT.

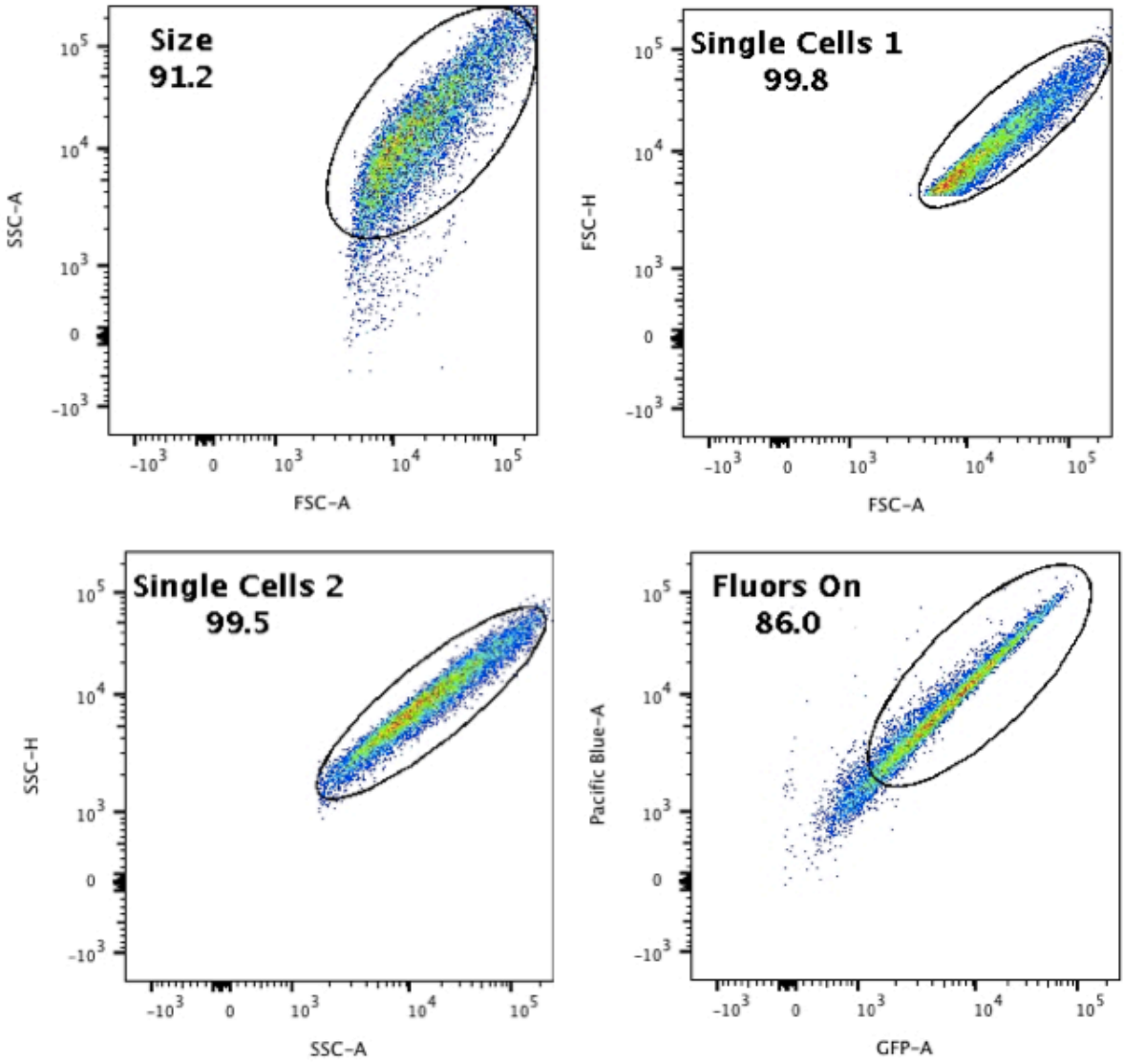

Fig 3.10: Flow sort method for *B. subtilis*.
Cells were sorted using the following gating strategy. All cells in the 'Fluors On' gate were analyzed.

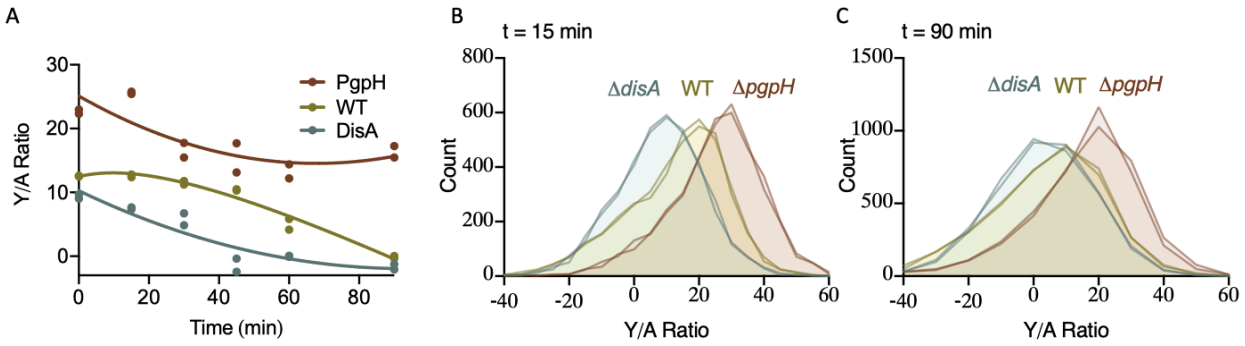

Figure 3.11: CDA5 detects varied c-di-AMP dynamics in *B. subtilis* mutants
(A) WT (yellow), ΔpgpH (red), and ΔdisA (blue) *B. subtilis* back diluted into 10% LB media and grown at 37°C and analyzed for FRET response by flow cytometry presented as Y/A ratios **(B-C)** CDA5 WT FRET ratio of single cells divided by the average CDA5 Y34A FRET ratio plotted as histograms at indicated time points. Data in all panels are presented as individual data points of n=2 biological replicates.

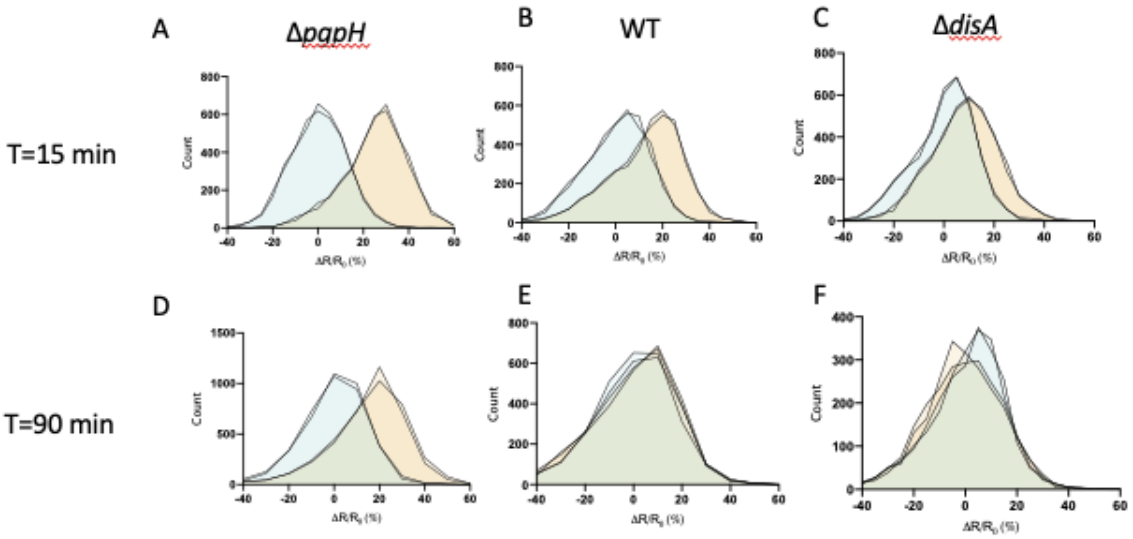

Fig 3.12: CDA5 WT and CDA5 Y34A single cell data. (A-F)
CDA5 WT and CDA5 Y34A FRET ratios of single cells divided by the average CDA5 Y34A FRET ratio plotted as histograms of indicated time points and *B. subtilis* strains

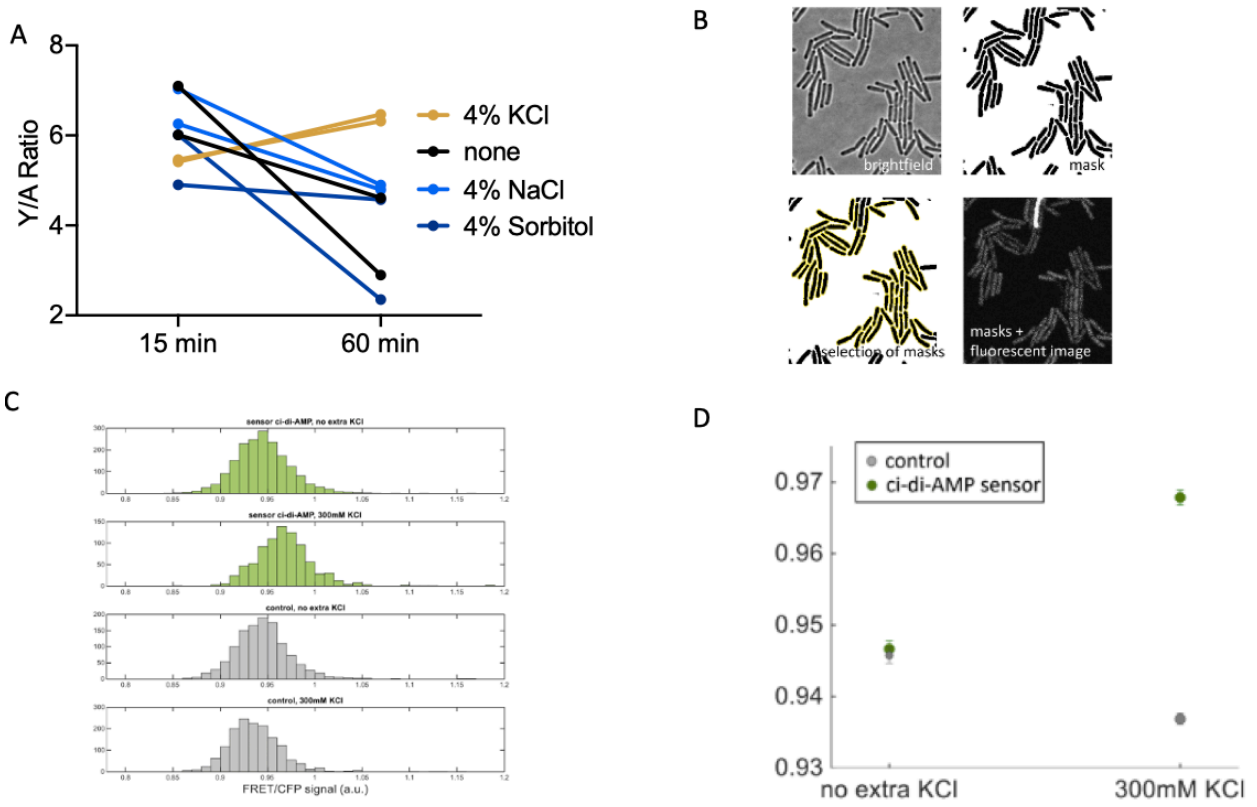

Figure 3.13: Potassium is an environmental factor that controls c-di-AMP
(A) WT *B. subtilis* back diluted into 10% LB media supplemented with various osmolytes and grown at 37°C and analyzed for FRET response by flow cytometry at 15 and 60 minutes, presented as Y/A ratios. **(B)** Method of cell segregation used in panels **C** and **D**. **(C)** Preliminary data indicating a unimodal FRET increase in the presence of potassium. **(D)** Average FRET ratios for panel **C**. Data in panel **A** is presented as individual data points of n=2 biological replicates.

Table 1: Summary of Crystallographic Information

	Lmo0553-c-di-AMP complex	Free Lmo0553
Space Group	$P3_121$	$P2_1$
Cell dimensions a, b, c (Å) α, β, γ (°)	87.8, 87.8, 107.2 90, 90, 120	37.2, 70.6, 88.7 90, 99.8, 90
Resolution[1]	50-1.60 (1.66-1.60)	50-2.48 (2.57-2.48)
*R*merge (%)	5.5 (43.4)	9.7 (37.3)
I/σI	32.9 (5.2)	10.3 (2.6)
Redundancy	8.1 (8.1)	2.9 (2.7)
Completeness	100 (100)	97 (97)
R_{work} (%)	16.7 (19.8)	22.1 (31.5)
R_{free} (%)	20.2 (22.7)	28.1 (38.6)
Average B-factors Protein Ligand/ion Water	21.3 15.7 28.7	46.5 – –
R.m.s deviation bond lengths (Å)	0.014	0.011
R.m.s deviation bond angles (°)	1.6	1.5
PDB Accession Code		

Table 2: Primers used in this study

Primer	Sequence	Name	Description
1	GAGGAGactagtatgTTGATAAAAAACCTTTGTATCCCTAAAATAAATTTAACAAC	lmo0553 CBS F	Amplify the CDA5 Lmo0553 scaffold
2	GAGGAGggtaccATTCCAGCCATCTTGGAGCAAAC	lmo0553 CBS R	
3	tgatcactagcgtacgaccATGGTTAGCAAGGGAGAGGAGC	CDA5 pSLIK F	Amplify CDA5 for lentiviral expression
4	tcttccaattcgtacgTTACTTATAAAGCTCATCCATTCCATGTGTAATTCC	CDA5 pSLIK R	
5	GGCTATCCATTTACTTGAAGAATCTGGTGCTCGCTGTGTTCCTGTATTAGACG	CDA5 Y34A F	Quickchange to make Y34A
6	CGTCTAATACAGGAACACAGCGAGCACCAGATTCTTCAAGTAAATGGATAGCC	CDA5 Y34A R	
7	GAGGAGggcggccgcATGGTAAGTAAAGGAGAGGAGTTGTTC	Bs CDA5 gBlock F	Amplify Bs-CDA5 gBlock for subcloning
8	GAGGAGgcggccgccTTTATACAGTTCGTCCATACCGTGTG	Bs CDA5 gBlock R	
9	CTTCTGGAGGAGTCCGGGGCCAGATGCGTCCCTGTGC	Bs CDA5 Y34A F	Quickchange to make Bs-CDA5-Y34A
10	GCACAGGGACGCATCTGGCCCCGGACTCCTCCAGAAG	BS CDA5 Y34A R	
11	GAGGAGggatccATGGTAAGTAAAGGAGAGGAGTTGTTC	pHT264 BS CDA5 F	Amplify Bs-CDA5 for B. subtilis expression
12	GAGGAGcccgggTTATTTATACAGTTCGTCCATACCGTGTG	pHT264 BS CDA5 R	

Table 3: Plasmids used in this study

Plasmid	Name	Description	Source
1	pET28b-lmo0553	E. coli expression vector for Lmo0553	[1]
2	pet20b-DisA	E. coli expression vector for DisA	[1]
3	pSPEEDET-mRECON	E. coli expression vector for RECON	[2]
4	pET28b-PdeA(84-657)	E. coli expression vector for soluble PdeA	[3]
5	pcDNA3-empty vector	Control transient expression vector	Gift from Genhong Cheng
6	pcDNA4-DisA	Transient expression vector for DisA	Gift from Philip Kranzusch
7	pcDNA4-WspR*	Transient expression vector for WspR*	Gift from Philip Kranzusch
8	pcDNA3-cGAS	Transient expression vector for cGAS	Gift from Genhong Cheng
9	pET15b-eCFP-12AA-eYFP	Vector for FRET cloning	Gift from Samuel Miller
10	pET15b-CDA5	E. coli expression vector for CDA5	This study
11	pSLIK-CDA5	Lentiviral expression vector for CDA5	This study
12	pET15b-CDA5-Y34A	E. coli expression vector for CDA5-Y34A	This study
13	pET15b-Bs-CDA5	Subcloning vector for Bs-CDA5	This study
14	pET15b-Bs-CDA5-Y34A	Subcloning vector for BS-CDA5-Y34A	This study
15	pHT264 BS CDA5	B. subtilis expression vector for CDA5	This study
16	pHT264 BS CDA5 -Y34A	B. subtilis expression vector for CDA5-Y34A	This study

Table 3 references:

1. Sureka, K. *et al.* The cyclic dinucleotide c-di-AMP is an allosteric regulator of metabolic enzyme function. *Cell* **158**, 1389–1401 (2014).
2. McFarland, A. P. *et al.* Sensing of Bacterial Cyclic Dinucleotides by the Oxidoreductase RECON Promotes NF-κB Activation and Shapes a Proinflammatory Antibacterial State. *Immunity* **46**, 433–445 (2017).

3. Witte, C. E. *et al.* Cyclic di-AMP is critical for Listeria monocytogenes growth, cell wall homeostasis, and establishment of infection. *MBio* **4**, e00282–13 (2013).

Table 4: Strains used in this study

Number	Name	Description	Source
1	WT	*B. subtilis* strain 168	Purchased from Bacillus Genetic Stock Center
2	Δ*disA*	*B. subtilis* strain 168 Δ*disA*	
3	Δ*pgpH*	*B. subtilis* strain 168 Δ*pgpH*	

Chapter 5

Conclusions and future directions

SUMMARY OF FINDINGS

Our understanding of 3′3′-c-di-AMP and 2′3′-cGAMP has rapidly expanded in the past 10 years. Knowledge of c-di-AMP has grown from its identification as a bacterial molecule which stimulates an interferon response to wide investigations of c-di-AMP's essentiality and roles in virulence, central metabolism, cell wall homeostasis, osmoregulation, and even Cyanobacteria light/dark cycling. Interest in cGAMP has expanded even more rapidly from its identification as a small molecule produced by cGAS in response to double stranded DNA to clinical trials utilizing non-hydrolysable cGAMP analogues as immune adjuvants and to synergize with immunotherapies.

Despite its increasing clinical relevance, there is a remarkable lack of tools for cGAMP measurement. Mass spectrometry, EIA assays, and, more recently, a coupled enzyme assay, are the only options for quantitative detection. These assays are sensitive but only provide a destructive population level snapshot of nucleotide levels. Qualitatively, there is both fluorescently tagged STING which transits to the nucleus upon stimulation and, more recently, interferon regulated florescent reporters. Although these are useful tools, they are highly qualitative and only indirectly report on cGAMP. To remedy this problem, we developed a reversible, sensitive, and genetically encodable Förster resonance energy transfer (FRET) based biosensor using murine STING as a scaffold which we deemed BioSTING. In this work, we show that recombinant BioSTING is a useful kinetic tool for cyclic-di-nucleotide detection that may facilitate drug screening campaigns and that BioSTING is an exceptionally sensitive intracellular tool for cGAMP detection. Expressed in mammalian cells, we are not only able to detect physiologically relevant concentrations of cGAMP but also can localize BioSTING to specific compartments to detect spatiotemporal cGAMP dynamics. In all, BioSTING is a powerful tool which will facilitate both academic and applied investigations of this important immune signaling molecule.

C-di-AMP, despite increasing recognition of its importance, also lacks powerful quantification methods. C-di-AMP quantification is limited to mass spectrometry and an EIA assay which, similarly, only provides snapshots of the population average and is not amenable to screening campaigns. There is also a reported c-di-AMP riboswitch-based biosensor but its dependence on an exogenous ligand, uncontrolled signal, and physiological irreversibility have prohibited use beyond its development. To remedy this lack of tools, we generated both a rationally designed c-di-AMP FRET biosensor which we deemed CDA5 and a luminescence-based coupled enzyme assay which we deemed CDA-Luc. CDA5 was designed based on the crystal structure of the c-di-AMP binding protein, Lmo0553. CDA5 detects c-di-AMP specifically, reversibly, in single cells, and at physiological concentrations. While characterizing CDA5 we discovered that, interestingly, c-di-AMP levels follow a unimodal distribution across *B. subtilis* populations in all conditions for all mutants tested. Furthermore, we found that our coupled enzyme assay, CDA-Luc, allows for equivalent sensitivity to commercial c-di-AMP EIA assays at a fraction of the cost. Together, these tools make possible both targeted and unbiased elucidation of c-di-AMP dynamics. Such investigations will greatly improve our understanding of this essential signaling molecule.

FUTURE DIRECTIONS

This work opens the opportunity for a wealth of exciting investigations elucidating new facets of cyclic dinucleotide biology. Due to our FRET biosensors' compatibility with flow cytometry, these assays are amenable to high throughput screens. Additionally, the kinetic response of these biosensors allows for targeted time course investigations to elucidate subtle subpopulation dynamics. Finally, the genetic encodability of these sensors allow for flexible expression between cell types and subcellularly.

CDA5 will facilitate diverse investigations of bacterial c-di-AMP regulation. Currently, very few environmental signals are known to regulate c-di-AMP. Pairing the *B. subtilis* system established here with arrayed media plates (such a Biolog) will elucidate environmental signals influencing c-di-AMP regulation. Further investigations using both CDA5 and CDA-Luc will help uncover the underlying molecular pathways. Similarly, flow sorting of an arrayed or stochastic mutant library expressing CDA5 would allow for the identification of new factors that contribute to c-di-AMP homeostasis.

In addition to unbiased screens, CDA5 will also facilitate targeted studies of c-di-AMP regulation. Due to c-di-AMP's link to cell wall homeostasis, we hypothesize that c-di-AMP levels may be linked to bacterial replication, during which, cell wall must be rapidly remodeled. Following FRET levels through individual cells lifecycle will provide a unique opportunity to investigate such growth dependent regulation patterns. Similarly, investigations can be performed to investigate c-di-AMP regulation during infection. Due to the severe virulence defect of mutants with high and low c-di-AMP, we hypothesize that c-di-AMP is regulated during pathogenesis. If the eCFP/eYFP fluorophores are replaced with a FRET pair having less overlap with mammalian cell autofluorescence, such as the far red shifted 'Booster' or the mTFP/mKO2 FRET pair, c-di-AMP levels could be measured in mammalian cells to elucidate such regulation.

BioSTING is similarly amenable to diverse unbiased and targeted investigations. Currently, there is immense interest in identifying factors influencing the cGAS/STING pathway for use in applied therapies. Use of BioSTING in an unbiased CRISPR screen setting could facilitate the identification of a multitude of new factors. For example, screening for high FRET in a cGAS inactive background would identify proteins which are either negative regulators of cGAS or which directly interact with the CBS domain of BioSTING. Screening in a cGAS active background for low FRET would identify proteins which influence cGAS activation. Screens which have been carried out to date are based on indirect, downstream interferon reporters which can be influenced by many factors. A BioSTING-based screen would only be influenced by genes altering DNA access to cGAS, cGAS activity, and proteins which directly bind BioSTING. Such targeted results would greatly facilitate follow-up investigations.

BioSTING is also useful for a wealth of targeted investigations. For example, BioSTING is a powerful tool for the investigation of contentious aspects of cGAS regulation such as activity localization. Time course investigations with differentially localized BioSTING in response to various stimuli will provide key evidence as to the localization of cGAS activity. Additionally, BioSTING can detect of cGAS activity in single cells within a population. Such studies which will

help elucidate which cells within a population are responsible for cGAMP production and any stochasticity.

BioSTING's utility can be expanded with the replacement of mTFP/mKO2 with the recently described 'Booster' FRET pair which acts in the far-red spectrum. This FRET pair is compatible with *in vivo* and *ex vivo* imaging and would provide a powerful tool for academic and clinical investigations. For example, 'Booster' BioSTING expressed in a mouse would make possible diverse investigations of cGAMP accumulation and localization during infection. Follow up studies could even extract single cells and implicate specific cell types with this response. Clinically, a tumor model expressing 'Booster' BioSTING could be employed in a mouse model to investigate the thoroughness of cGAMP or cGAMP analogue penetration into the tumor microenvironment. Such investigations would be invaluable to preclinical investigations and help improve therapies.

Finally, with a strong pipeline for engineering FRET biosensors in place, future FRET biosensors can be developed to investigate other important pathways. Currently, no alternative methods appear likely to replace intramolecular FRET biosensors. Protein design, although powerful, is still in its infancy in regards to small molecule binding, particularly to small molecules with flexibility. Additionally, binding affinity is difficult to accurately predict. Until protein design is further developed, use of natural FRET biosensors is preferrable due to existing physiologically relevant binding kinetics. Additional FRET biosensors could be generated for molecules such as oligo-adenylate, which is produced by oligoadenylate synthase (OAS) upon recognition of double stranded RNA (dsRNA), by adapting the effector protein RNAseL. Similarly, FRET biosensors could be generated for nucleotides produced by cyclic-oligonucleotide-based anti-phage signaling systems (CBASS) such as 3′3′-cGAMP by adapting effector proteins.

In summary, the field of cyclic dinucleotide research is largely untapped. Future investigations will elucidate important biology relevant in human health. The tools I have developed during my PhD will help uncover this fascinating biology in the years to come.

Literature Cited

1. Janeway, C. A. & Medzhitov, R. Innate Immune Recognition. *Annual Review of Immunology* **20**, 197–216 (2002).
2. Zaver, S. A. & Woodward, J. J. Cyclic dinucleotides at the forefront of innate immunity. *Current Opinion in Cell Biology* **63**, 49–56 (2020).
3. Sun, L., Wu, J., Du, F., Chen, X. & Chen, Z. J. Cyclic GMP-AMP Synthase Is a Cytosolic DNA Sensor That Activates the Type I Interferon Pathway. *Science* **339**, 786 (2013).
4. Wu, J. *et al.* Cyclic GMP-AMP Is an Endogenous Second Messenger in Innate Immune Signaling by Cytosolic DNA. *Science* **339**, 826 (2013).
5. Zhou, W. *et al.* Structure of the Human cGAS–DNA Complex Reveals Enhanced Control of Immune Surveillance. *Cell* **174**, 300-311.e11 (2018).
6. Ablasser, A. *et al.* cGAS produces a 2′-5′-linked cyclic dinucleotide second messenger that activates STING. *Nature* **498**, 380 (2013).
7. Zhang, X. *et al.* Cyclic GMP-AMP Containing Mixed Phosphodiester Linkages Is An Endogenous High-Affinity Ligand for STING. *Molecular Cell* **51**, 226–235 (2013).
8. Diner, E. J. *et al.* The Innate Immune DNA Sensor cGAS Produces a Noncanonical Cyclic Dinucleotide that Activates Human STING. *Cell Reports* **3**, 1355–1361 (2013).
9. Hall, J. *et al.* The catalytic mechanism of cyclic GMP-AMP synthase (cGAS) and implications for innate immunity and inhibition. *Protein Sci.* **26**, 2367–2380 (2017).
10. Shang, G., Zhang, C., Chen, Z. J., Bai, X. & Zhang, X. Cryo-EM structures of STING reveal its mechanism of activation by cyclic GMP–AMP. *Nature* **567**, 389–393 (2019).
11. McWhirter, S. M. *et al.* A host type I interferon response is induced by cytosolic sensing of the bacterial second messenger cyclic-di-GMP. *The Journal of Experimental Medicine* **206**, 1899–1911 (2009).
12. Burdette, D. L. *et al.* STING is a direct innate immune sensor of cyclic di-GMP. *Nature* **478**, 515–518 (2011).
13. Woodward, J. J., Iavarone, A. T. & Portnoy, D. A. c-di-AMP Secreted by Intracellular *Listeria monocytogenes* Activates a Host Type I Interferon Response. *Science* **328**, 1703 (2010).
14. Wang, C. *et al.* Synthesis of All Possible Canonical (3′–5′-Linked) Cyclic Dinucleotides and Evaluation of Riboswitch Interactions and Immune-Stimulatory Effects. *Journal of the American Chemical Society* **139**, 16154–16160 (2017).
15. Ishikawa, H. & Barber, G. N. STING is an endoplasmic reticulum adaptor that facilitates innate immune signalling. *Nature* **455**, 674–678 (2008).
16. Ishikawa, H., Ma, Z. & Barber, G. N. STING regulates intracellular DNA-mediated, type I interferon-dependent innate immunity. *Nature* **461**, 788–792 (2009).
17. Zhang, C. *et al.* Structural basis of STING binding with and phosphorylation by TBK1. *Nature* **567**, 394–398 (2019).
18. Zhao, B. *et al.* A conserved PLPLRT/SD motif of STING mediates the recruitment and activation of TBK1. *Nature* **569**, 718–722 (2019).

19. de Oliveira Mann, C. C. *et al.* Modular Architecture of the STING C-Terminal Tail Allows Interferon and NF-κB Signaling Adaptation. *Cell Reports* **27**, 1165-1175.e5 (2019).
20. Luteijn, R. D. *et al.* SLC19A1 transports immunoreactive cyclic dinucleotides. *Nature* **573**, 434-438 (2019).
21. Ablasser, A. *et al.* Cell intrinsic immunity spreads to bystander cells via the intercellular transfer of cGAMP. *Nature* **503**, 530 (2013).
22. Mardjuki, R. E., Carozza, J. A. & Li, L. Development of cGAMP-Luc, a sensitive and precise coupled enzyme assay to measure cGAMP in complex biological samples. *Journal of Biological Chemistry* **295**, 4881–4892 (2020).
23. Bose, D., Su, Y., Marcus, A., Raulet, D. H. & Hammond, M. C. An RNA-Based Fluorescent Biosensor for High-Throughput Analysis of the cGAS-cGAMP-STING Pathway. *Cell Chemical Biology* **23**, 1539–1549 (2016).
24. Webb, M. R. A continuous spectrophotometric assay for inorganic phosphate and for measuring phosphate release kinetics in biological systems. *Proceedings of the National Academy of Sciences* **89**, 4884–4887 (1992).
25. Brune, M., Hunter, J. L., Corrie, J. E. T. & Webb, M. R. Direct, Real-Time Measurement of Rapid Inorganic Phosphate Release Using a Novel Fluorescent Probe and Its Application to Actomyosin Subfragment 1 ATPase. *Biochemistry* **33**, 8262–8271 (1994).
26. Surdo, N. C. *et al.* FRET biosensor uncovers cAMP nano-domains at β-adrenergic targets that dictate precise tuning of cardiac contractility. *Nature Communications* **8**, 15031 (2017).
27. Börner, S. *et al.* FRET measurements of intracellular cAMP concentrations and cAMP analog permeability in intact cells. *Nature Protocols* **6**, 427–438 (2011).
28. Calamera, G. *et al.* FRET-based cyclic GMP biosensors measure low cGMP concentrations in cardiomyocytes and neurons. *Communications Biology* **2**, 394 (2019).
29. Christen, M. *et al.* Asymmetrical Distribution of the Second Messenger c-di-GMP upon Bacterial Cell Division. *Science* **328**, 1295–1297 (2010).
30. Kulasekara, B. R. *et al.* c-di-GMP heterogeneity is generated by the chemotaxis machinery to regulate flagellar motility. *eLife* **2**, (2013).
31. Mills, E., Petersen, E., Kulasekara, B. R. & Miller, S. I. A direct screen for c-di-GMP modulators reveals a *Salmonella* Typhimurium periplasmic L-arginine–sensing pathway. *Science Signaling* **8**, ra57–ra57 (2015).
32. Christen, M. *et al.* Identification of Small-Molecule Modulators of Diguanylate Cyclase by FRET-Based High-Throughput Screening. *ChemBioChem* **20**, 394–407 (2019).
33. Petersen, E., Mills, E. & Miller, S. I. Cyclic-di-GMP regulation promotes survival of a slow-replicating subpopulation of intracellular *Salmonella* Typhimurium. *Proceedings of the National Academy of Sciences* **116**, 6335–6340 (2019).
34. Dippel, A. B., Anderson, W. A., Park, J. H., Yildiz, F. H. & Hammond, M. C. Development of Ratiometric Bioluminescent Sensors for *in Vivo* Detection of Bacterial Signaling. *ACS Chemical Biology* acschembio.9b00800 (2020) doi:10.1021/acschembio.9b00800.
35. Roy, R., Hohng, S. & Ha, T. A practical guide to single-molecule FRET. *Nature Methods* **5**, 507–516 (2008).
36. Rowland, C. E., Brown, C. W., Medintz, I. L. & Delehanty, J. B. Intracellular FRET-based probes: a review. *Methods and Applications in Fluorescence* **3**, 042006 (2015).

37. Shrestha, D., Jenei, A., Nagy, P., Vereb, G. & Szöllősi, J. Understanding FRET as a Research Tool for Cellular Studies. *International Journal of Molecular Sciences* **16**, 6718–6756 (2015).
38. Huang, Y.-H., Liu, X.-Y., Du, X.-X., Jiang, Z.-F. & Su, X.-D. The structural basis for the sensing and binding of cyclic di-GMP by STING. *Nature Structural & Molecular Biology* **19**, 728–730 (2012).
39. Krasteva, P. V. & Sondermann, H. Versatile modes of cellular regulation via cyclic dinucleotides. *Nature Chemical Biology* **13**, 350 (2017).
40. Kranzusch, P. J. *et al.* Ancient Origin of cGAS-STING Reveals Mechanism of Universal 2′,3′ cGAMP Signaling. *Molecular Cell* **59**, 891–903 (2015).
41. Chin, K.-H. *et al.* Novel c-di-GMP recognition modes of the mouse innate immune adaptor protein STING. *Acta Crystallographica Section D Biological Crystallography* **69**, 352–366 (2013).
42. Day, R. N., Booker, C. F. & Periasamy, A. Characterization of an improved donor fluorescent protein for Förster resonance energy transfer microscopy. *Journal of Biomedical Optics* **13**, 031203 (2008).
43. Sun, Y. *et al.* Characterization of an orange acceptor fluorescent protein for sensitized spectral fluorescence resonance energy transfer microscopy using a white-light laser. *Journal of Biomedical Optics* **14**, 054009 (2009).
44. Chen, X., Zaro, J. L. & Shen, W.-C. Fusion protein linkers: Property, design and functionality. *Advanced Drug Delivery Reviews* **65**, 1357–1369 (2013).
45. Koshiba, T. & Chan, D. C. The Prefusogenic Intermediate of HIV-1 gp41 Contains Exposed C-peptide Regions. *Journal of Biological Chemistry* **278**, 7573–7579 (2003).
46. Roelofs, K. G., Wang, J., Sintim, H. O. & Lee, V. T. Differential radial capillary action of ligand assay for high-throughput detection of protein-metabolite interactions. *Proceedings of the National Academy of Sciences* **108**, 15528–15533 (2011).
47. Hall, J. *et al.* Discovery of PF-06928215 as a high affinity inhibitor of cGAS enabled by a novel fluorescence polarization assay. *PLoS One* **12**, 1–16 (2017).
48. Carozza, J.A. *et al*. Extracellular cGAMP is a cancer-cell-produced immunotransmitter involved in radiation-induced anticancer immunity. *Nature Cancer* 2020, **1**, 184–196 (2020).
49. Shin, K.-J. *et al.* A single lentiviral vector platform for microRNA-based conditional RNA interference and coordinated transgene expression. *Proceedings of the National Academy of Sciences* **103**, 13759–13764 (2006).
50. Shu, C. *et al.* Structure of STING bound to cyclic di-GMP reveals the mechanism of cyclic dinucleotide recognition by the immune system. *Nature Structural & Molecular Biology* 19, 722–724 (2012).
51. Eaglesham, J.B., Pan, Y., Kupper, T.S., Kranzusch, P.J. Viral and metazoan poxins are cGAMP-specific nucleases that restrict cGAS–STING signalling. *Nature* **566**, 259–263 (2019).
52. Ritchie, C. *et al.* SLC19A1 Is an Importer of the Immunotransmitter cGAMP. *Molecular Cell* **75**, 372-381 (2019).
53. Kato, K. *et al.* Structural insights into cGAMP degradation by Ecto-nucleotide pyrophosphatase phosphodiesterase 1. *Nature Communications* **9**, 4424 (2018).

54. Marcus, A. *et al.* Tumor-Derived cGAMP Triggers a STING-Mediated Interferon Response in Non-tumor Cells to Activate the NK Cell Response. *Immunity* **49**, 754-763.e4 (2018).
55. Li, X.D. *et al.* Pivotal Roles of cGAS-cGAMP Signaling in Antiviral Defense and Immune Adjuvant Effects. *Science* **341**, 1390–1394 (2013).
56. Lau, L., Gray, E. E., Brunette, R. L. & Stetson, D. B. DNA tumor virus oncogenes antagonize the cGAS-STING DNA-sensing pathway. *Science* **350**, 568 (2015).
57. Barnett, K.C. *et al.* Phosphoinositide Interactions Position cGAS at the Plasma Membrane to Ensure Efficient Distinction between Self- and Viral DNA. *Cell* **176**, 1432-1446 (2019).
58. Liu, H. *et al.* Nuclear cGAS suppresses DNA repair and promotes tumorigenesis. *Nature* **563**, 131–136 (2018).
59. Gentili, M. *et al.* The N-Terminal Domain of cGAS Determines Preferential Association with Centromeric DNA and Innate Immune Activation in the Nucleus. *Cell Reports* **26**, 2377-2393 (2019).
60. Zierhut, C. *et al.* The Cytoplasmic DNA Sensor cGAS Promotes Mitotic Cell Death. *Cell* **178,** 302-315 (2019).
61. Volkman, H. E., Cambier, S., Gray, E. E. & Stetson, D. B. Tight nuclear tethering of cGAS is essential for preventing autoreactivity. *eLife* **8**, (2019).
62. Collins, A. C. *et al.* Cyclic GMP-AMP Synthase Is an Innate Immune DNA Sensor for Mycobacterium tuberculosis. *Cell Host & Microbe* **17**, 820–828 (2015).
63. Dey, B. *et al*. A bacterial cyclic dinucleotide activates the cytosolic surveillance pathway and mediates innate resistance to tuberculosis. *Nature Medicine* **21**(4) (2015).
64. Huynh, T.N. *et al*. An HD-domain phosphodiesterase mediates cooperative hydrolysis of c-di-AMP to affect bacterial growth and virulence *Proceedings of the National Academy of Sciences* **112**, 7 (2015).
65. Whiteley, A.T. *et al*. Bacterial cGAS-like enzymes synthesize diverse nucleotide signals. *Nature* **567**, 194–199. (2019).
66. Ozawa, T., Kaihara, A., Sato, M., Tachihara, K. & Umezawa, Y. Split Luciferase as an Optical Probe for Detecting Protein−Protein Interactions in Mammalian Cells Based on Protein Splicing. *Analytical Chemistry* **73**, 2516–2521 (2001).
67. Littmann, T., Ozawa, T., Hoffmann, C., Buschauer, A. & Bernhardt, G. A split luciferase-based probe for quantitative proximal determination of Gαq signalling in live cells. *Scientific Reports* **8**, 17179 (2018).
68. Filonov, S.G. *et al*. Bright and stable near infra-red fluorescent protein for *in vivo* imaging. *Nature Biotechnology* **29**, 757-761 (2012).
69. Chu, J. *et al*. Non-invasive intravital imaging of cellular differentiation with a bright red-excitable fluorescent protein. *Nature Methods.* **11**, 572-578 (2014).
70. Bajar, B., Wang, E., Zhang, S., Lin, M. & Chu, J. A Guide to Fluorescent Protein FRET Pairs. *Sensors* **16**, 1488 (2016).
71. P.V. Krasteva, H. Sondermann, H, *Nat. Chem. Biol.* **2017**, *13*, 350-359.
72. S.A. Zaver, J. J. Woodward, J. J, *Curr. Opin. Cell Biol.* **2020**, *63*, 49–56.
73. C.E. Witte, A. T. Whiteley, T. P. Burke, J. D. Sauer, D. A. Portnoy, J. J. Woodward, *mBio* **2013**, *4*, e00282-13.
74. A. T. Whiteley, N. E. Garelis, B. N. Peterson, P. H. Choi, L. Tong, J. J. Woodward, D. A. Portnoy, *Mol. Microbiol.* **2017**, *104*, 212–233.

75. K. Sureka, P.H. Choi, M. Precit, M. Delince, D.A. Pensinger, T.N. Huynh, A. R. Jurado, Y. A. Goo, M. Sadilek, A. T. Iavarone, J.-D. Sauer, L. Tong, J. J. Woodward, *Cell* **2014**, *158*, 1389–1401.
76. T. N. Huynh, P. H. Choi, K. Sureka, H. E. Ledvina, J. Campillo, L. Tong, J. J. Woodward, *Mol. Microbiol.* **2016**, *102*, 233–243.
77. L. Townsley, S. M. Yannarell, T. N. Huynh, J. J. Woodward, E. A. Shank, *mBio* **2018**, *9*, e00341-18.
78. J. Gundlach, L. Krüger, C. Herzberg, A. Turdiev, A. Poehlein, I. Tascón, M. Weiss, D. Hertel, R. Daniel, I. Hänelt, V. T. Lee, J. Stülke, *J. Biol. Chem.* **2019**, *294*, 9605–9614.
79. L. Krüger, C. Herzberg, R. Warneke, A. Poehlein, J. Stautz, M. Weiß, R. Daniel, I. Hänelt, J. Stülke, *J. Bacteriol.* **2020**, *202*, e00138-20.
80. J. Stülke, L. Krüger, *Annu. Rev. Microbiol.* **2020**, *74*, 159-179.
81. A. T. Whiteley, J. B. Eaglesham, C. C. de Oliveira Mann, B. R. Lowey, E. A. Nieminen, O. Danilchanka, D. S. King, A. S. Y. Lee, J. J. Mekalanos, P. J. Kranzusch, *Nature* **2019**, *567*, 194-199.
82. D. Cohen, S. Melamed, A. Millman, G. Shulman, Y. Oppenheimer-Shaanan, A. Kacen, S. Doron, G. Amitai, R. Sorek, R. *Nature* **2019**, *574*, 691-695.
83. J. J. Woodward, A. T. Iavarone, D. A. Portnoy, *Science* **2010**, *328*, 1703-1705.
84. McFarland, S. Luo, F. Ahmed-Qadri, M. Zuck, E. F. Thayer, Y. A. Goo, K. Hybiske, L. Tong, J. J. Woodward, *Immunity* **2017**, *46*, 433–445.
85. A. P. McFarland, T. P. Burke, A. A. Carletti, R. C. Glover, H. Tabakh, M. D. Welch, J. J. Woodward, *MBio* **2018**, *9*, e00526-18.
86. S. M. McWhirter, R. Barbalat, K. M. Monroe, M. F. Fontana, M. Hyodo, N. T. Joncker, K. J. Ishii, S. Akira, M. Colonna, Z. J. Chen, K. A. Fitzgerald, Y. Hayakawa, R. E. Vance, *J. Exp. Med*. **2009**, *206*, 1899–1911.
87. D. L. Burdette, K. M. Monroe, K. Sotelo-Troha, J. S. Iwig, B. Eckert, M. Hyodo, Y. Hayakawa, R. E. Vance, *Nature* **2011**, *478*, 515–518.
88. X. Gui, H. Yang, T. Li, X. Tan, P. Shi, M. Li, F. Du, Z. J. Chen, *Nature* **2019**, *567*, 262–266.
89. K. Parvatiyar, Z. Zhang, R. M. Teles, S. Ouyang, Y. Jiang, S. S. Iyer, S. A. Zaver, M. Schenk, S. Zeng, W. Zhong, Z. J. Liu, R. L. Modlin, Y. Liu, G. Cheng, *Nat. Immunol.* **2012**, *13*, 1155–1161.
90. T. N. Huynh, J. J. Woodward, *Curr. Opin. Microbiol*. **2016**, *30*, 22–29.
91. T. N. Huynh, S. Luo, D. Pensinger, J.-D. Sauer, L. Tong, J. J. Woodward, *Proc. Natl. Acad. Sci.* **2015**, *112*, E747–E756.
92. A. T. Whiteley, A. J. Pollock, D. A. Portnoy, *Cell Host Microbe* **2015**, *17*, 788–798.
93. H. T. Pham, N. T. H. Nhiep, T. N. M. Vu, T. N. Huynh, Y. Zhu, A. L. D. Huynh, A. Chakrabortti, E. Marcellin, R. Lo, C. B. Howard, N. Bansal, J. J. Woodward, Z.-X. Liang, M. S. Turner, *PLoS Genet.* **2018**, *14*, e1007574.
94. R. M. Corrigan, L. Bowman, A. R. Willis, V. Kaever, A. Gründling, *J. Biol. Chem*. **2015**, *290*, 5826–5839.
95. C. A. Kellenberger, C. Chen, A. T. Whiteley, D. A. Portnoy, M. C. Hammond, *J. Am. Chem. Soc.* **2015**, *137*, 6432–6435.
96. R. E. Mardjuki, J. A. Carozza, L. Li, *J. Biol. Chem.* **2020**, *295*, 4881–4892.
97. J. Yang, Y. Bai, Y. Zhang, V. D. Gabrielle, L. Jin, G. Bai, *Mol. Microbiol*. **2014**, *93*, 65–79.

98. K. Manikandan, V. Sabareesh, N. Singh, K. Saigal, U. Mechold, K. M. Sinha, *PLoS One* **2014**, *9* e86096.
99. Q. He, F. Wang, S. Liu, D. Zhu, H. Cong, F. Gao, B. Li, H. Wang, Z. Lin, J. Liao, L. Gu, *J. Biol. Chem.* **2016**, *291* 3668–3681.
100. Q. Tang, Y. Luo, C. Zheng, K. Yin, M. K. Ali, X. Li, J. He, *Int. J. Biol. Sci.* **2015**, *11*, 813–824.
101. A. Latoscha, D. J. Drexler, M. M. Al-Bassam, A. M. Bandera, V. Kaever, K. C. Findlay, G. Witte, N. Tschowri, *Proc. Natl. Acad. Sci.* **2020**, *117*, 7392–7400.
102. A. J. Pollock, S. A. Zaver, J. J. Woodward, *Nat. Commun.* **2020**, *11*, 3533.
103. R. D. Luteijn, S. A. Zaver, B. G. Gowen, S. K. Wyman, N. E. Garelis, L. Onia, S. M. McWhirter, G. E. Katibah, J. E. Corn, J. J. Woodward, D. H. Raulet, *Nature*, **2019**, *573*, 434-438.
104. J. Gibhardt, J. L. Heidemann, R. Bremenkamp, J. Rosenberg, R. Seifert, V. Kaever, R. Ficner, F. M. Commichau, *Environ. Microbiol.* **2020**, *22*, 2771–2791.
105. T. Tosi, F. Hoshiga, C. Millership, R. Singh, C. Eldrid, D. Patin, D. Mengin-Lecreulx, K. Thalassinos, P. Freemont, A. Gründling, *PLoS Pathog*. **2019**, *15*, e1007537.
106. Stülke, J. & Krüger, L. Cyclic di-AMP Signaling in Bacteria. Annu. Rev. Microbiol. 74, 159–179 (2020).
107. Gomelsky, M. cAMP, c-di-GMP, c-di-AMP and now cGMP: bacteria use them all! Mol. Microbiol. 79, 562–565 (2011).
108. Krasteva, P. V. & Sondermann, H. Versatile modes of cellular regulation via cyclic dinucleotides. Nat. Chem. Biol. 13, 350–359 (2017).
109. Commichau, F. M., Heidemann, J. L. & Ficner, R. Making and breaking of an essential poison: the cyclases and phosphodiesterases that produce and degrade the essential second messenger cyclic di-AMP in …. Journal of (2019).
110. Zaver, S. A. & Woodward, J. J. Cyclic dinucleotides at the forefront of innate immunity. Curr. Opin. Cell Biol. 63, 49–56 (2020).
111. Bowman, L., Zeden, M. S., Schuster, C. F., Kaever, V. & Gründling, A. New insights into the cyclic di-adenosine monophosphate (c-di-AMP) degradation pathway and the requirement of the cyclic dinucleotide for acid stress resistance in Staphylococcus aureus. J. Biol. Chem. 291, 26970–26986 (2016).
112. Zeden, M. S. et al. Cyclic di-adenosine monophosphate (c-di-AMP) is required for osmotic regulation in Staphylococcus aureus but dispensable for viability in anaerobic conditions. J. Biol. Chem. 293, 3180–3200 (2018).
113. He, J., Yin, W., Galperin, M. Y. & Chou, S.-H. Cyclic di-AMP, a second messenger of primary importance: tertiary structures and binding mechanisms. Nucleic Acids Res. 48, 2807–2829 (2020).
114. Fahmi, T., Port, G. C. & Cho, K. H. c-di-AMP: An Essential Molecule in the Signaling Pathways that Regulate the Viability and Virulence of Gram-Positive Bacteria. Genes 8, (2017).
115. Yin, W. et al. A decade of research on the second messenger c-di-AMP. FEMS Microbiol. Rev. (2020).
116. Witte, C. E. et al. Cyclic di-AMP is critical for Listeria monocytogenes growth, cell wall homeostasis, and establishment of infection. MBio 4, e00282–13 (2013).

117. Whiteley, A. T. et al. c-di-AMP modulates Listeria monocytogenes central metabolism to regulate growth, antibiotic resistance and osmoregulation. Mol. Microbiol. 104, 212–233 (2017).
118. Sureka, K. et al. The cyclic dinucleotide c-di-AMP is an allosteric regulator of metabolic enzyme function. Cell 158, 1389–1401 (2014).
119. Pham, H. T. et al. Enhanced uptake of potassium or glycine betaine or export of cyclic-di-AMP restores osmoresistance in a high cyclic-di-AMP Lactococcus lactis mutant. PLoS Genet. 14, e1007574 (2018).
120. Massa, S. M. et al. c-di-AMP Accumulation Impairs Muropeptide Synthesis in Listeria monocytogenes. J. Bacteriol. 202, (2020).
121. Huynh, T. N. et al. An HD-domain phosphodiesterase mediates cooperative hydrolysis of c-di-AMP to affect bacterial growth and virulence. Proc. Natl. Acad. Sci. U. S. A. 112, E747–56 (2015).
122. Corrigan, R. M. et al. Systematic identification of conserved bacterial c-di-AMP receptor proteins. Proceedings of the National Academy of Sciences vol. 110 9084–9089 (2013).
123. Corrigan, R. M., Abbott, J. C., Burhenne, H., Kaever, V. & Gründling, A. c-di-AMP is a new second messenger in Staphylococcus aureus with a role in controlling cell size and envelope stress. PLoS Pathog. 7, e1002217 (2011).
124. Whiteley, A. T., Pollock, A. J. & Portnoy, D. A. The PAMP c-di-AMP Is Essential for Listeria monocytogenes Growth in Rich but Not Minimal Media due to a Toxic Increase in (p)ppGpp. Cell Host Microbe 17, 788–798 (2015).
125. Bai, Y. et al. Two DHH Subfamily 1 Proteins in Streptococcus pneumoniae Possess Cyclic Di-AMP Phosphodiesterase Activity and Affect Bacterial Growth and Virulence. Journal of Bacteriology vol. 195 5123–5132 (2013).
126. Bai, Y. et al. Cyclic Di-AMP Impairs Potassium Uptake Mediated by a Cyclic Di-AMP Binding Protein in Streptococcus pneumoniae. Journal of Bacteriology vol. 196 614–623 (2014).
127. Huynh, T. N. et al. Cyclic di-AMP targets the cystathionine beta-synthase domain of the osmolyte transporter OpuC. Molecular Microbiology vol. 102 233–243 (2016).
128. Townsley, L., Yannarell, S. M., Huynh, T. N., Woodward, J. J. & Shank, E. A. Cyclic di-AMP Acts as an Extracellular Signal That ImpactsBacillus subtilisBiofilm Formation and Plant Attachment. mBio vol. 9 (2018).
129. Gundlach, J. et al. Sustained sensing in potassium homeostasis: Cyclic di-AMP controls potassium uptake by KimA at the levels of expression and activity. Journal of Biological Chemistry vol. 294 9605–9614 (2019).
130. Krüger, L. et al. Two Ways To Convert a Low-Affinity Potassium Channel to High Affinity: Control of Bacillus subtilis KtrCD by Glutamate. Journal of Bacteriology vol. 202 (2020).
131. Rubin, B. E. et al. High-throughput interaction screens illuminate the role of c-di-AMP in cyanobacterial nighttime survival. PLOS Genetics vol. 14 e1007301 (2018).
132. Tosi, T. et al. Inhibition of the Staphylococcus aureus c-di-AMP cyclase DacA by direct interaction with the phosphoglucosamine mutase GlmM. PLoS Pathog. 15, e1007537 (2019).
133. Zhu, Y. et al. Cyclic-di-AMP synthesis by the diadenylate cyclase CdaA is modulated by the peptidoglycan biosynthesis enzyme GlmM in Lactococcus lactis. Mol. Microbiol. 99, 1015–1027 (2016).

134. Pham, T. H., Liang, Z.-X., Marcellin, E. & Turner, M. S. Replenishing the cyclic-di-AMP pool: regulation of diadenylate cyclase activity in bacteria. Curr. Genet. 62, 731–738 (2016).
135. Woodward, J. J., Iavarone, A. T. & Portnoy, D. A. c-di-AMP secreted by intracellular Listeria monocytogenes activates a host type I interferon response. Science 328, 1703–1705 (2010).
136. Underwood, A. J., Zhang, Y., Metzger, D. W. & Bai, G. Detection of cyclic di-AMP using a competitive ELISA with a unique pneumococcal cyclic di-AMP binding protein. J. Microbiol. Methods 107, 58–62 (2014).
137. Kellenberger, C. A., Chen, C., Whiteley, A. T., Portnoy, D. A. & Hammond, M. C. RNA-Based Fluorescent Biosensors for Live Cell Imaging of Second Messenger Cyclic di-AMP. J. Am. Chem. Soc. 137, 6432–6435 (2015).
138. Zaver, S., Pollock, A., Boradia, V. & Woodward, J. A luminescence based coupled enzyme assay enables high throughput quantification of the bacterial second messenger 3′3′-cyclic-di-AMP. Chembiochem (2020).
139. Surdo, N. C. et al. FRET biosensor uncovers cAMP nano-domains at β-adrenergic targets that dictate precise tuning of cardiac contractility. Nat. Commun. 8, 15031 (2017).
140. Murai, S. et al. A FRET biosensor for necroptosis uncovers two different modes of the release of DAMPs. Nat. Commun. 9, 4457 (2018).
141. Börner, S. et al. FRET measurements of intracellular cAMP concentrations and cAMP analog permeability in intact cells. Nat. Protoc. 6, 427–438 (2011).
142. Calamera, G. et al. FRET-based cyclic GMP biosensors measure low cGMP concentrations in cardiomyocytes and neurons. Commun Biol 2, 394 (2019).
143. Christen, M. et al. Asymmetrical distribution of the second messenger c-di-GMP upon bacterial cell division. Science 328, 1295–1297 (2010).
144. Kulasekara, B. R. et al. c-di-GMP heterogeneity is generated by the chemotaxis machinery to regulate flagellar motility. Elife 2, e01402 (2013).
145. Mills, E., Petersen, E., Kulasekara, B. R. & Miller, S. I. A direct screen for c-di-GMP modulators reveals a Salmonella Typhimurium periplasmic L-arginine–sensing pathway. Sci. Signal. 8, ra57–ra57 (2015).
146. Christen, M. et al. Identification of Small-Molecule Modulators of Diguanylate Cyclase by FRET-Based High-Throughput Screening. Chembiochem 20, 394–407 (2019).
147. Petersen, E., Mills, E. & Miller, S. I. Cyclic-di-GMP regulation promotes survival of a slow-replicating subpopulation of intracellular Salmonella Typhimurium. Proc. Natl. Acad. Sci. U. S. A. 116, 6335–6340 (2019).
148. Dippel, A. B., Anderson, W. A., Park, J. H., Yildiz, F. H. & Hammond, M. C. Development of Ratiometric Bioluminescent Sensors for in Vivo Detection of Bacterial Signaling. ACS Chem. Biol. 15, 904–914 (2020).
149. Pollock, A. J., Zaver, S. A. & Woodward, J. J. A STING-based biosensor affords broad cyclic dinucleotide detection within single living eukaryotic cells. Nat. Commun. 11, 3533 (2020).
150. Calamera, G. et al. Construction of novel cGMP FRET-sensors based on PKG from Plasmodium falciparum. BMC Pharmacology and Toxicology vol. 16 (2015).
151. Jalink, K. Spying on cGMP with FRET. Nature Methods vol. 3 11–12 (2006).
152. Roy, R., Hohng, S. & Ha, T. A practical guide to single-molecule FRET. Nat. Methods 5, 507–516 (2008).

153. Rowland, C. E., Brown, C. W., Medintz, I. L. & Delehanty, J. B. Intracellular FRET-based probes: a review. Methods Appl Fluoresc 3, 042006 (2015).
154. Shrestha, D., Jenei, A., Nagy, P., Vereb, G. & Szöllősi, J. Understanding FRET as a research tool for cellular studies. Int. J. Mol. Sci. 16, 6718–6756 (2015).
155. Hochreiter, B., Garcia, A. P. & Schmid, J. A. Fluorescent proteins as genetically encoded FRET biosensors in life sciences. Sensors 15, 26281–26314 (2015).
156. Algar, W. R., Russ Algar, W., Hildebrandt, N., Vogel, S. S. & Medintz, I. L. FRET as a biomolecular research tool — understanding its potential while avoiding pitfalls. Nature Methods vol. 16 815–829 (2019).
157. Bajar, B. T., Wang, E. S., Zhang, S., Lin, M. Z. & Chu, J. A Guide to Fluorescent Protein FRET Pairs. Sensors 16, (2016).
158. Denay, G., Schultz, P., Hänsch, S., Weidtkamp-Peters, S. & Simon, R. Over the rainbow: A practical guide for fluorescent protein selection in plant FRET experiments. Plant Direct 3, e00189 (2019).
159. Roelofs, K. G., Wang, J., Sintim, H. O. & Lee, V. T. Differential radial capillary action of ligand assay for high-throughput detection of protein-metabolite interactions. Proc. Natl. Acad. Sci. U. S. A. 108, 15528–15533 (2011).
160. Wang, F. et al. BrlR from Pseudomonas aeruginosa is a receptor for both cyclic di-GMP and pyocyanin. Nat. Commun. 9, 2563 (2018).
161. Dey, B. et al. A bacterial cyclic dinucleotide activates the cytosolic surveillance pathway and mediates innate resistance to tuberculosis. Nat. Med. 21, 401–406 (2015).
162. Nurunnabi, M., Khatun, Z., Reeck, G. R., Lee, D. Y. & Lee, Y.-K. Near infra-red photoluminescent graphene nanoparticles greatly expand their use in noninvasive biomedical imaging. Chem. Commun. 49, 5079–5081 (2013).
163. Chu, J. et al. Non-invasive intravital imaging of cellular differentiation with a bright red-excitable fluorescent protein. Nat. Methods 11, 572–578 (2014).
164. Ozawa, T., Kaihara, A., Sato, M. & Tachihara, K. Split luciferase as an optical probe for detecting protein− protein interactions in mammalian cells based on protein splicing. Analytical (2001).
165. Littmann, T., Ozawa, T., Hoffmann, C., Buschauer, A. & Bernhardt, G. A split luciferase-based probe for quantitative proximal determination of Gαq signalling in live cells. Sci. Rep. 8, 17179 (2018).
166. Whiteley, A. T. et al. Bacterial cGAS-like enzymes synthesize diverse nucleotide signals. Nature 567, 194–199 (2019).
167. Hendrickson, W. A., Horton, J. R. & LeMaster, D. M. Selenomethionyl proteins produced for analysis by multiwavelength anomalous diffraction (MAD): a vehicle for direct determination of three-dimensional structure. EMBO J. 9, 1665–1672 (1990).
168. Otwinowski, Z. & Minor, W. [20] Processing of X-ray diffraction data collected in oscillation mode. in Methods in Enzymology vol. 276 307–326 (Academic Press, 1997).
169. Adams, P. D. et al. PHENIX: building new software for automated crystallographic structure determination. Acta Crystallogr. D Biol. Crystallogr. 58, 1948–1954 (2002).
170. , P. & Cowtan, K. Coot: model-building tools for molecular graphics. Acta Crystallogr. D Biol. Crystallogr. 60, 2126–2132 (2004).
171. Murshudov, G. N., Vagin, A. A. & Dodson, E. J. Refinement of macromolecular structures by the maximum-likelihood method. Acta Crystallogr. D Biol. Crystallogr. 53, 240–255 (1997).